MARMARA UNIVERSITY
INSTITUTE FOR GRADUATE STUDIES
IN PURE AND APPLIED SCIENCES

# PREPARATION AND CHARACTERIZATION OF ANTIFOULING $TiO_2$-POLYSULFONE ULTRAFILTRATION MEMBRANES

BÜŞRA MERVE CERRAH

**MASTER THESIS**
Department of Environmental sciences

**Thesis Supervisor**
Y. Doç. Dr. Elif SOYER

ISTANBUL, 2016

# MARMARA UNIVERSITY
# INSTITUTE FOR GRADUATE STUDIES IN PURE AND APPLIED SCIENCES

Busra Merve CERRAH, a Master of Science student of Marmara University Institute for Graduate Studies in Pure and Applied Sciences, defended her thesis entitled "Preparation and Characterization of Antiofouling $TiO_2$-Polysulfone Ultrafiltration Membranes" on Sep.06,.2016 and has been found to be satisfactory by the jury members.

**Jury Members**

Assist. Prof. Dr. Elif SOYER (Advisor)
Marmara University ..... (SIGN) .....

Assist.Prof. Dr. Esra ERDİM (Jury Member)
Marmara Üniversitesi ..... (SIGN) .....

Prof. Dr. Mehmet ÇAKMAKÇI (Jury Member)
Yıldız Teknik Üniversitesi ..... (SIGN) .....

## APPROVAL

Marmara University Institute for Graduate Studies in Pure and Applied Sciences Executive Committee approves that Büşra Merve CERRAH be granted the degree of Master of Science in Department of Environmeltal Sciences, Environmental Sciences Program on 26.09.2016 (Resolution no: 2016/22-02)

**Director of the Institute**
**Prof. Dr. Uğur YAHSİ**

## ACKNOWLEDGEMENT

I dedicate this long work to the time I spent in ISAM Library and to my beloved mother.

**August, 2016** **Büşra Merve CERRAH**

# TABLE OF CONTENTS

## ABSTRACT

In this study membranes were prepared by phase inversion method using polysulfone (PSf), polyvinylpyrrolidone (PVP) in solvent N-methyl-2-pyrrolidone (NMP) with four different loadings of titania nanoparticles ($TiO_2$-NPs), 0.0%, 0.5%, 2.0% and 4.0% by weight.

Because of its unique characteristics, such as obtaining high water flux, semi-conductivity, propensity to photocatalytic membrane reactions, titania has been gaining more attention for producing nanoparticles embedded membranes. Therefore, this study is focused on the production and characterization of titania ($TiO_2$) nanoparticles entrapped membrane sheets.

The morphology of the fabricated membranes was analyzed by using scanning electron microscope (SEM). The membranes were subjected to ultrafiltration tests, such as measurement of pure water flux, fouling behavior including flux decline and flux recoveries. Besides, this study includes particle size evaluation of nanoparticles, mechanical tests, water uptake and contact angle measurements of fabricated membranes. Titania release under interaction with different chemical agents (HCl, NaOH and NaOCl) was also investigated. Finally, potential photocatalytic activity of released titania was examined.

## ÖZET

Bu çalışmada, membranlar polisülfon (PSf), polivinilpirolidon (PVP) ve çözücü olarak N-metil-2-pirolidon (NMP) kulllanılarak faz dönüşümü metodu ile, kütlece %0, %0,5, %2 ve % 4 olmak üzere dört farklı nanoparçacık ($TiO_2$) bileşim oranlarında hazırlanmıştır.

Titanyum dioksit, yüksek akı değeri sağlayabilme, fotokatalitik membran reaksiyonlarına karşı eğilim ve yarıiletkenlik gibi özellikleri sebebiyle son yıllarda nanoparçacık katkılı membran üretiminde oldukça ilgi çekici bir bileşiktir. Bu sebeple, bu çalışmada titanyum dioksit ($TiO_2$) nanoparçacık katkılı membran üretimi ve karakterizasyonu üzerinde durulmuştur.

Üretilen membranların morfolojisi taramalı elektron mikroskobu (SEM) ile analiz edilmiştir. Membranlar, saf su akısı ölçümü, tıkanma davranışlarının (akı azalması ve akı gerikazanımları) belirlenmesi gibi ultrafiltrasyon testlerine tabi tutulmuştur. Ayrıca, bu çalışma üretilmiş membranlarda ve üretim aşamalarında nanoparçacık boyutu değerlendirmeleri, mekanik testler, su çekme deneyleri ve temas açısı ölçümlerini de içermektedir. Membranların üç farklı kimyasalla temasında oluşan titanyum dioksit nanoparçacık geri salımları da ayrıca incelenmiştir. Son olarak, geri salınan $TiO_2$ nanoparçacıklarının potensiyel fotokatalitik aktivitesi de bu çalışmada bahsedilmiştir.

## SYMBOLS

**a :** Area ($m^2$)

**Ag:** Silver

**$Al_2O_3$ :** Aluminium Oxide

**$CO_2$ :** Carbon Dioxide

**$CH_4$ :** Methane

**cm :** Centimeter

**CNT:** Carbon nanotube

**d :** Day

**g :** Gram

**h :** Hour

**HCl :** Hydrochloric Acid

**J :** Flux ($g/m^2.h$)

**kDa:** Kilodalton

**Km :** Membrane Resistance Coefficient, $m^{-1}$

**km :** Kilometer

**kPa :** Kilopascal

**kV :** Kilovolts

**L :** Liter

**m :** Meter

**$m^2$ :** Meter square

**$m^3$ :** Cubic meter

**mg :** Milligram

**µg :** Micro Gram

**mgd :** Millions of gallons per day

**ml :** Milliliter

**MWCNT:** Multiwall Carbon Nanotube

**N :** Normality

**NaOCl :** Sodium Hypochlorite

**NaOH :** Sodium Hydroxide

**O2 :** Oxygen

**PSi :** Pound per square inch

**Q :** Volumetric flow rate of pure water ($m^3$/h)

**rpm :** Revolution per minute

**$TiO_2$ :** Titanium Dioxide

**t :** Time (day, hour)

**w% :** Weight Percent

**% :** Percentage

**°C :** Degree Celcius

**µm :** Micro Meter

**$ZrO_2$ :** Zirkonium Dioxide

**ΔP :** Pressure Difference (bar)

**µ :** Dynamic Viscosity of Water, kg/ m.s

## ABBREVIATIONS

**ED :** Electrodialysis

**EWC :** Equilibrium water content

**HA:** Humic Acid

**ICP-MS :** Inductively Coupled Plasma Mass Spectrometer

**MF :** Microfiltration

**NF :** Nanofiltration

**NMP :** N-Methyl Pyrolidone

**PEG:** Polyethylene Glycol

**PES :** Polyethersulfone

**PP :** Polypropylene

**PSf :** Polysulfone

**PVP :** Polyvinylpyrolidone

**RO :** Reverse Osmosis

**SEM :** Scanning Electron Microscopy

**UF :** Ultrafiltration

## LIST OF FIGURES

## LIST OF TABLES

# 1.INTRODUCTION

Membranes are influential materials on separating components in water, and they are permeable to water but not to other substances. Membranes have propensity to permeate some substances and water due to their pore sizes and this mechanism results a less concentrated permeate water with impermeable matter than retentate. Membrane processes are used in many fields such as potable water treatment, wastewater treatment, pharmaceutical industry, food industry and biotechnology (AWWA, 2005; Crittenden et al., 2005).

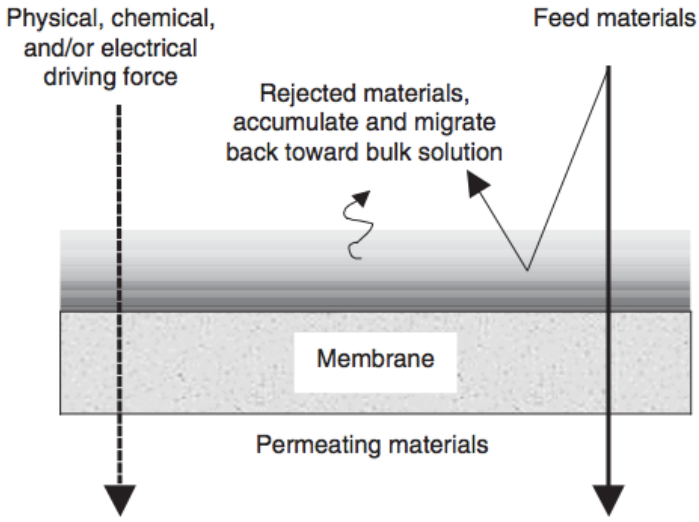


**Figure 1.1.** Understanding how a membrane basically works

Polysulfone (PSF) membranes have been widely used as UF membranes in many industrial fields for their low cost, superior film forming ability, good mechanical and anti-compaction properties, strong chemical and thermal stabilities and exclusive acidic and alkaline resistance (Yang et al., 2007).

Many efforts have been made to control membrane fouling, which generally is divided into three categories: the hydrophilic modification of membrane, pretreatment of the feed solution, and optimization of membrane process (Li et al., 2006). Many studies have been done to enhance the hydrophilic properties of polysulfone membrane surface. These studies can be differentiated in three categories:

- Blending PSF with hydrophilic nanoparticles such as $SiO_2$, $ZrO_2$ and $TiO_2$,
- Grafting with hydrophilic polymers, monomers or functional groups,
- Coating with hydrophilic polymers.

Blending with nanoparticles spearheads among those options in the past 10 years due to their convenient operation conditions (Richards et al., 2012).

**Table1.1.** Literature review on nanocomposite UF membranes (Goh et al., 2015)

| Poly-mer | Filler | Filler loading (wt%) | TMP (MPa) | Contact Angle (°) | Feed | Initial Flux ($L/m^2h$) | Pure Water Flux ($L/m^2h$) | FRR(%) |
|---|---|---|---|---|---|---|---|---|
| PSf | $TiO_2$ | 2.00 | 0.20 | Neat=84.7<br>NC=41.4 | Oil-in-water | Neat=239.4<br>NC=305.3 | Neat=289<br>NC=488 | |
| PES | $TiO_2$ | 2.00 | | Neat=70<br>NC=60 | | Neat=88<br>NC=93 | Neat=217<br>NC=236 | |
| PES | $TiO_2$ | 2.00 | 0.10 | Neat=72<br>NC=48 | BSA | | Neat=17<br>NC=55 | Neat=83.3<br>NC=61.5 |
| PSf | $TiO_2$ | 2.00 | 0.10 | Neat=<br>NC=72 | BSA | Neat=239.4<br>NC=305.3 | | Neat=71.8<br>NC=83.4 |
| PES | $TiO_2$ | 0.40 | | Neat=52.3<br>NC=44.1 | BSA | | Neat=181<br>NC=197 | |
| PES | $Al_2O_3$ | 1.00 | 0.50 | Neat=66.3<br>NC=41.4 | Whey | Neat=1.2<br>NC=1.99 | Neat=3.9<br>NC=4.63 | Neat=58.2<br>NC=96.1 |
| PES | $Al_2O_3$ | 0.40 | | Neat=52.3<br>NC=37.8 | BSA | | Neat=181<br>NC=209 | |
| PES | $ZrO_2$ | 0.40 | | Neat=52.3<br>NC=48.6 | BSA | | Neat=181<br>NC=188 | |
| PES | $Ce/SiO_2$ | | 0.05 | Neat=78.6<br>NC=41.7 | Oil-in-water | | Neat=181<br>NC=188 | |
| PES | | | | Neat=52.3<br>NC=48.6 | BSA | | | |
| PSf | $SiO_2$ | 3.00 | 0.30 | | Oil-in-water | Neat=1.08<br>NC=17.32 | | Neat=10.3<br>NC=34.01 |
| PES | $SiO_2$ | 3.00 | 0.50 | Neat=78.6<br>NC=58 | BSA | | Neat=249.4<br>NC=510.7 | Neat=80.6<br>NC=98 |
| PES | MWCNT | 2.00 | 0.35 | | BSA | | Neat=12<br>NC=70 | |

| | | | | | | | | |
|---|---|---|---|---|---|---|---|---|
| PES | MWCNT | 1.00 | 0.30 | Neat=69.1<br>NC=51.9 | BSA | | Neat=124<br>NC=184 | Neat=27<br>NC=46 |
| PES | Ag/Zr | 0.10 | 0.10 | Neat=71.5<br>NC=58.4 | BSA | | Neat=82.1<br>NC=100.6 | |
| PSf | Ag | 4.00 | 0.30 | Neat=81.2<br>NC=60.9 | BSA | Neat=42<br>NC=147 | Neat=48<br>NC=168 | |
| PSf | Ag | 0.50 | 0.30 | Neat=70<br>NC=60 | BSA | Neat=94.2<br>NC=43.2 | | |
| PES | HNT/Ag | 3.00 | | Neat=88<br>NC=55 | PEG | | Neat=112.8<br>NC=375.6 | Neat=88.7<br>NC=97.6 |
| PSf | Zeolite | 15.00 | 0.20 | Neat=70.6<br>NC=66.1 | HA | Neat=13.56<br>NC=35.81 | | |
| PSf | $CaCO_3$ | 10.00 | | Neat=82.8<br>NC=72.5 | BSA | | | Neat=44<br>NC=71 |

According to review that Goh et al. published, blending nanoparticles with polymers other than polysulfone and polyethersulfone, such as PVDF (polyvinylidene fluoride), PPESK (poly(phthalazinone ether sulfone ketone)), BPPO (brominated polyphenylene oxide), PAN (polyacrylonitrile) and CA (cellulose acetate) is also extensive. Most commonly composed nanoparticles with before cited materials are $SiO_2$, $TiO_2$, MWCNT, Ag, Zeolite/Ag, graphene oxide, Ag/Zr, $Al_2O_3$, Ce/ $SiO_2$ and halloysite nanotubes.

Zhang et al. examined in 2008 the photocatalytic activity of $TiO_2$-NPs embedded nanowire membranes on humic acid solution and they achieved to remove total organic matter of a ratio of 93.6% under UV irradiation. Li et al. tried to modify the inorganic titanium dioxide nanoparticles in order to avoid the agglomeration and increase the solubility of nanoparticles in organic solvent. They reported that with the introduction of $TiO_2$ into the casting solution, the number of macrovoids of the membrane decreases, at the same time the thickness of the skin layer increases. They compared the unmodified membranes and modified porous skin layer structure due to $TiO_2$ addition. For hydrophilicity analyses in terms of contact angle measurements it is approached that the higher concentration of $TiO_2$, the lower the contact angle is.

Li et al. also evaluated that the flux of $TiO_2$ embedded PPESK membranes increases owing to more porous surface and skin layer which reduces the resistance of water permeation, but not over 3% (w/w) of $TiO_2$. It is claimed that after 3% wt. the flux starts decreasing due to

particle agglomeration, which is relatedly figured out of sponge-like structure of membrane cross-section. Meanwhile, it is investigated that the PPESK membranes with embedded $TiO_2$ are less susceptible to fouling than the plain membrane.

A. Sotto et al. indicated that with the addition of $TiO_2$- NPs into PES nanofiltration membranes contact angle decreases from 68° to 63° whereas the extent of membrane fouling decreases considerably by around 22%.

Yang et al. did examine the morphology and characteristics of 18wt.% PSF which was entrapped with nanosized $TiO_2$. When the amount of $TiO_2$ -NPs 2 wt.% in dope solution, permeability, hydrophilicity, mechanical strength and anti-fouling ability of membrane became improved. They claimed that the higher $TiO_2$ content than 2% wt. leads nanoparticle agglomeration and owing to that, membrane performance decreases. According to UF and fouling experiments done in this study, membrane performance of 0-2wt. % $TiO_2$ embedded membranes show an incline unlike 2-5 wt. % $TiO_2$ entrapped membrane, which have a downward trend. Teli et al. tried to modify commercial titanium nanoparticles with polyaniline (PANI) to avoid particle agglomeration and thus, to enhance membrane anti-fouling properties.

You et al. reported that $TiO_2$-film photocatalyses followed by ultrafiltration process improves the removal of total organic carbon 47.13% and 49.94% for the case of 5 kDa and 10 kDa membranes, respectively. Permeate flux also increased about 23% for 6 hours operation with 10 kDa membranes.

Vatanpour et al. evaluated the effect of different size and types of nanoparticles on antifouling and performance for polyethersulfone nanofiltration membranes and they achieved that 20 nm particle sized titanium oxide (80% anatase, 20% rutile) entrapped membranes which contains 4wt.% nanoparticles, represents highest pure water flux, flux recovery ratio and have the best antifouling properties among plain and 8 nm and 15-25 nm particle sized $TiO_2$ embedded PES membranes. But before permeation tests, they activated antibiofuling properties of each membrane under UV light irradiation (160 W) for 15 minutes.

## 1.2. General Background

### 1.2.1. Historical Aspect

Although in 18th and 19th century some researches went on about membrane processes, the first patented microporous membranes produced in 1920's. Till 1950's membranes had been used in laboratory scale.

As membrane filtration started being used for sterilization of liquid pharmaceuticals and intravenous solutions in 1950's, the U.S. Public Health Service (U.S. PHS) framed membrane filtration to indicate bacteria in 1957. Followingly, membrane filtrations were used in food-processing industries for clarifying, concentrating, purifying, or sterilizing products like fruit juices, dairy products, vegetable oils. Membrane filtration also started to be used for industrial process and waste treatment, such as oily wastewater treatment, caustic acid, and brine recovery and treatment or recovery of diverse other industrial waste streams.

Because of the concern about microbiological contamination an interest to membrane filtration for potable water occurred in the 1980's. Unlike granular filtration, due to its indisputable advantages -such as its being attractive, highly automated, operationally simple- even small utilities began to consider membrane filtration.

The first membrane filtration plant was installed for potable water production in the United States was a 225-m3/d (0.06-mgd) plant at Keystone Resorts in Colorado in 1987 and a 250-m3/d (0.07-mgd) UF plant was built in France in 1988.

Till 1993 the use of membrane systems were still slow that is indicated being of only eight systems installed in U.S., which are considered small with the capacity lower than 3800 $m^3$/d. In 1993, passing through of *Cryptosporidium oocysts* in conventional water treatment plant caused over 400,000 illnesses and 50 deaths. After that incident a considerable need of membrane treatment occurred, since membrane filtration removes particles by straining which means complete protozoa is assured. Followingly, a rapid increase on installation of membrane filtration plants occurred with the capacity of 50 to 100 per cent per years. Since then interests in membrane filtration keeps on (Crittenden et al., 2012).

Nowadays, membrane technologies are playing a capital role for environmental quality control, resource recovery, pollution prevention, energy production, and environmental monitoring (Wiesner et al., 2007).

In recent years, inorganic nanometer sized particles has gained great popularity for the

modification of separation membrane. (Li Jin-Bo et al., 2006). Among them titania has remarkable attention because of its unique characteristics, such as high water flux, semi-conductivity, catalysis and their potential applications in photocatalytic membrane reactions (Ding et al., 2006).

### 1.2.2. Membrane Systems

Membranes can be categorize by following properties:

- Membrane pore size,
- Molecular weight cut-off (MWCO),
- Membrane material and geometry,
- Targeted materials to be removed,
- Type of water quality to be treated,
- Treated water quality (Mackenzie, 2010).

Also, membrane systems can be classified by driving force that makes processes work: pressure driven, electrically driven processes and others. Electrodialysis (ED) is an electrical voltage driven process and microfiltration (MF), ultrafiltration (UF), nanofiltration (NF) and reverse osmosis (RO) are pressure driven ones.

Electrodialysis is briefly an electrochemical membrane process driven by electric potential for removing ions from an aqueous stream. Feed water enters the bulk under a pressure of about 50 psi (340 kPa), ions are removed and less concentrated stream stays as product water (AWWA, 2005).

Microfiltration (MF) and ultrafiltration (UF) are pressure driven membrane processes, which use porous membranes to separate micrometer-sized and nanometer-sized particles, respectively. Other pressure driven membrane systems – nanofiltration (NF) and reverse osmosis (RO) – use less porous (dense) membranes for the separation of solutes such as macromolecules, nanoparticles and larger ions in terms of nanofiltration, of simple salts and very small organic compounds in terms of reverse osmosis (Wiesner et al., 2007).

Additional to those systems there are other membrane systems using driving force except pressure and electrical potential, such as dialysis, pervaporation, forward osmosis, membrane distillation and thermoosmosis. These techniques are driven by concentration gradient,

pressure gradient, osmosis, vapor pressure and temperature gradient, respectively (Crittenden et al., 2012).

Dialysis is defined as a membrane separation of two solutions but in different compositions. The concentration gradient across the membrane leads a flow of solute and solvent from one side of the membrane to the other. In the case of pervaporation, a liquid mixture comes toward one side of a membrane, and the permeate is removed as a vapor from the other with the help of low vapor pressure (Baker, 2004).

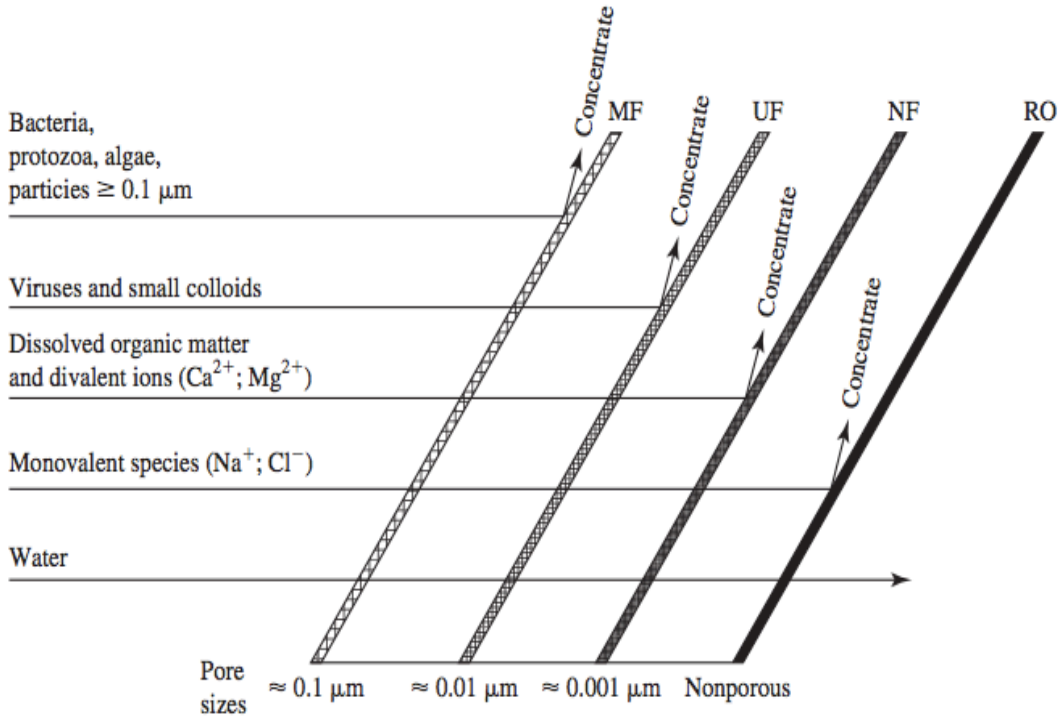


**Figure 1.2.** Hierarchical representation of pressure-driven membrane processes (Mackenzie, 2010)

For industrially operating membrane separations membranes should be effectively packaged so as to require low cost and small areas. Thus, membranes are designed in the form of modules.

### 1.2.2.1. Plate –and- frame Modules

Plate –and- frame modules are earliest form of membrane applications. Membrane feed-and-product spacers gathered together between two end plates. The feed mixture contacts the surface of the membrane. Permeate goes through the membrane, enters the permeate channel and then get collected. Those modules are relatively expensive among other alternatives. Nowadays, they have been used for only electrodialysis and pervaporation systems and limitedly for reverse osmosis and ultrafiltration systems. General representation of plate and frame modules can be seen on Figure 1.3**.**

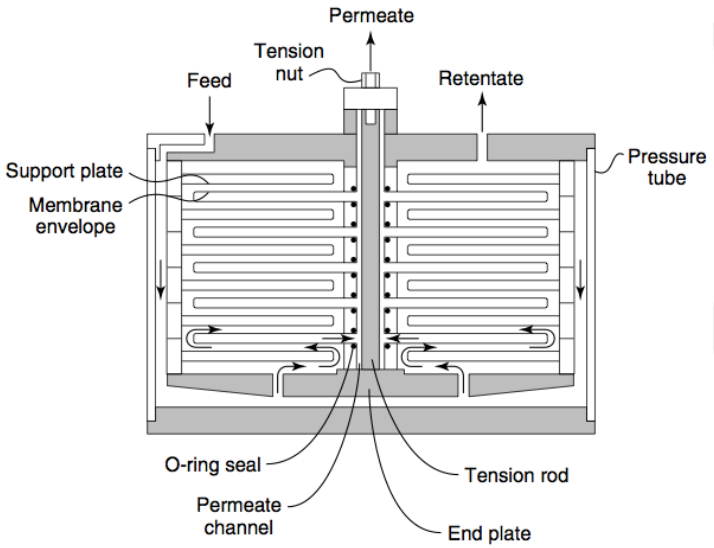


**Figure 1.3.** Schematic representation of Plate & Frame Modules

### 1.2.2.2. Tubular Modules

Owing to the resistance to membrane fouling tubular modules are now used for ultrafiltration systems. There is membrane inside of the tube and a support made of porous paper or fiberglass as well.

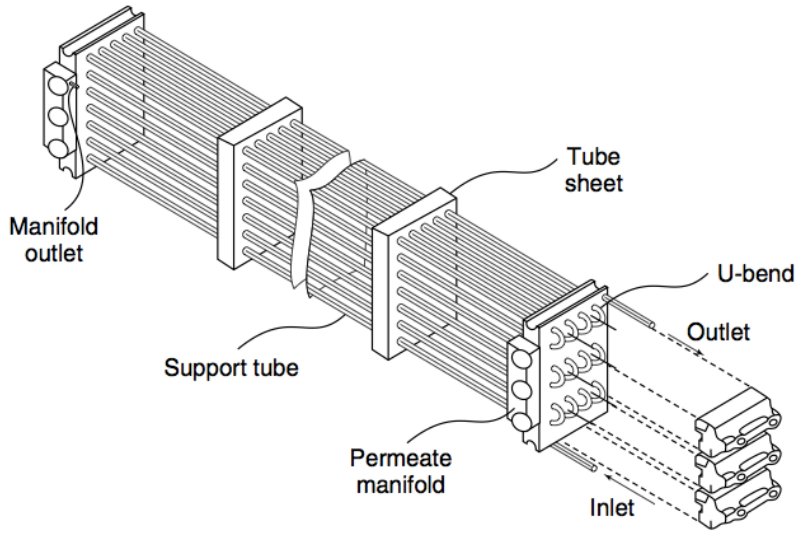


**Figure 1.4.** Illustration for 30-tube model system

In a typical tubular membrane system a large number of tubes are multiplied in series. Permeate is taken from each tube and transferred to a permeate collection header. An illustration for 30-tube module system can be seen on Figure 1.4.

### 1.2.2.3. Spiral Wound Modules

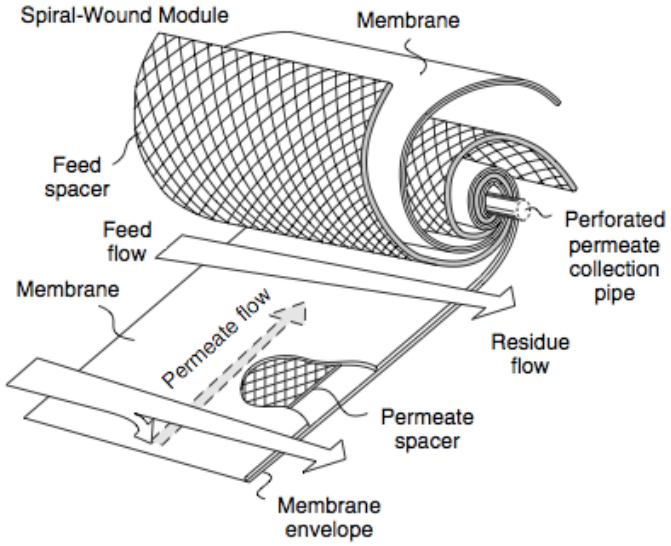


**Figure 1.5.** Representative figure for a spiral-wound module (Baker, 2004)

Flat-sheet membranes are grouped together in layers separated by permeate and retentate

spacers and these layers rolled around a central tube by this way the permeate follows a spiral flow path toward the central collection tube. It is extensively used in NF and RO membranes but not in widespread use for membrane filtration because of clogging of flow paths with particulate matter and troubles with backwashing efficiency (Crittenden et al., 2012).

#### 1.2.2.4. Hollow Fiber Modules

In this case of hollow fiber membrane modules membranes are cast in the shape of hollow tubes. While the water passes through the wall of fibers, filtration occurs. This geometry is so similar to tubular modules but tubular membranes have a much larger diameter (Wiesner et al., 2007).

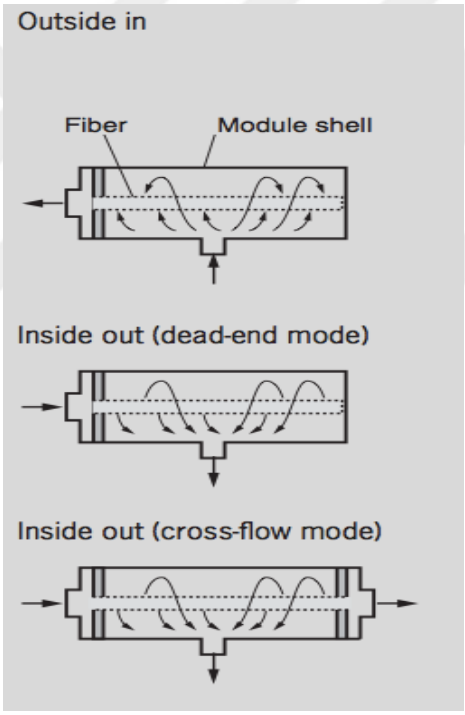


**Figure 1.6.** Drawing for hollow fiber modes

Hollow fiber modules are represented in two configurations: outside in and inside out. *Outside in* configuration basically can treat more water comparing to *inside out* at same flux due to its larger surface area and it is less susceptible to presence of large solids in feed water. However, *outside in* configuration cannot be operated in cross-flow mode. *Inside out* mode is also divided into two options: *Dead-end* and *cross-flow*. In dead-end filtration mode the feed water flow contacts in a vertical way to and toward the membrane surface. Therefore, during

dead-end filtration cycle, all solids accumulate on the membrane and can be removed with the help of backwash cycle. But in *cross-flow* filtration mode bulk water flows parallel to membrane surface and that leads a shear force that reduces the development of fouling. *Inside out dead-end* filtration system is cheaper than *cross flow mode.* Under the circumstances of *inside out (dead-end)* configuration large solids can cause clogging. Due to its surface area it can filtrate less water. *Inside out cross-flow mode* can be operated at higher flux with even high-turbidity bulk water because cross-flow velocity carries away solids. For this case, large particles can cause clogging and pumping costs can be expensive. Treatment capacity due to surface area is same with *inside out (dead-end)* mode (Crittenden et al., 2012).

### 1.2.2.5. Vibrating and Rotating Modules

In this kind of modules membranes can move faster than fluids toward membrane surface with the effect of vibration and rotation. On Figure 1.7 an example design is shown. These modules can be used for ultrafiltration of extremely viscous, concentrated solutions, however it is too expensive.

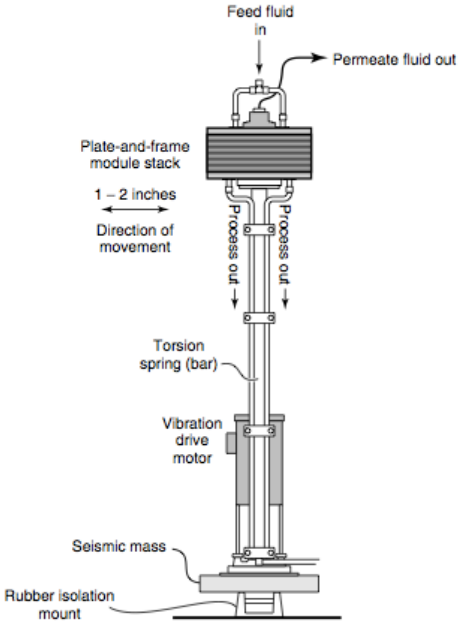


**Figure 1.7.** Vibrating plate –and- frame module design

#### 1.2.2.6. Flat sheet Membranes

Flat sheet membranes are cast in the shape of a sheet and used as a single layer or a batch of sheets. These kinds of membranes are generally operating in laboratory scale for MF, UF and NF processes. In this study fabricated and characterized ultrafiltration membranes are also flat sheet formed.

### 1.2.3. Membrane Fabrication Techniques

The choice of membrane fabrication techniques depends on the type of polymer and designed structure of membrane such as pore size, pore size distribution on surface layer, thickness because all of these properties have effects on membrane performance. Most common methods have been used for membrane fabrication are phase inversion, interfacial polymerization, stretching, track-etching and electrospinning which are described as it follows.

#### 1.2.3.1. Phase Inversion

Phase inversion method is defined as a process of transformation of initially homogenous solution into a solid form in an controlled environment. This transformation can show variety in terms of the type of solvent, non-solvent and the environment. The diversity explained in the following topics.

##### 1.2.3.1.1. Immersion Precipitation

Immersion precipitation is a phase inversion process where a polymer solution is cast on a convenient support (e.g. glass plate), after that immersed in a coagulation bath, which contains a non-solvent (e.g. water). Through an exchange of solvent and non-solvent solid polymeric film formation occurs in coagulation bath. The exchange of solvent and non-solvent keeps on for a while till the solution turns into the state of thermodynamically instable and the demixing occurs. Formed polymeric film usually has an asymmetric structure. Desired membrane's pore structure depends on the selection of solvents and non-solvents, precipitation time and bath temperature as well as the selection of polymer, additives and so on. Other important parameters, which build up the pore structure of membrane film during

immersion precipitation process are chemical nature of polymer and concentration of polymer.

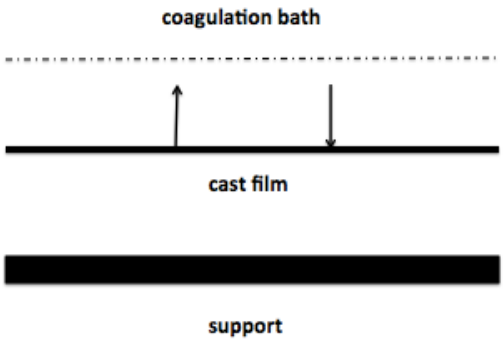


**Figure 1.8.** An illustration for immersion precipitation method

### 1.2.3.1.2. Evaporation-induced Phase Separation

The viscous polymer solution is prepared in a solvent (or in binary/ternary mixture of them) and a volatile non-solvent. Afterwards, prepared polymer solution is casted on a flat porous surface using a casting knife. The solvent could evaporate, with the help of precipitation or demixing/precipitation process a thin polymer film is formed. This technique is also known as a solution casting method. Desired membrane's morphology depends on the difference of using solvents' boiling points (Lalia et al., 2013).

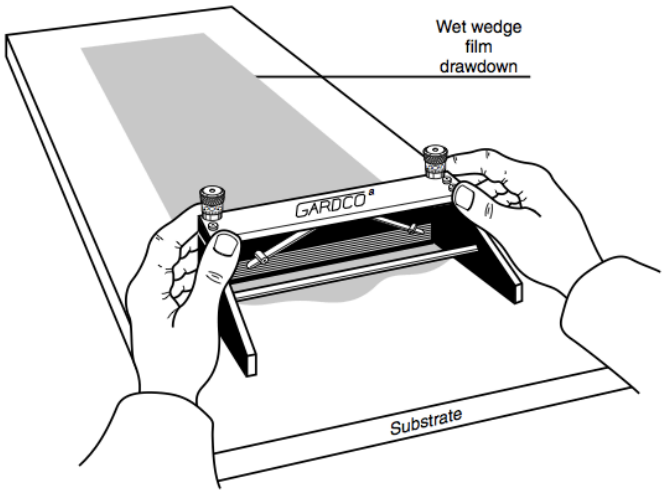


**Figure 1.8.** A hand-casting knife figure (Baker, 2004)

#### 1.2.3.1.3. Thermally Induced Phase Separation

Thermally induced phase separation method is basically about the phenomenon that the solvent quality usually decreases when the temperature is decreased. After demixing takes place, the solvent is removed by extraction, evaporation or freeze drying.

#### 1.2.3.1.4. Vapor-induced Phase Separation

The prepared polymer solution is exposed to an environment, which contains a non-solvent (e.g. water) where absorption of non-solvent causes demixing/precipitation.

### 1.2.3.2. Interfacial Polymerization

Interfacial polymerization (IP) is reported as the most important method for industrial scale of fabrication of thin-film composite (TFC) reverse osmosis and nanofiltration membranes (Lalia et al., 2013). In this method, an aqueous solution of a reactive prepolymer (e.g. polyamine), is first loaded in the pores of a microporous support membrane, such as a polysulfone ultrafiltration membrane. The polyamine deposited microporous support is then immersed in a solvent solution, which cannot be mixed with water containing a reactant, for instance diacid chloride in hexane. The polyamine and acid chloride react at the interface of the two immiscible solutions to form a membrane layer, which is densely cross-linked and reasonably thin (Baker, 2004).

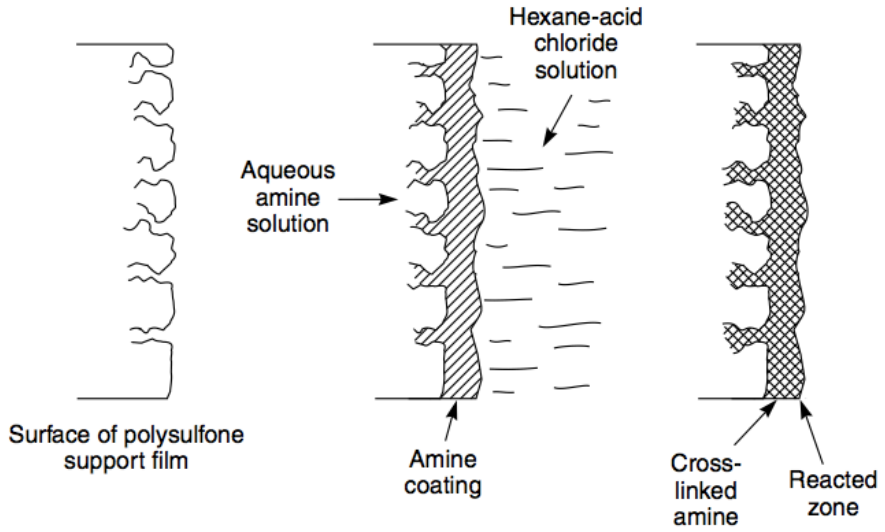


**Figure 1.9.** Interfacial Polymerization Process

### 1.2.3.3. Stretching

Stretching is a method, which proceeds under solvent free conditions. The polymer is heated above the melting point, compressed into thin sheet shape and after that, stretched to give a porous shape. It is assumed that material's physical properties, such as crystallinity, melting point, tensile strength etc. and the applied processing parameters have an important effect on the final porous structure and properties of the membranes.

### 1.2.3.4. Track-etching

In track-etching technique a nonporous polymeric film is exposed to irradiation with fission particles that causes to formation of linear damaged tracks through breaking polymer chains. These tracks behave like excited molecules. The exposure time of irradiation determines the number of membrane pore and the etch time specifies the pore diameter. This method is important because it provides to precise control on the pore size distribution.

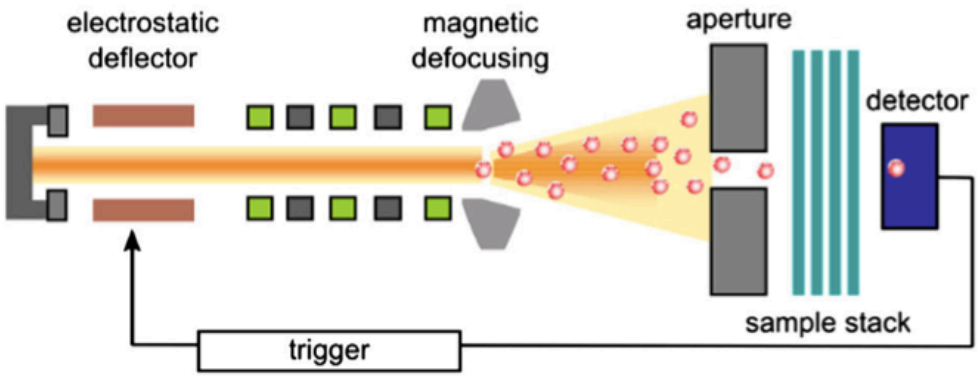


**Figure 1.10.** Schematic illustration of track-etched membrane setup

### 1.2.3.5. Electrospinning

Electrospinning technique is comparatively new one of fabrication methods. High electrical voltage is applied polymer solution droplet and grounded collector. When the voltage is high enough, it overcomes the surface tension of polymer droplets and fibrous membranes occur. Owing to the controllable production on the fiber size, shape and morphology of electrospun fibrous membranes have been used for filtration and membrane distillation processes (Lalia et al., 2013).

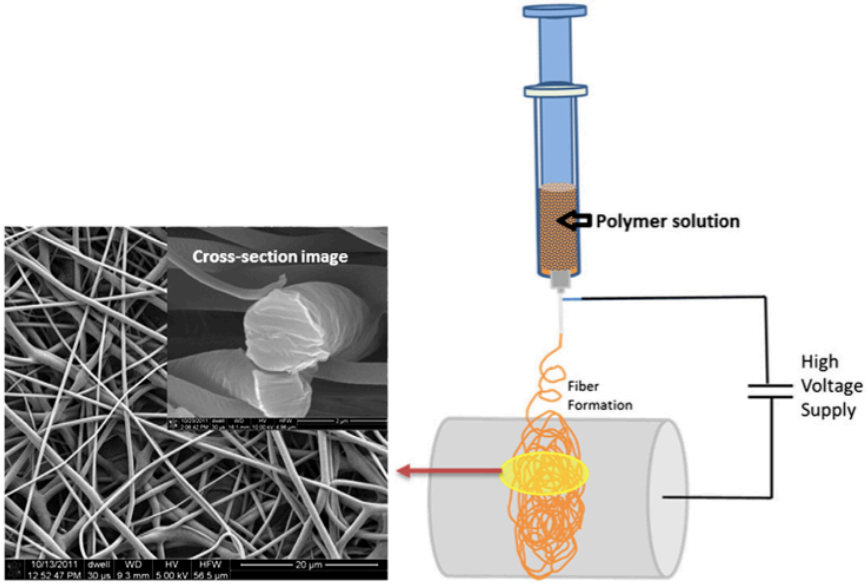


**Figure 1.11.** Electrospinning of polymer solution

### 1.2.4. Characteristics of Common Membrane Materials

According to Crittenden et al. ideal membrane material should produce a high flux and should not be clogged or fouled at the same time. It also should be chemically stable and resistant, physically durable, inexpensive and nonbiodegradable.

Because of the lacking the existence of ideal membrane material there is a variety among the materials and properties they have.

Cellulose acetate (CA) is known as the most hydrophilic commercial membrane material. Because of the hydrophilicity, it provides high flux through minimizing fouling and clogging. CA is easy to manufacture, inexpensive and exists in a wide range of pore sizes. Biodegradability of CA deports it from being ideal, because it is intolerant to continuous exposure or high concentrations of free chlorine and to aggressive cleaning agents or temperatures above 30$^{\circ}$C.

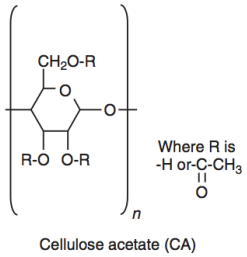


**Figure 1.12.** Cellulose acetate molecule

Polyvinylidene fluoride (PVDF) is described as hydrophobic to some extent, perfectly durable, chemically tolerant and biologically resistant. It can endure to continuous free chlorine contact to any concentration, pH values between 2 and 10, and temperatures to 75°C, which makes aggressive cleaning and disinfecting possible.


**Figure 1.13.** PVDF and PP molecules

Polypropylene (PP) has the highest hydrophobicity among common commercial membrane materials. Since it is too hydrophobic to allow water pass through the membrane in UF processes, it is only available for MF membranes. It is chemically and biologically resistant, durable and it tolerates high temperatures to some degree and pH values between 1-13, where it is possible to clean aggressively. Intolerance to chlorine deports it from being ideal, because biological growth cannot be controlled any more.

Ceramic membranes are designed as rigid monolithic elements, reported Crittenden et al.. Ceramic is hydrophilic, rough and can endure high temperatures and pressure and also it has perfect chemical and pH tolerance, which makes aggressive cleaning and disinfecting possible.

Polysulfone (PSf) and polyethersulfone (PES) are the most common polymeric materials currently used in water treatment, beside PVDF. They are partly hydrophobic and very tolerant to chemicals and resistant to biologic exposure. They can endure free chlorine contact to 200 mg/L for short periods of time for cleaning. Aggressive cleaning and disinfecting is possible, because they are resistant to pH values between 1 and 13 and temperatures to 75°C. For this study polysulfone is chosen as main polymer for membrane solution.

### 1.2.5. Mechanisms of Filtration

There are three filtration mechanism described in literature as shown in Figure 1.14 and explained as following:

- **Straining**

Straining as known as sieving and steric exclusion is the main filtration mechanism in membrane filtration. In the case of straining, particles are physically rejected because they are larger than the pore size of membrane, but water and smaller particles pass through the membrane. When the particle size is close to membrane retention rating, which is a declaration of materials retained, when pore size of dimensions varies, shape of the particles are nonspherical or an interaction such as electrostatic repulsion exists, a nonideal performance occurs that cause straining.

- **Adsorption**

Adsorption occurs when materials filtrating are small enough to enter pores and then adsorb to the walls of the pores of membrane. In the early stages of filtration with a clean membrane adsorption may be an important mechanism for removing soluble and insoluble materials, which have dimensions much smaller than the membrane pore size. Since the adsorption capacity becomes quickly exhausted, the adsorbed material can narrow the pores and hereby increase the ability of the membrane to retain particles smaller than the nominal pore size (Mackenzie, 2010).

- **Cake Formation**

Cake filtration takes place when particles that are small enough to pass through the membrane

but they are already retained by a cake of larger particles, which accumulates on or near the membrane surface. This cake layer acts as a filtration medium leads to another mechanism for rejection. The cake layer acts as a ‘‘dynamic’’ filter and can retain additional smaller material, but also generates hydraulic resistance to flow as it does so. The cake layer can prevent particles smaller than the retention rating from reaching the membrane, improving filtration effectiveness and probably minimizing fouling from pore constriction. During backwashes cake layer can be removed partially or wholly (Crittenden et al., 2012).

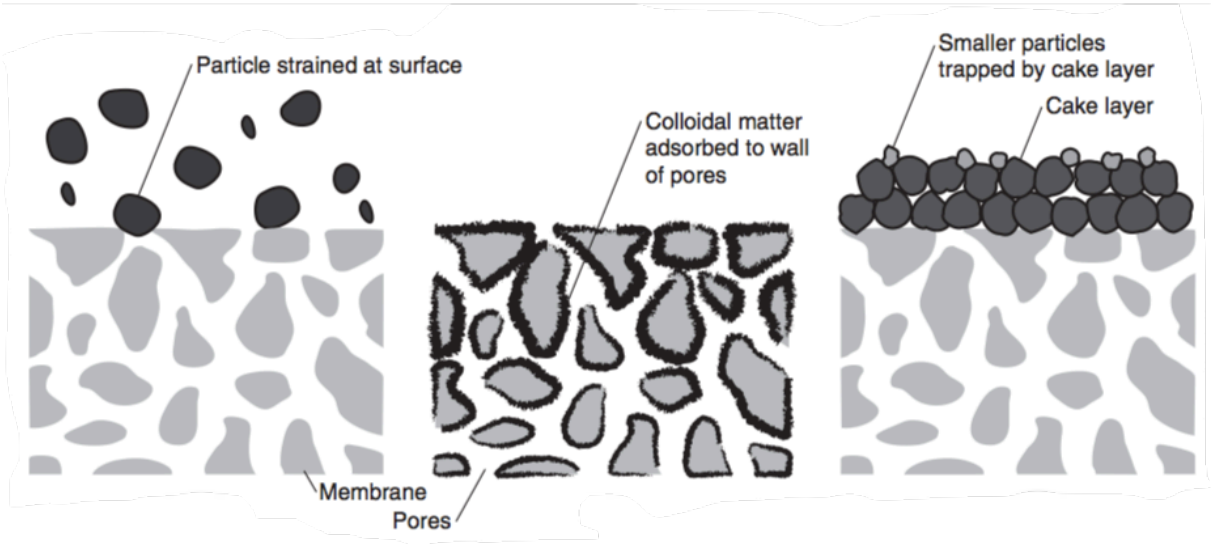


**Figure 1.14.** Mechanisms of filtration: straining, adsorption and cake formation, respectively.

### 1.2.6. Properties of Titania

Titanium is the one of the most widely found metal on the earth. It was discovered in 1791 in England by Reverend William Gregor. Titanium metal is not found unbound to other elements and that are present in various rocks and sediments. Its most common compound titanium dioxide ($TiO_2$) is one of the members of to the family of transition metal oxides. In the beginning of the 20th century, industrial production of $TiO_2$ was started with the use of it as pigment for white paint. Presently, the annual production of $TiO_2$ exceeds 4 million tons. 31% of total production of $TiO_2$ is used as white pigment in paints, plastic, cosmetic and paper industries. The rest can be assorted in the various possible applications (Natarajan et al., 1998). For instance, because of its high refractive index, it is used as anti-reflection coating in thin-film optical device (Macleod, 1999). Owing to its biocompatibility with the human body,

$TiO_2$ appears as a biomaterial in biological or biomedical applications, such as fabrication of vital heart tissue (Polunchеck et al., 2000). It is also applied in solar cells for the production hydrogen and electric energy.

The photo-induced phenomena of $TiO_2$ were unwound case till avant-garde research of Fujishima and Honda in the early 1970's. They evaluated the possibility of water splitting by $TiO_2$ photoelectrochemical cell and then the application of $TiO_2$ photocatalysis extended to environmental frontiers. In 1977, Frank and Bard for the first time, pointed out the photocatalytic application of $TiO_2$ for oxidation of $CN^-$ and $SO_3^{2-}$ in aqueous medium under solar light irradiation (Frank et al., 1977). Later on, numerous researches have been done on decomposition of different pollutants utilizing photo-assisted $TiO_2$ systems, on account of stable chemical-physical property, non-toxicity, low cost, innocuity and high photoactive nature of $TiO_2$.

In membrane technology nanoparticles have gained a tremendous popularity since they contribute mechanical strength with CNT (Wiesner et al., 2007), antibacterial properties with silver and copper, high membrane permeability and low fouling with $Al_2O_3$ and $ZrO_2$, improved antifouling property with silica…etc.. (Zhao et al., 2013). Among them titania has much considerable interest because of its previously mentioned properties.

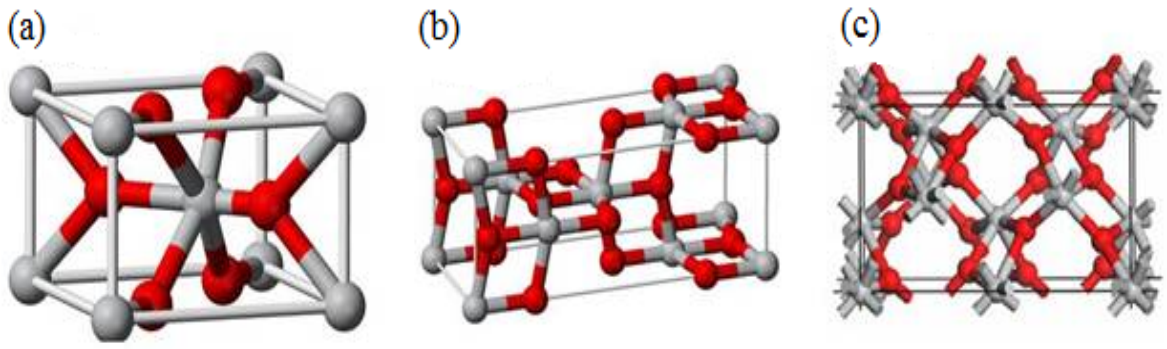


**Figure 1.15.** Crystal structures of rutile (a), anatase (b) and brookite (c) $TiO_2$

UVA irradiation (400-315 nm) is absorbed by TiO2 that catalyzes the generation of reactive oxygen species, such as superoxide anion radicals, hydrogen peroxide, free hydroxyl radicals, and singlet oxygen in aqueous media. Those hydroxyl radicals are initiators for oxidation process **(**Monteiro-Riviere and Orsiere**,** 2007). In addition to that anatase crystalline form of

$TiO_2$ is assumed more photoactive because of the difference between their band gap.

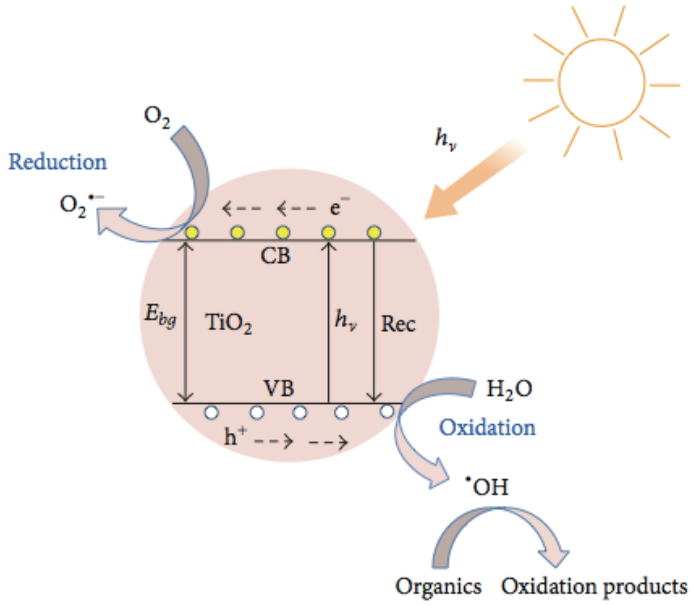


**Figure 1.16.** General Mechanism for of $TiO_2$ under UV light exposure

$$TiO_2 \rightarrow e^- + h^+$$

$$h^+ + H_2O \rightarrow \cdot OH + H^+$$

$$h^+ + OH^- \rightarrow \cdot OH$$

$$e^- + O_2 \rightarrow \cdot O^-$$

In general solar photocatalysis process, the electrons ($e^-$) on the photocatalyst surface can be excited from valence band to conduction band by photons which are provided by energy larger than its band gap under solar light irradiation, that forms $e^-$ on conduction and holes ($h^+$) on valence band. The photogenerated electrons and holes participate in redox reactions with adsorbed species on photocatalyst surface and than they turn into superoxide radical anion ($\cdot O^-$) and hydroxyl radical ($\cdot OH$), respectively. The photogenerated reactive oxygen species are very strong oxidizers and play the dominant roles in the degradation of organic

pollutants in water. The organics in water can be completely degraded to $CO_2$ and $H_2O$, therefore there is no secondary pollution (Zhang et al., 2014).

#### 1.2.6.1. Short Overview on Environmental Impacts of Titania Nanoparticles

In this study consideration of environmental impacts of nanomaterial used is one of motivation factors we have carried. Photocatalytic degradation ability on organic pollutants of titania was an encouragement, besides that, the investigation of release characteristics titania embedded membranes have, was an inspiration because of its reported toxicological properties.

European Union described nanomaterials, which are natural, random or manufactured material containing unbound, aggregate or agglomerate stated particles; where 50% or more of the particles exhibited, one or more external dimensions are in the size range of 1–100 nm. Others have defined NPs as matter with at least one of their three dimensions in the range of 1–100 nm (Shi et al., 2013).

Titanium dioxide particles ($TiO_2$), which are larger than 100 nm, are generally defined as to be biologically inert to both humans and animals. Several studies have shown that the cytotoxicity of nano-sized $TiO_2$ was very low or negligible as compared with other nanoparticles, but size cannot be the only predictor of cytotoxicity. Titanium dioxide has inflammatory effects on human endothelial cells.

As $TiO_2$ reflects and scatters UVB and UVA in sunlight, nano-sized $TiO_2$ is used in numerous sunscreens. However, it has been noted that photogenerated $TiO_2$ causes DNA damage both in vitro and in human cells. $TiO_2$ nanoparticles have been shown to be photogenotoxic, but according to Wiesner M. (2007) there is insufficient information on the genotoxic properties of unirradiated $TiO_2$ nanoparticles. In the absence of photoactivation, nanoscale $TiO_2$ (10 and 20 nm) in the anatase form can increase lipid peroxidation and oxidative DNA damage, but particles larger than 200 nm do not have same effect. The size of the particles and the crystalline form are extremely important factors as 200 nm rutile size particles can increase oxidative DNA damage. Besides, levels of major end-product of lipid peroxidation, are increased under 10 and 20 nm anatase $TiO_2$ treatments but not with >200 nm anatase or 200 nm rutile treatments. These results indicated that nanoscale anatase could encourage oxidative

damage to lipids and DNA.

Finally, cell treatments with anatase $TiO_2$ nanoparticles showed an increase in nitric oxide levels and hydrogen peroxide that predictably leads to chromosomal damage. These results are strongly related to the size of the particles, the smaller particles being the more destructive. Therefore, the anatase form of titania could increase reactive oxygen species and chromosome damage *in vitro* in the absence of UV photoactivation.

Titanium dioxide in the form of anatase and rutile accelerates solar disinfection of Escherichia coli as an effect of photocatalytic activity and reactive oxygen species (Rincon et al., 2004). Also, titania coated surfaces oxidize E. coli and Micrococcus luteus with the help of photocatalysis (Maness et al., 1999).

# 2.MATERIALS AND METHODS

## 2.1. Chemicals

Polysulfone polymer (PSf, Mw 35000 g/mol), polyvinylpyrolidone polymer (PVP, Mw 40000 g/mol) and alginic acid sodium powder were obtained from Sigma Aldrich. N-Methyl-2-pyrrolidone (NMP, purity 99.5%), sodium hydroxide pellets, hydrochloric acid (HCl, 37%) were obtained from Merck. Titanium dioxide ($TiO_2$) nano powder (particle size ~40 nm) was provided by Inframat Advanced Materials. All chemicals were used as received. Sodium hypochloride (NaOCl) solution was prepared from commercial bleach solution, which has NaOCl component less than 4%. Polyethylene glycol (PEG, Mw 35,000 Da) purchased from Fluka, Analytical.

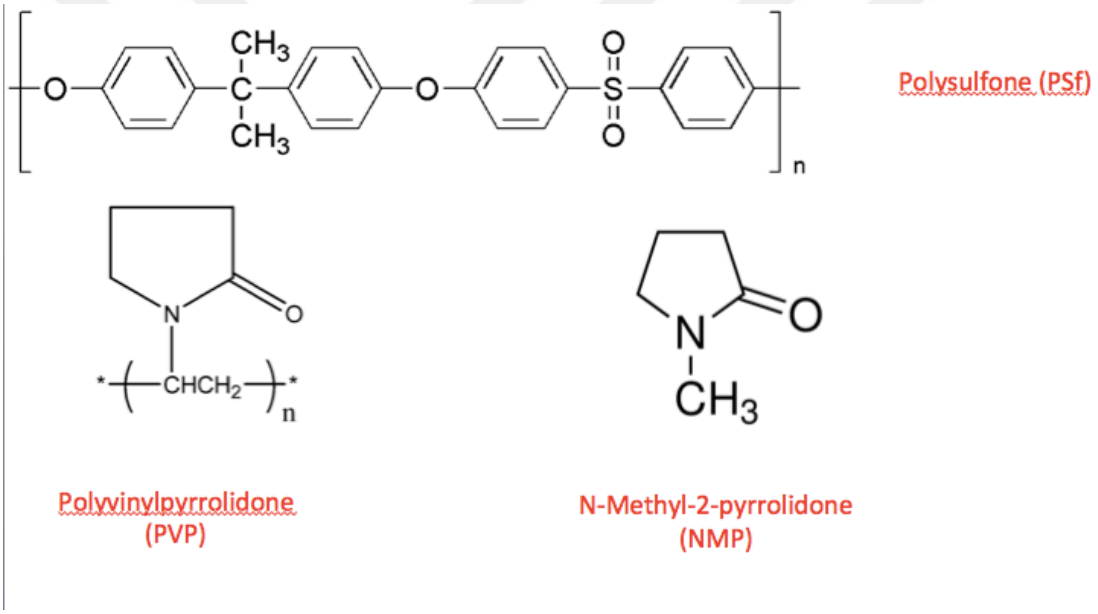


**Figure 2.1.** Molecular Structure of PSf, PVP and NMP

## 2.2. Materials

### 2.2.1. Bandelin Sonopuls Ultrasonic Homogenizer ( Sonopuls HD3220)

Equipments ultrasonic homogenizer has mentioned below:

*High-frequency generator:* Low-frequency voltage of 50 Hz is transformed into high-frequency voltage of 20 kHz by HF generator.

*Ultrasonic converter:* It turns the electrical energy delivered from the generator into mechanical vibrations of 20 kHz.

*Standard and booster horns:* Horns increase the amplitude because of their uniqe shape. The external thread is designed for close connection of vessels.

*Probes:* It sends the ultrasonic energy into the sample. Microtips, tapered and flattips dia. 2, 3, 6, 13, 19 and 25 mm for use in different volumes. For our experimental studies flattips with 13 mm dia. had been used.

*Cooling vessels:* They are using for temperature-sensitive samples. The cooling jacket provides the circulation of cool liquid (generally water) around the sample during sonication.

*Soundproof boxes:* They are used to guard the environment from ultrasonic sound level. The inner walls of the boxes were coated plastics.

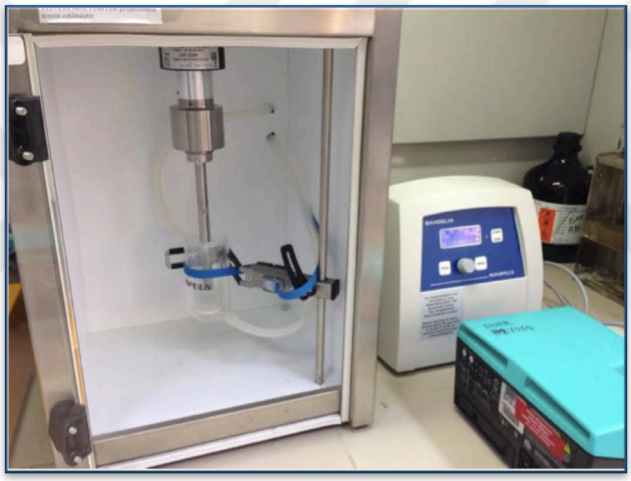

**Figure 2.2.** Ultrasonication Homogenizer

### 2.2.2. Magnetic Stirrer with Heater

Heidolph MR Hei-Standard magnetic stirrer with heater was used for the purpose of dissolving membrane polymers in a solvent at a constant temperature and stirring rate.


**Figure 2.3.** Heidolph MR Hei-Standard magnetic stirrer with heater

### 2.2.3. Stainless Steel Casting Knife

Stainless steel casting knife (Figure 2.4.) was used to cast the membrane solution by hand on a glass plate. It has three parts on it. Two of them are attached by screws on the main part to limit the frame and thickness that future membrane will have.

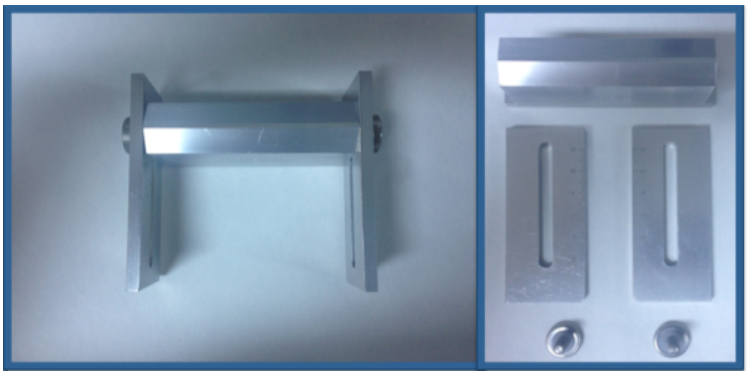

**Figure 2.4.** Stainless steel casting knife

### 2.2.4. Sterlitech™ HP4750 Stirred Cell

A dead-end filtration cell was used for ultrafiltration experiments (Figure 2.5.).The cell is made of stainless steel and has 49 mm inner diameter, which makes the active membrane area 14.6 cm². Inner volume of the cell is 300 mL. Maximum pressure is 69 bar and ultrafiltration cell can work temperatures up to 120 °C.

**Figure 2.5.** Sterlitech™ HP4750 Stirred Cell

Equipments:

- Stainless steel cell body
- Cell top
- Cell bottom
- Cell top coupling
- Cell bottom coupling
- Porous stainless steel membrane support disk
- Two o-rings
- Top gasket
- Permeate tube
- Stir bar assembly

- Stir bar retriever

### 2.2.5. Pressure Tank

Pressure tank was used as a water supply storage (Figure 2.6.). It is made of stainless steel and its volume is about 4L. Pressure tank was used for long term ultrafiltration and fouling tests because stirred cell's volume (300 mL) was inadequate alone.

**Figure 2.6.** Pressure tank

### 2.2.6. GFL Shaking Incubator 3031

Shaking incubator was used for the release experiments of $TiO_2$-NP from membrane by the existence of cleaning agents. Shaking incubator is used for applications requiring exactly reproducible orbital motions and temperatures up to +70 °C. It is microprocessor-controlled, PID type and has RS 232 serial interface. Temperature, time and shaking frequency can be controlled both on the device menu or PC. It has a shaking frequency up to 250 rpm.

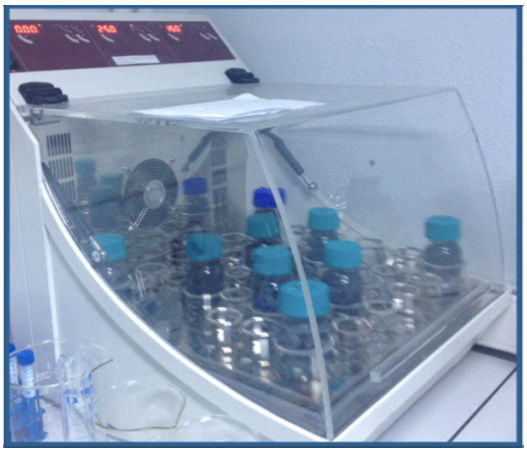

**Figure 2.7.** Shaking Incubator

### 2.2.7. Scanning Electron Microscope (SEM)

Jeol JSM-5910LV scanning electron microscope (Figure 2.8.) was used for the morphology analyses of membrane produced. It has accelerating voltage 0.3 to 30 kV, magnification up to 300.000. It's resolution is 3.0 nm at 30 kV. SEM has secondary electron and backscattered electron imaging. The specimens were attached by carbon tape on a steel stub to be covered with golden and palladium to provide electrical conductivity.

**Figure 2.8.** Scanning Electron Microscope (SEM)

### 2.2.8. Inductively Coupled Plasma- Mass Spectroscopy (ICP-MS)

The Agilent 7500ce ICP-MS is an instrument, which is specifically designed and optimized for the analysis of trace metals in high matrix samples including environmental, clinical, geological, and other. Titanium release analyses investigated by ICP-MS.

### 2.3. Preparation of Membrane Casting Solutions

All plain membrane formulations mentioned on Table 2.2. are tested and 15% PVP and 18% PSf composition is chosen to proceed.

**Table 2.1.** Plain membrane formulations with changing PVP ratio

| | **PSf** | **NMP** |
|---|---|---|
| **0.0% PVP** | 18 % | 82 % |
| **2.0 % PVP** | 18 % | 80 % |
| **5.0 % PVP** | 18 % | 77 % |
| **7.5 % PVP** | 18 % | 74.5 % |
| **10 % PVP** | 18 % | 72 % |
| **12.5 % PVP** | 18 % | 69.5 % |
| **15 % PVP** | 18 % | 67 % |

**Table 2.2.** Compositions of membrane casting solutions

| **Component** | **0.0%$TiO_2$** | **0.5%$TiO_2$** | **2%$TiO_2$** | **4%$TiO_2$** |
|---|---|---|---|---|
| PSf | 18% | 18% | 18% | 18% |
| PVP | 15% | 15% | 15% | 15% |
| NMP | 67% | 66.5% | 65% | 63% |
| $TiO_2$ | 0.0% | 0.5% | 2% | 4% |

#### 2.3.1. Preparation of 0.0% $TiO_2$ Membrane Casting Solution

0.0%TiO2 containing membrane solution was composed of two polymer compounds and one solvent: polysulfone (PSf), polyvinylpyrrolidone (PVP) and N-Methyl-2-pyrrolidone (NMP). Polysulfone is the main polymer compound. Since PSf has very high hydrophobic character, PVP was added to the solution to reduce hydrophobicity of the solution.

According to the concentrations by weight of all components were given on Table 2.2 quantities calculated for 50 grams of solution are below:

- 9 grams of polysulfone
- 7.5 grams of polyvinylpyrrolidone
- 33.5 grams of N-Methyl-2-pyrrolidone

Since NMP is a liquid component under room temperature and pressure, the amount of NMP was used was calculated below:

$$\rho NMP = 1.03\ \frac{g}{mL}$$

$$The\ amount\ of\ solvent = \frac{grams\ of\ solvent}{density\ of\ solvent} = \frac{33.5\ g}{1.03\ \frac{g}{mL}} = 32.52\ mL$$

At the beginning of membrane casting solution preparation procedure PVP was weighed and added into the flask with the existence of magnetic fish. The flask was positioned on the magnetic stirrer. Calculated volume of NMP was transferred to the flask containing calculated mass of PVP with the help of automatic pipette. After that calculated mass of PSf was added to the mixture of NMP and PVP. The final blend was allowed to stir overnight (approximately 15 hours) at 50 °C and 250 rpm until the solution was homogenized. If the homogenization of the solution did not happen properly, stirring was kept on.

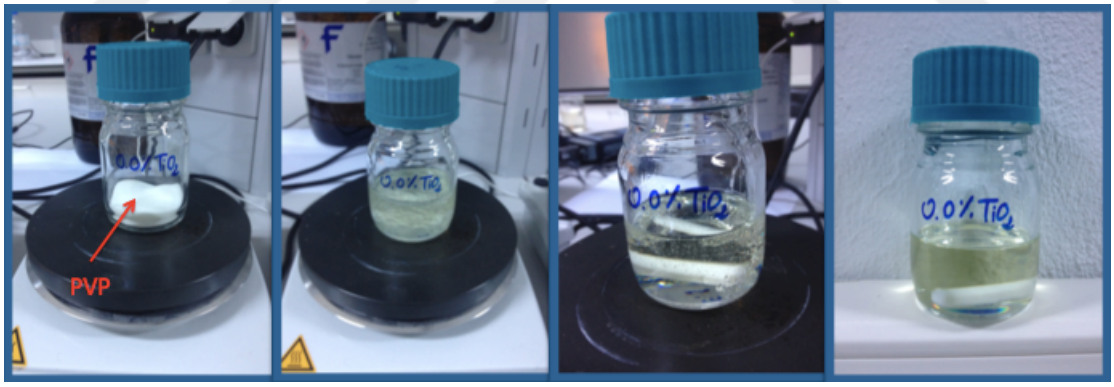


**Figure 2.9.** Homogenization of casting solution step by step

After the completion of the homogenization of membrane solution, the flask was removed from magnetic stirrer and allowed to wait at least 1 hour for the removal of possible air bubbles in solution. Otherwise, air bubbles can cause flaws on membrane sheets during fabrication.

### 2.3.2. Preparation of 0.5% $TiO_2$, 2% $TiO_2$ and 4% $TiO_2$ Membrane Casting Solution

The concentrations by weight of components of 0.5% $TiO_2$ embedded membranes:

- Polysulfone (PSf), 18%
- Polyvinylpyrrolidone (PVP), 15%
- N-Methyl-2-pyrrolidone (NMP), 66.5
- Titanium dioxide nanoparticles ($TiO_2$ ), 0.5%

Quantities required for 50 grams of solution:

- 9 grams of polysulfone (PSf)
- 7.5 grams of polyvinylpyrrolidone (PVP)
- 33.25 grams (32.28 mL) of N-Methyl-2-pyrrolidone (NMP)
- 0.25 gram of titanium dioxide nanoparticles ($TiO_2$ )

The volume of NMP that is required calculated below:

$$The\ amount\ of\ solvent = \frac{grams\ of\ solvent}{density\ of\ solvent} = \frac{33.25\ g}{1.03\frac{g}{mL}} = 32.28\ mL$$

The concentrations by weight of components of 2% TiO2 embedded membranes:

- Polysulfone (PSf), 18%
- Polyvinylpyrrolidone (PVP), 15%
- N-Methyl-2-pyrrolidone (NMP), 65%
- Titanium dioxide nanoparticles ($TiO_2$ ), 2%

Quantities required for 50 grams of solution:

- 9 grams of polysulfone (PSf)
- 7.5 grams of polyvinylpyrrolidone (PVP)
- 32.5 grams (31.55 mL) of N-Methyl-2-pyrrolidone (NMP)
- 1 gram of titanium dioxide nanoparticles ($TiO_2$ )

The volume of NMP that is required calculated below:

$$The\ amount\ of\ solvent = \frac{grams\ of\ solvent}{density\ of\ solvent} = \frac{32.5\ g}{1.03\frac{g}{mL}} = 31.55\ mL$$

The concentrations by weight of components of 2% $TiO_2$ embedded membranes:

- Polysulfone (PSf), 18%
- Polyvinylpyrrolidone (PVP), 15%
- N-Methyl-2-pyrrolidone (NMP), 63%
- Titanium dioxide nanoparticles ($TiO_2$ ), 4%

Quantities required for 50 grams of solution:

- 9 grams of polysulfone (PSf)
- 7.5 grams of polyvinylpyrrolidone (PVP)
- 31.5 grams (30.58 mL) of N-Methyl-2-pyrrolidone (NMP)
- 2 grams of titanium dioxide nanoparticles ($TiO_2$)

The volume of NMP that is required calculated below:

$$The\ amount\ of\ solvent = \frac{grams\ of\ solvent}{density\ of\ solvent} = \frac{31.5\ g}{1.03\frac{g}{mL}} = 30.58\ mL$$

The preparation of titanium dioxide nanoparticles embedded membranes have almost same procedure as in the case of plain membrane which is written above, but only one additional step differs: Dispersion of nanoparticles.

To start less than calculated volume of NMP (25 mL) and required amount of $TiO_2$ nanoparticles transferred into cooling vessel, which is one of the equipment ultrasonic homogenizer has. For ultrasonication step the sample placed in soundproof box and the probe (TT13) was immersed into the $TiO_2$ – NMP sample we prepared. Ultrasonic homogenizer was run until $TiO_2$ nanoparticles became dispersed in the solvent, which is limited by 15 minutes for this study. PVP was weighed and added into the flask with the existence of magnetic fish. The flask was positioned on the magnetic stirrer. Ultrasonicated $TiO_2$ – NMP blend was transferred with the help of pipette into the weighed PVP. Before that magnetic stirrer was already run. The remaining volume of required NMP was used for the wash of residuals in cooling vessel, which must be taken or for draining on inner wall of flask. After that calculated mass of PSf pellets were added to the mixture of NMP, PVP and $TiO_2$ . The final

blend was allowed to stir overnight (approximately 15 hours) at 50 °C and 250 rpm until the casting solution was uniformed and homogenized. If the homogenization of the solution did not happen properly, stirring was kept on.

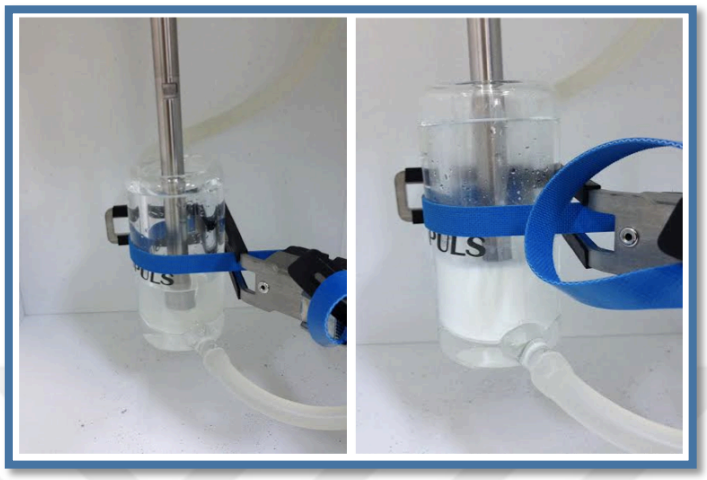

**Figure 2.10.** Ultrasonication of $TiO_2$ Nanoparticles

After the completion of the homogenization of membrane solution, the flask was removed from magnetic stirrer and allowed to wait almost 1 hour for the removal of air bubbles.

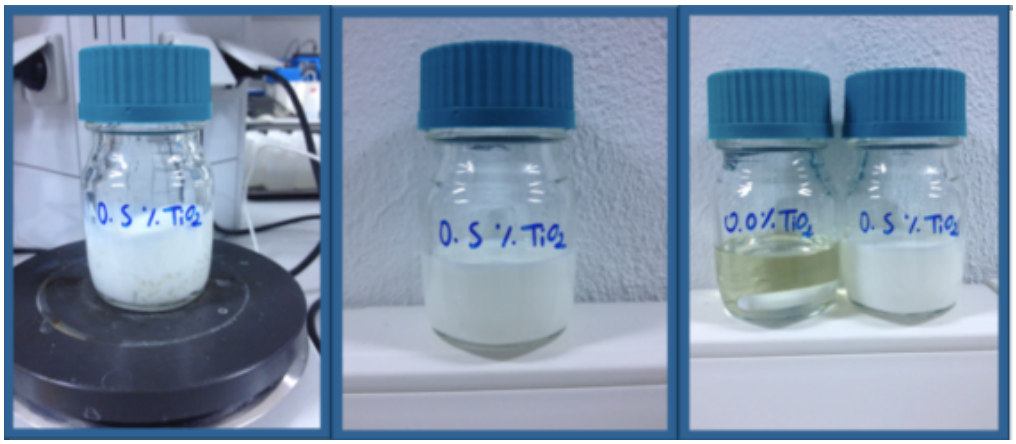


**Figure 2.11.** Representative figure of homogenization of 0.5% $TiO_2$ embedded membrane casting solution

### 2.4. Fabrication of Membranes

Membranes (plain and nanoparticle embedded) prepared in this study are fabricated using the immersion precipitation method, which is demonstrated before.

Stainless steel casting knife was used to homogenously flatten the membrane solutions. The casting knife was placed on a clean, smooth glass plate. Already prepared membrane solution was poured gently in front of the main part of the casting knife. In very few seconds the knife was pulled under possible constant speed and force in direction where membrane solution poured and thin membrane film was formed. After that, the glass plate was taken under constant speed into de-ionized water bath, which is also called coagulation bath. A few seconds after immersion membrane sheet formed because it started to leave glass plate. During the formation process of membrane sheets the color changes from transparent to white. Fabricated membrane sheets preserved in water bath at +4 °C.

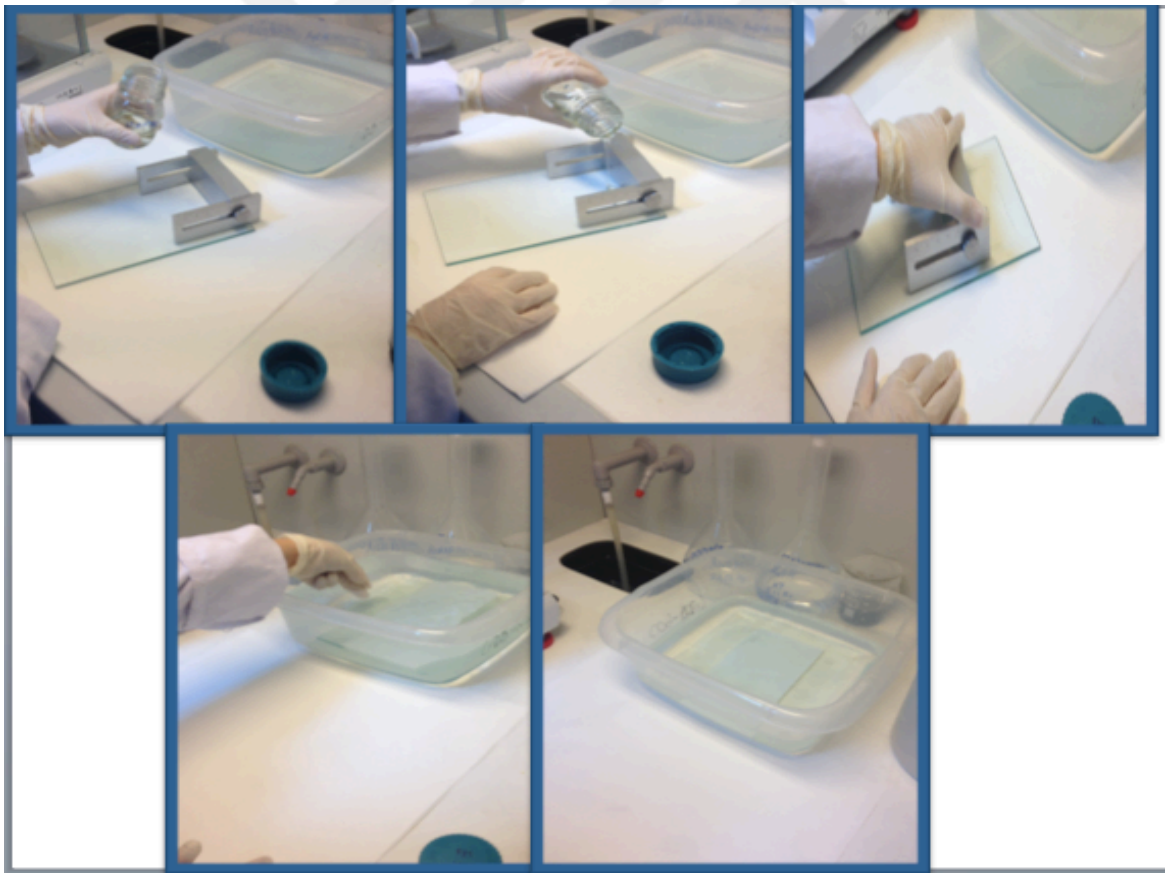

**Figure 2.12.** Casting of thin film membrane on a glass plate

## 2.5. Characterization of Membranes

Plain and nanoparticle embedded membranes that were fabricated in this study were characterized by permeation experiments, morphology analyses and their release behavior. Membrane performances were evaluated by their flux, fouling and rejection rates, and equilibrium water content. Surface and cross section morphologies investigated by scanning electron microscopy ( SEM- Jeol JSM-5910LV). Titanium release analyses carried out by ICP-MS (Agilent 7500ce).

### 2.5.1. Preparation of Membrane Coupons

Membrane coupons were cut from flat membrane sheets in a specific circular shape having 49 mm and 38 mm diameter. The coupons having 49 mm diameter were used for experiments carried out with dead-end filtration cell. For titanium release studies followed out with the help of coupons having 38 mm diameter.

### 2.5.2. Flux

Flux is defined as volumetric flow rate per unit of membrane area.

$$J = \frac{Q}{a} = \frac{\Delta P}{\mu K m}$$

J= volumetric water flux through membrane, L/m². h or m/s

Q= flow rate, L/h

a= membrane area, m²

$\Delta P$ = differential pressure across membrane, bar

$\mu$= dynamic viscosity of water, kg/ m.s

Km= membrane resistance coefficient, $m^{-1}$

To explain the relationship shown on the equation flux can be maximized by operating at the highest possible transmembrane pressure. This expression may be true for the case of deionized water, high pressure operation may not be preferable during filtration of raw water. Fouling can be intensified by high-pressure operation, which requires a balance between fouling and flux. Additionally, membrane flux has a relationship with the fluid viscosity, which means flux is also related to temperature of fluids and membrane flux can be varied by the change of seasons. (Crittenden et al., 2012)

During the filtration of fluids (e.g. raw rater) a decrease of membrane performance occurs. With the help of backwash and chemical cleaning recovery of performance can be achieved. Flux decline is formulated and represented by a graph below:

$$Reversible\ Flux\ Decline = Flux_{After\ Backwash} - Flux_{Before\ Backwash}$$

$$Irreversible\ Flux\ Decline = 1 - Flux_{After\ Backwash}$$

$$Total\ Flux\ Decline = Reversible\ Flux\ Decline + Irreversible\ Flux\ Decline$$

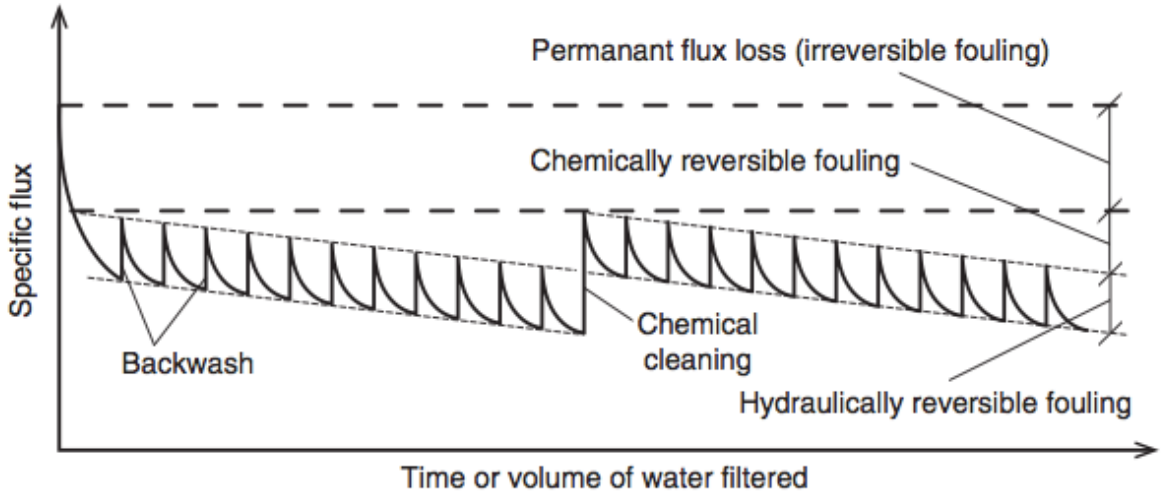


**Figure 2.13.** Representative graph for membrane fouling, backwashes, chemical cleaning, reversible and irreversible fouling (Crittenden et al., 2012)

After backwash and chemical cleaning of the fouled membrane acquired, reversible and irreversible fouling behavior of the membrane can be evaluated. Flux recovery ration can be calculated with the help of data of clean membrane flux and fouled and chemically cleaned membrane flux. This relationship is formulated below:

$$Flux\ Recovery\ Ratio = \frac{Water\ flux_{Fouled\ and\ cleaned\ membrane}}{Water\ flux_{Clean\ membrane}}$$

### 2.5.3. Fouling

Membrane fouling that is a common obstacle to the progress of water-treatment membrane technologies, including microfiltration, ultrafiltration (UF), nanofiltration, and osmosis

processes, reduces process productivity, increases operating costs, and shortens membrane lifespan (Liang S., 2014). Fouling is characterized by three mechanisms: pore blockage, pore constriction, cake formation. In terms of removal tendency of fouling, it can be *reversible* or *irreversible*. Fouling is also defined by the material causing it, which can be particles, biofouling or natural organic matter (Crittenden et al, 2012).

$$J = \frac{\Delta P}{\mu(Km + K_{ir} + K_{hr} + K_{cr})}$$

$$J = \frac{\Delta P}{\mu(K_m + K_c + K_p)}$$

Where;

$J = Volumetric\ water\ flux\ through\ membrane, m^3/h.m^2$

$\Delta P = Transmembrane\ pressure, kPa \quad \mu = Dynamic\ viscosity\ of\ water, Pa.s$

$R_m = Membrane\ resistance\ coefficient, m^{-1}$

$K_{ir} = Irreversible\ membrane\ resistance\ coefficient, m^{-1}$

$K_r = Reversible\ membrane\ resistance\ coefficient, m^{-1}$

$K_c = Cake\ layer\ membrane\ resistance\ coefficient, m^{-1}$

$K_a = Pore\ constriction\ resistance\ coefficient, m^{-1}$

### **2.5.4**. **Membrane Porosity**

The membrane porosity, ε (%), is described as the volume of the pores divided by the total volume of the porous membrane. The porosity of different membranes was calculated as it follows (Chakrabarty et al., 2008):

$$\varepsilon\ (\%) = \frac{(W_W - W_D)/D_W}{((W_W - W_D)/D_W) + (W_D/D_P)} x100$$

Where; $\varepsilon = Membrane\ porosity\ (\%)$

$W_W = Wet\ membrane\ weight, grams$

$W_D = Dry\ membrane\ weight, grams$

$D_W = Density\ of\ water, g/cm^3$

$D_P = Density\ of\ polymer, g/cm^3$

### 2.5.5. Water Contact Angle

Contact angle is a method of determination of hydrophobicity/hydrophilicity and presents the interfacial tension between water and membrane material. Hydrophilic membrane materials like water and this makes the interfacial tension lower comparing to hydrophobic materials. To minimize experimental error membrane bands which were cut from fabricated membrane sheets dried in 50 °C convection oven for 30 minutes. Contact angle measurements are examined using Attension tensiometer. All the measurements were carried out 8 times for each and then contact angles were averaged.

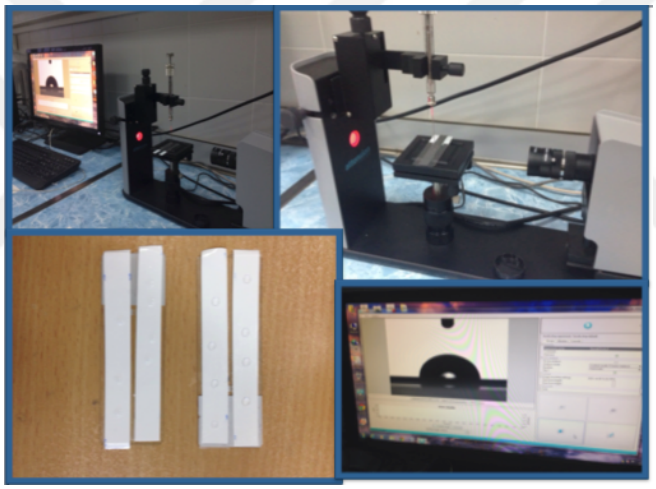

**Figure 2.14.** Experimental setup during contact angle experiments

### 2.5.6. Equilibrium Water Content

Equilibrium water content is one of the important characterization parameter which explains the porosity of membranes and also represents the degree of hydrophilicity or hydrophobicity of membranes. Firstly, wet membrane coupons were weighed after wiping the excess of surface water of membrane with a clean tissue paper. The wet membranes were dried in vacuum desiccator for 48h at room temperature. Perfectly dried membrane coupons weighed again (Arthanareeswaran et al., 2009). The equilibrium water content (EWC) is calculated as below:

$$EWC(\%) = \frac{wet\ membrane\ weight - dry\ membrane\ weight}{wet\ membrane\ weight} \times 100$$

### 2.5.7. Morphology Observation

Qualitative data of surfaces and cross-sections of the membranes was investigated by SEM analysis by use of Jeol JSM-5910LV scanning electron microscope. Before analysis all samples were dried in room temperature and kept in desiccator to avoid natural humidity. Cross-sections were prepared by fracturing by but not with a cutting device. Also, all specimens were coated with gold and palladium before observation.

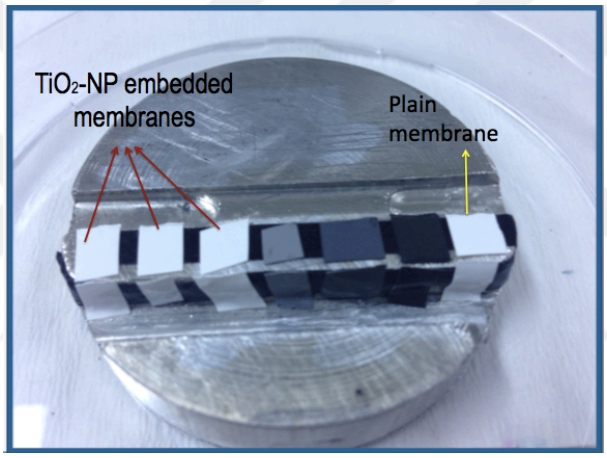


**Figure 2.15.** Surfaces and cross-sections before Au-Pd coating

### 2.5.8. Permeation Experiments

Permeation experiments were carried out by dead-end stirred ultrafiltration cell (Sterlitech) with the exictance of nitrogen ($N_2$) gas as driving force. The ultrafiltration cell has 14.6 cm² effective membrane area. The driving force effects the cell from the top of it and permeates can be collected from the bottom of the cell.

All membrane coupons were compacted in the cell under 100 kPa approximately 5 minutes before experiments begin.

#### 2.5.8.1. Pure Water Flux

Since pure water flux is one of characterization method for membranes deionized water flux measurements were carried out in dead-end ultrafiltration cell without using magnetic stirrer.

Membrane coupon having 49 mm dia. was placed onto porous disk and locate on the bottom of the cell, tightened with the rings and the cell filled with 300 mL deionized water. Flux was measured at five different pressure points being 80-100-120-140-160 kPa, respectively. The permeate was collected from the bottom of the cell onto a digital balance which was connected to computer with RS 232 cable. At each pressure point app. four different data for 2 minutes with 30 seconds of interval time were taken. A diagram for experimental setup can be seen on Figure 2.15.

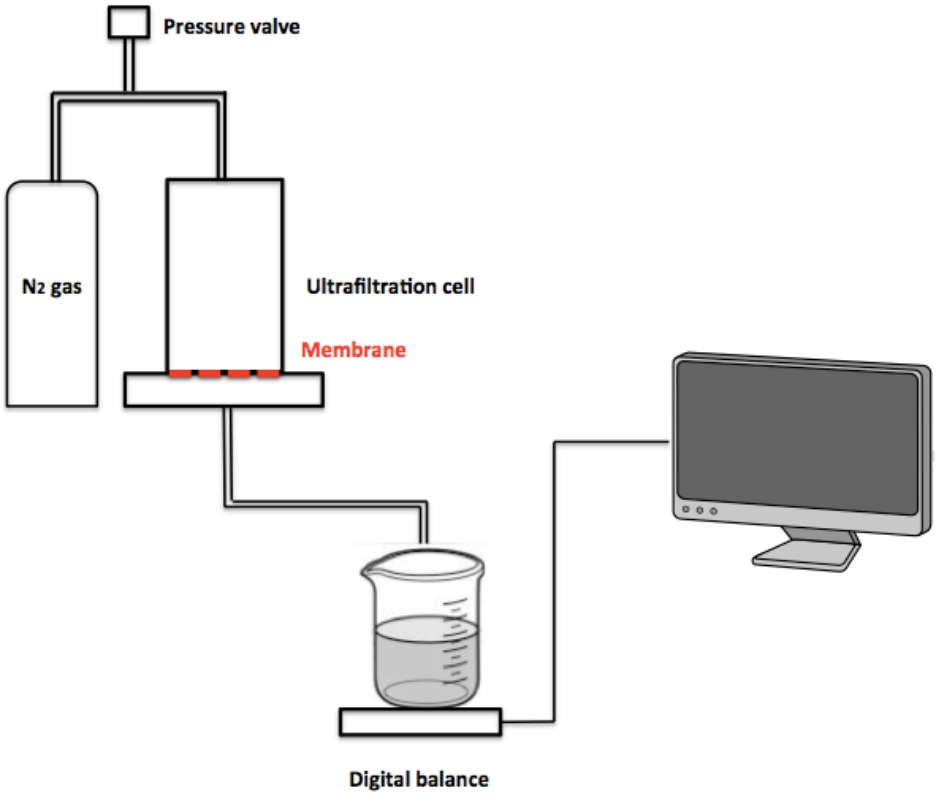


**Figure 2.16.** Diagram for experimental setup

### 2.5.8.2. Fouling Tests

Fouling tests were carried out with raw water obtained from a drinking water treatment plant reservoir in Istanbul, which is called Cumhuriyet Drinking Water Treatment Plant. Before experiments start the raw water was filtered with 5µm cartridge filter and after that filtered raw water used as feed water. Alginic acid sodium salt powder solution is also used as a second indicator of fouling test. Alginate solution concentration was 500 ppm.

During raw water and alginate experiments Sterlitech HP4750 dead-end ultrafiltration cell with the cell stirrer was used. The operating condition was 100 kPa (1 bar) constant pressure,

625 rpm stirring rate for 1 hour on each step. After 1 hour ran out, pressure was released and backwash procedure has taken place. Backwashing was made with 50 mL of pure water filled into ultrafiltration cell which was also containing cell stirrer and it was stirred at 625 rpm for 5 minutes to clean the fouling in which form it was occurring. Backwashing process ingeminated after each raw water/alginate ultrafiltration step. Totally 4 raw water / alginate filtration and 3 backwashing steps took place before chemical cleaning. After the $4^{th}$ raw water / alginate permeation, membrane coupons were immersed into 50 mL of HCl (1N) / NaOH (1N) / NaOCl (500 ppm) solution for 0.5 h under constant temperature of 25 $^{o}$C and a shaking speed of 150 rpm. After chemical cleaning completed, membrane coupons washes with distilled water for couple of times. Then membranes were placed into the filtration cell and pure water fluxes were measured for each membrane. To conclude, raw water/alginate filtration carried on for an hour under a constant pressure of 100 kPa (1 bar).

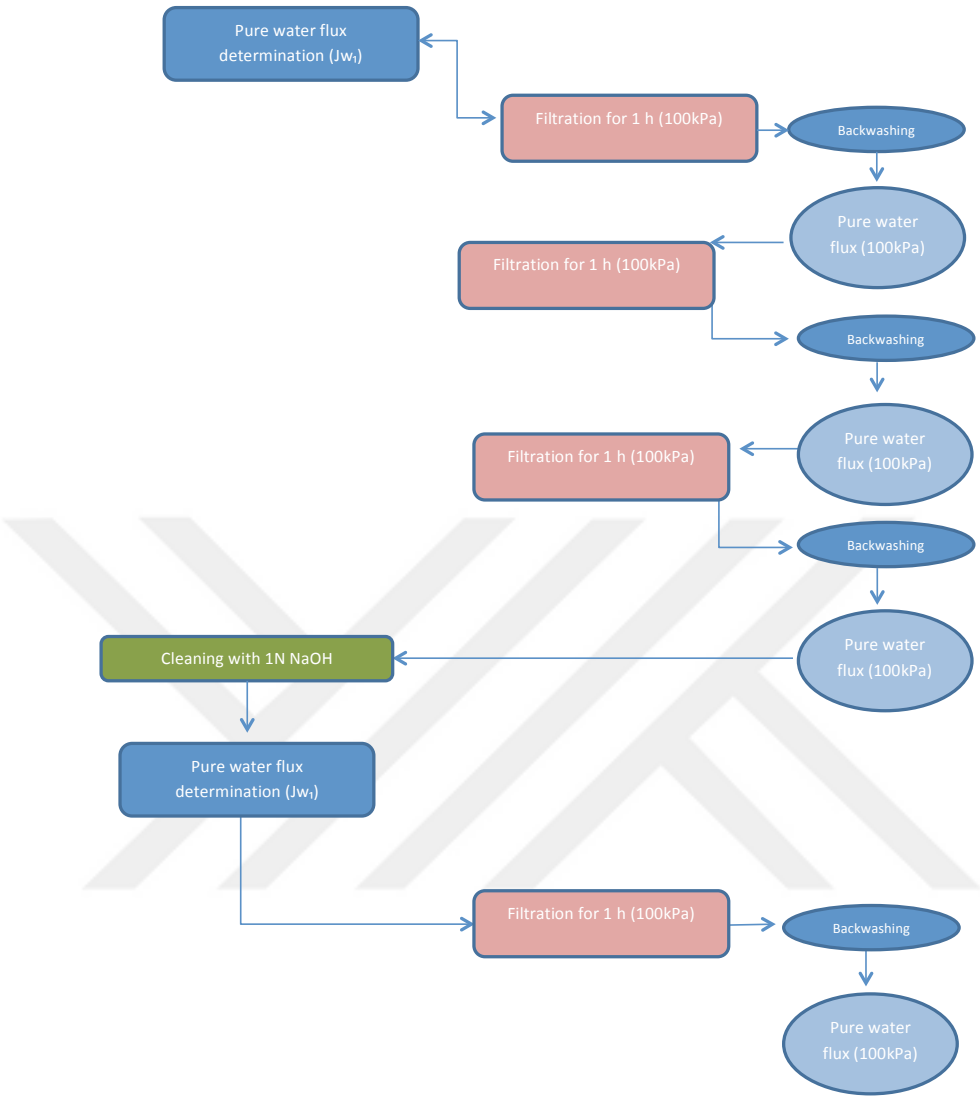


**Figure 2.17.** Experimental procedure of fouling tests

### 2.5.8.3. Effects of Membrane Cleaning Agents on Permeability

To observe the effect of cleaning agents on the water permeabilities of fabricated PSf/PVP ultrafiltration membranes embedded with 0-4% (w/w) $TiO_2$ -NPs loadings, all membranes were exposed to:

- 1N HCl
- 1N NaOH
- 500 ppm NaOCl

The total surface area of the membrane sheets casted was 10x10 $cm^2$. Filtration coupons were cut from those membrane plates with a diameter of 49 mm, so as to fit to diameter of the porous support disk. The experimental procedure for this step as it is below;

- Pure water fluxes of the membrane coupons were measured at five different pressure points and their permeability coefficients were calculated.
- Filtration coupons were exposed to chemicals at mentioned concentrations with the volume of 50 mL. They were shaked for 30 minutes in shaking incubator.
- After 30 minutes of shaking, solutions were collected for titanium analyses and coupons were washed with deionized water and their pure water fluxes were measured again just like in the first step.
- After evaluation of pure water fluxes for the second time, membrane coupons were exposed to the same chemicals for further 30 min.
- At the end of the 30 min of shaking, solutions were collected for titanium analyses and coupons were washed with deionized water and their pure water fluxes were measured again.
- After that step the whole same procedure repeated for 2 and 24 hours.

Transmembrane pressure and the cumulative volume of filtered water were recorded and a "pressure - flux change graph" generated, from slope of the graph membrane permeability constant was calculated according to Darcy's law since it is as it follows:

$$Km = \frac{J}{\Delta P} \text{ (L/m}^2\text{/h/bar)}$$

**2.5.8.4. Titanium Release Analyses**

To determine the titanium release, chemical-cleaning agents e.g. hydrochloric acid, sodium hydroxide and sodium hypochlorite were applied where they were also used in the backwash cycles of the membranes. Samples were collected during each chemical cleaning step and each backwashing sequences. After taking the samples the pH level was made lower than 7 with the help $HNO_3$ with a purity of 65%, and stored up in +4 $^oC$ until the investigation with ICP-MS. The experiment has been run in replicates to have a better evaluation with the combined results.

Additionally, to evaluate the titanium release from different concentrations of $TiO_2$-NPs embedded membranes, they were exposed to different chemicals such as 1N HCl, 1N NaOH

and 500 ppm NaOCl (Figure 2.18.). The surface area of small membrane coupons was 11.34 $cm^2$. Release experiments were carried out in room temperature of 20-22 $^oC$, in a shaker with a shaking speed of 150 rpm. The experiments were run as replicates for different amounts of time. The procedure of the experiment as it is below;

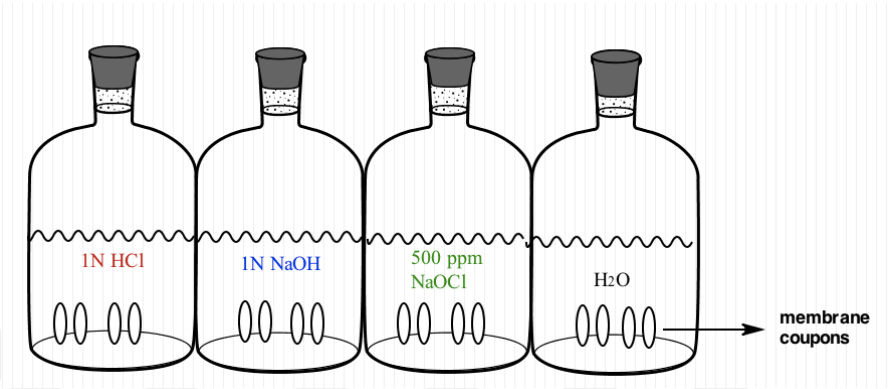


**Figure 2.18.** Representative Figure for Release Experiments

- The coupons with the same area were exposed to certain concentrations of chemicals, which the amounts are also known, in the shaker with 150 rpm shaking speed for 30 min.
- The solutions were collected for the release analyses and then membranes were cleaned with deionized water.
- Same coupons were exposed to the same concentrations for further 30 min.
- After 30 min, again the solutions were collected, membranes were washed with deionized water and exposed to the same concentrations for further 1 hour.
- After 1 hour, again the solutions were collected, membranes were washed with deionized water and exposed to the same concentrations for further 2 hours.
- After 2 hours, again the solutions were collected, membranes were washed with deionized water and exposed to the same concentrations for further 20 hours.

In all filtration experiments membrane coupons were cut from the fabricated membrane sheets with a diameter of 49 mm, so as to fit to diameter of the porous support disk. Those filtration coupons were also exposed to chemicals to see the change in membrane permeability, and to have a better determination for titanium release. The procedure for this experiment as it is below;

- Pure water fluxes of the membrane coupons were measured at five different pressure points and their permeability coefficients were calculated.
- Filtration coupons were exposed to chemicals at certain concentrations that is mentioned above with a certain volume. They were shaked in shaking incubator for 30 minutes.
- At the end of the 30 min. of shaking, solutions were collected for titanium analyses and coupons were cleaned with deionized water and their pure water fluxes were measured again just like in the first step.
- After determination of pure water fluxes for the second time, coupons were exposed to the same chemicals for further 30 min..
- After 30 min. of shaking, solutions were collected for titanium analyses and coupons were cleaned with deionized water and their pure water fluxes were measured again just like in the first step.
- After that step the same procedure ingeminated for 2 and 24 hours.

All measurements were investigated by Agilent 7500A model ICP-MS, therefore it was possible to detect the metal ion in such low concentrations level like ppb (μg/L).

### 2.5.9. Photocatalytic Oxidation

Titanium dioxide nanoparticles degrade organic compounds in the presence of UV irradiation. Because of this well knowing activity of titania, a simulation was carried out with natural organic matter, UV irradiation and $TiO_2$-NPs. Natural organic matter was represented by humic acid in this study. Titanium dioxide solutions were prepared based on the highest released titanium characteristics, which was shown by 4% $TiO_2$ embedded membranes under NaOCl exposure, in order to examine the change on organic matter in case of the evaluation of released titanium with the help of proper reactor design. Concentration of humic acid and titania solution was 150 mg/L and 16 mg/L, respectively. Humic acid and titanium dioxide solution were prepared separately and then they were mixed in the ratio of 3:5, and this final 200 mL mixture was exposed to UV-light irradiation. UV-light was synthetically provided by a 10-watt lamb with 1.8 cm diameter, which was also covered by quartz tube with 2.1 cm diameter. Before and after UV irradiation, samples were collected from mixture and the amount of organic matter was investigated by UV spectrophotometer (UV-2450 Shimadzu)

under 254 nm. But, to eliminate titania particles from mixture cartridge filter (0.45 μm pore size) was used before UV absorbance.


**Figure 2.19.** UV-2450 Shimadzu Spectrophotometer

### 2.5.10. Particle Size Evaluation

In order to evaluate the size of nanoparticles before they are incorporated with polymers and solvent, a series of measurements were carried out. Particle size analyses were investigated by Malvern Zetasizer ZS90. Titanium dioxide ($TiO_2$) nano powder was commercially obtained and has 40 nm sized particles. Before analyses start, nanoparticles were sonicated with solvent (NMP), which was used for membrane preparation as well. To fulfill the protocol given for membrane solution preparation previously, all quantities and durations were followed. After ultrasonication step, particle size measurements were immediately started to prevent undesired nanoparticle agglomeration and precipitation.


**Figure 2.20.** Malvern Zetasizer- Nano ZS90

### 2.5.11. Mechanical Resistance Tests

Mechanical resistance of fabricated membranes was evaluated with the help of stress-strain tests, which were carried out with Zwick Roell 500N testing device. During stress-strain tests pre-load was 0.01N and pre-load velocity was 5 $^{mm}/_{min.}$.

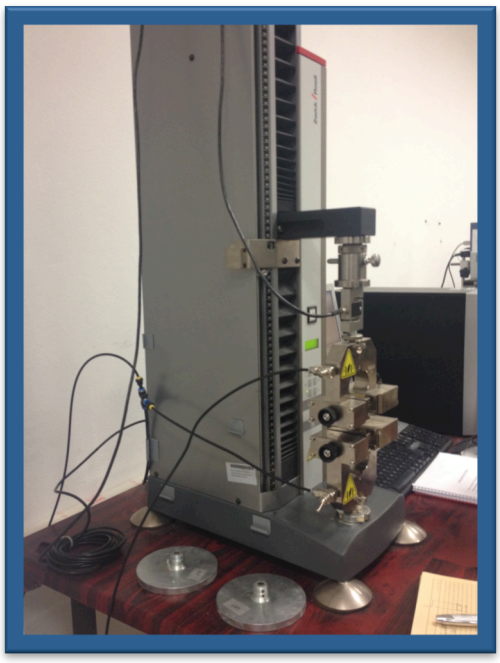

**Figure 2.21.** Zwick Roell mechanical resistance testing device

### 2.5.12. Rejection

Rejection is described as a method for determining the molecular weight cut-off (MWCO) of membranes. Membrane rejection is evaluated by dead-end filtration of 100 ppm PEG having 35,000 molecular weight and then permeates were collected. In order to determine the concentration of permeates TOC measurements and calculations were done according to equation below.

$$\text{Rejection}\ (\%) = \ (1 - \frac{\text{Cp}}{\text{Cf}}) * 100$$

For comparative measurements same procedure was carried out for commercial membrane, which has 20 kDa MWCO.

# 3. RESULTS AND DISCUSSION

## 3.1. Membrane Characterization

The characterization of the neat and titania nanoparticles embedded membranes was fulfilled in terms of pure water permeabilities, flux behaviors during raw water and sodium alginate filtration, rejection, contact angle, water uptake and scanning electron microscope (SEM) images.

### 3.1.1. Pure Water Fluxes of Different PVP Content

As it is already mentioned in material and methods part all membranes fabricated in this study are containing of polysulfone and polyvinylpyrrolidone. Using PVP in casting solution of PSf enlarges the pore size in the prepared membranes rather than the suppression of that structure (Kanagaraj et al., 2014) and increases viscosity (Tweddle et al., 1983). Because of the benefits that PVP contributes, membranes with different PVP ratio and constant PSf ratio were prepared and investigated in terms of permeation flux as it is shown on Figure 3.1. PSf and PVP ratio of membranes were given in materials and methods part on Table 2.1.

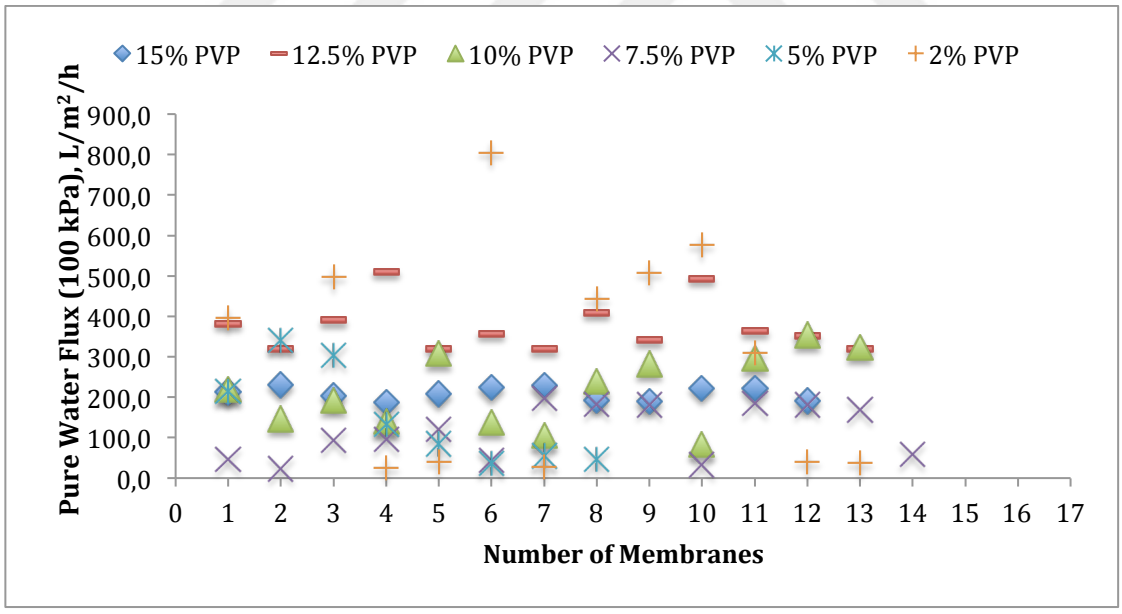


**Figure 3.1.** The effect of PVP content on membrane permeability

Figure 3.1 shows the relationship between different PVP concentrations with constant main

polymer (PSf) concentrations and permeates flux at constant transmembrane pressure (100 kPa). The range of PVP concentrations are 15%, 12.5%, 10%, 7.5%, 5% and 2% by weight. Permeation tests were carried out for each concentration value at least eight, at most fourteen times.

Operating transmembrane pressure, which is 100 kPa for this study, is among the values that are stated in literature. Typical permeate flux values are noted in literature with the range of 30-170 L/m².h (Crittenden et al., 2012).

On figure 3.1. permeation flux values are fluctuating between 37.2 and 805.5 L/m².h at 100 kPa. Among all membranes that are having different PVP compositions, membranes with 2% PVP by weight shows the most undulant behavior and also permeation flux values of 2% PVP having membranes are out of the range that ultrafiltration membranes typically have. Although 5%, 7.5%, 10% and 12.5% PVP by weight containing membranes do not have fluctuant characteristics like 2% PVP having membranes, they also do not indicate a desirable consistency. On the other hand, permeation flux values are in the range of 189,6 and 230,5 30-170 L/m².h, when the concentration of membranes is 15% PVP by weight. These values are slightly different from those, which were stated in literature previously. But, considering laboratory conditions, permeation flux values can be different even from each measurement of same membrane approximately ± 30 L/m².h. Therefore, permeation flux values that 15% PVP containing membranes have, are acceptable. Furthermore, as it can be seen on Figure 3.1, the permeation flux values of 15% PVP having membrane show reliable consistency for twelve measurement.

### 3.1.2. Membrane Permeabilities

To investigate the effect of $TiO_2$ addition on the permeability of PSf membranes, pure water flux was measured under a constant transmembrane pressure of 100 kPa. Figure 3.2. shows the results of pure water and specific fluxes of control membrane, 0.5% - 2.0% - 4.0 % titania nanoparticles entrapped membranes, respectively. For this graph, all pure water fluxes were measured at 100 kPa. For the case of pure water fluxes error bars were also included. The range of pure water flux values changes between 175.9 and 127.2 L/m²/h and the scale of specific flux values is formed between the values of 1.3 and 1.7 L/m²/h/kPa.

As it can be seen on figure asdf, control membrane and 0.5% $TiO_2$ by weight embedded membrane have similarity in terms of pure water flux. 0.5% $TiO_2$ by weight entrapped membranes' pure water fluxes are 6.34 % higher than control membranes' pure water flux on average. 2% $TiO_2$ entrapped membranes have lowest pure water flux among other nanoparticle concentration. 4% titania embedded membranes have %10.51 higher pure water permeability than 2% titania entrapped membranes averagely. Decline between plain membranes and 2% titania embedded membranes' pure water flux is equal to 22.74% of pure water flux of plain membrane. Pure water permeability of membranes is one of indicators of hydrophilic properties of membranes. Observed decrease in pure water fluxes at 100 kPa for the membranes with 2.0% and 4.0% $TiO_2$-NPs loadings is 19.5% and 6.9%, respectively.

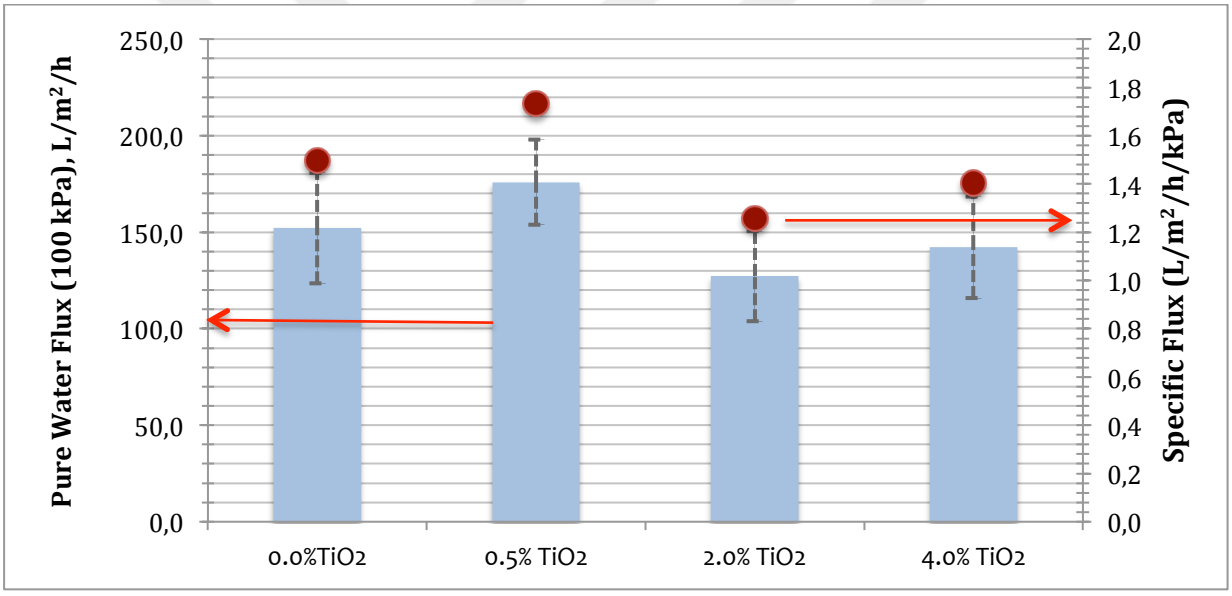


**Figure 3.2.** Membrane pure water flux-specific flux graph at 0.0% - 0.5% - 2.0% - 4.0% $TiO_2$ by weight

Standard deviation of plain membranes' pure water fluxes at 100 kPa is 28.54 among same kind of membranes, while 22.16, 23.34 and 26.31 for 0.5%, 2.0% and 4.0% titania entrapped membranes' pure water flux respectively. Error bars stand for standard deviation on figure 3.2. The increase of pure water fluxes from 2% titania entrapped membrane to 4% titania embedded membrane can be ignored, because 10.51% of difference can also be observed among same kind of membranes during repetition of experiments.

The addition of $TiO_2$ nanoparticles causes a more porous membrane surface and skin layer, reducing the resistance of water permeation through the membranes. Meanwhile, the better hydrophilicity can attract water molecules into the membrane and decrease the interface tension of membrane-water, consequently membrane flux becomes higher (Li et al., 2006). When titania concentration is more than 2% by weight, pure water flux of membranes are not improved. For the case of higher concentration than 2% by weight of titania, nanoparticles perform aggregation phenomenon, which prevents dispersion of nanoparticles inside polymer matrix.

Since membrane hydrophilicity can be determine in terms of the membrane flux as well as contact angle, it has been mentioned in several articles that nanoparticles can be in an attached state on membrane surface and inside membrane pores. The position of nanoparticles can cause reduction in membrane permeability and an incline in filtration resistance (Richards et al., 2012).

### 3.1.3. Water Uptake

To determine the effect of $TiO_2$ addition on water uptake ability of PSf membranes, membrane coupons were weighed in wet and dry position. Numbers were recorded and the calculation was done according to equilibrium water content, that was given in material and methods part previously. Results were transferred to graph, which can be seen on Figure 3.3. Error bars correspond to standard deviation on Figure 3.3.

The water uptake tests and the results of equilibrium water content showed that while the $TiO_2$ – NP content increases in membranes the water uptake percentage decreases. As it can be seen on Figure 3.3. the water uptake of 0.5% $TiO_2$ loaded membrane slightly differentiates from plain membrane, but is the highest. On the other hand, 4.0% $TiO_2$ embedded membrane shows the lowest water uptake propensity with the difference of ~4% and ~5% from 2.0% and 0.5% $TiO_2$ entrapped ones, respectively.

Distinguishable decrease between water uptake percentages of differently loaded membranes can be caused by nanoparticle agglomeration in membrane pores. The more the nanoparticles are embedded into membrane solution, the harder it becomes to homogenize the titania nanoparticles. As a result of less homogenization the nanoparticles tend to bond together which narrows membrane pores.

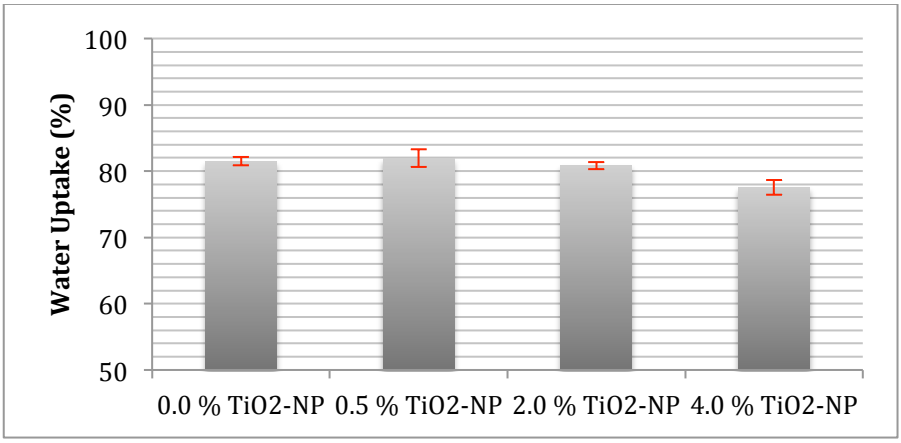


**Figure 3.3.** Water uptake changes at different $TiO_2$ loadings

### 3.1.4. Contact Angle

To examine the relationship between surface hydrophilicity and the addition of titania nanoparticles, contact angle measurements were carried out eight times for each and then contact angles were averaged. Figure 3.4. shows average contact angle values for four types of membranes: Neat membrane, 0.5%, 2.0% and 4.0% by weight $TiO_2$ embedded membranes. The hydrophilic properties of fabricated membranes can be identified by the help of relative contact angle measurements. Decreased contact angle ascribes a meaning to increased hydrophilicity of membranes (Oh S.J. et al., 2009). In theory, for an ideally hydrophilic membrane the contact angle should be 0 degrees (Richards et al., 2012).

As the measurement results show that contact angle decreases, while the concentration of titania nanoparticles inside the membrane increases. Neat membrane's contact angle is around 90° when 2% TiO2 loaded membrane has a contact angle around 85°**.** 0.5% $TiO_2$ embedded membrane shows a contact angle decline with the difference of ~4% from neat membrane and 4% $TiO_2$ embedded membrane has a scale-down with the difference of ~16% from plain membrane as well.

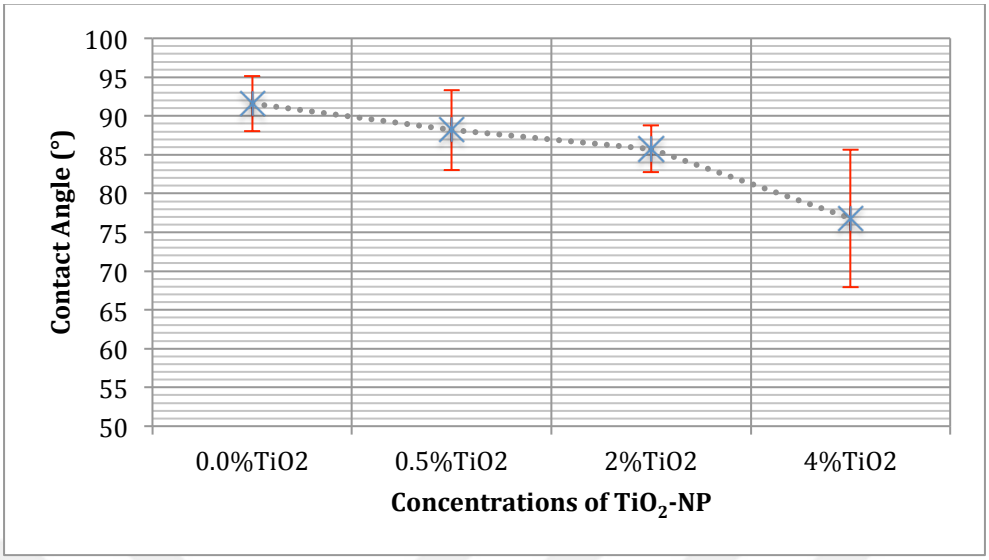


**Figure 3.4.** Contact angles at different $TiO_2$ loadings

### 3.1.2. Membrane Morphology

In order to observe $TiO_2$-NPs inside and on the membrane and to investigate surface and cross-section morphology of membranes, which was prepared with different titania loadings, scanning electron microscopy (SEM) technique was performed.

Figure 3.5. shows the cross-section SEM images of neat and titania nanoparticles embedded membranes in 50-micron magnitude. Membranes have a skin layer at top, an intermediate layer and a bottom layer. SEM images at all $TiO_2$-NPs loadings have asymmetric structure due to their preparation process, which is immersion precipitation.

The cross-section morphologies of membranes illustrate that the macrovoids grow and become permeable at low filler concentration. Then, the macrovoids are suppressed or disappear at higher filler concentration than 2% by weight. The skin layer of membranes thickens with the increase of filler concentration. In the case of 4 wt.% titania loaded membranes have much thicker skin layer, which causes low pure water permeation. According to Figure 3.5. 0.5 wt. % titania entrapped membranes have much significant fingerlike structure. Relatively high pure water flux that 0.5 wt. % titania loaded membrane have can be confirmed by its proper structure.

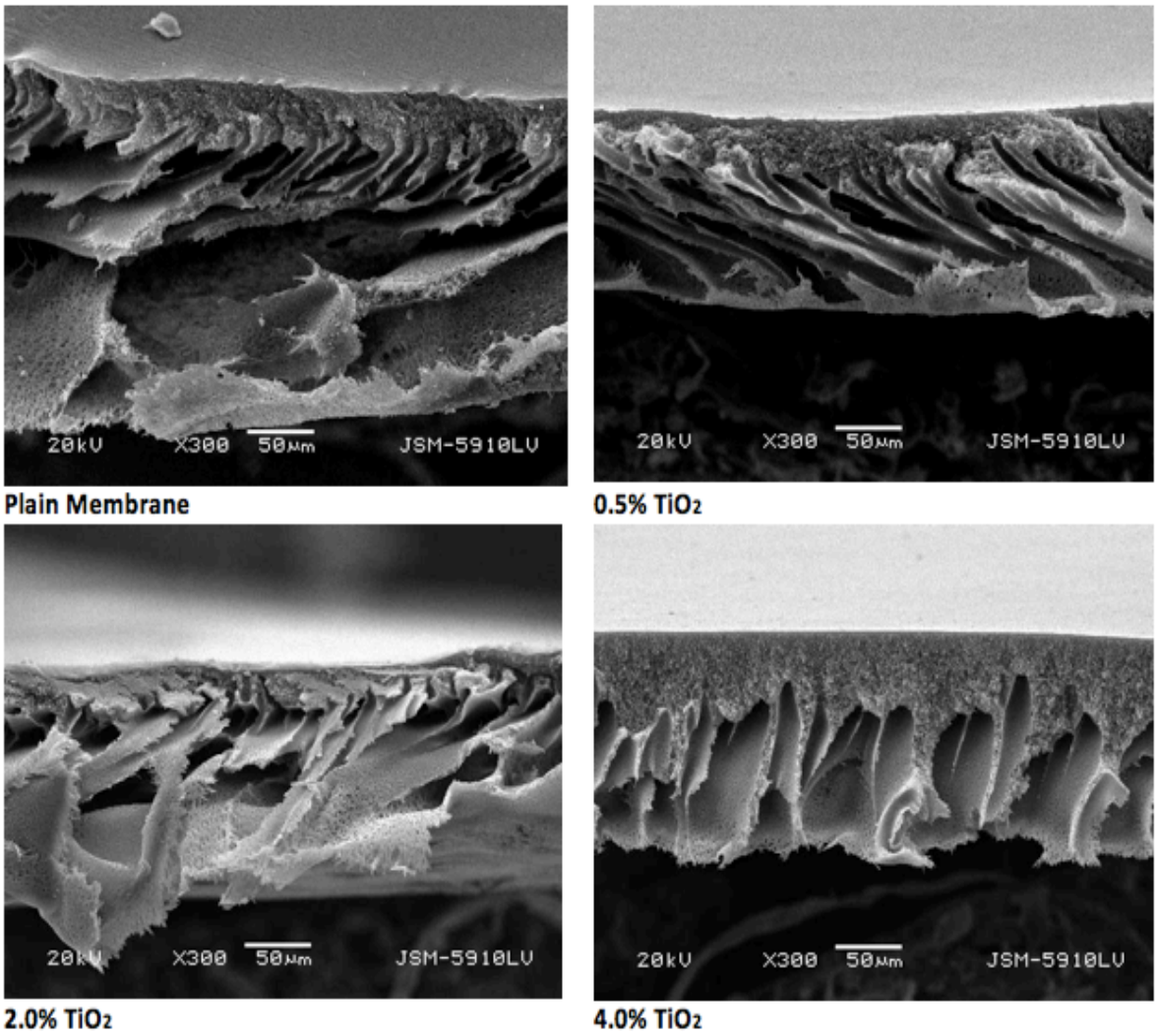


**Figure 3.5.** A picture of membrane cross-sections at different TiO2-NP concentrations

When the magnitude was made lower than 50-micron, nanoparticles were observed in 4wt.% $TiO_2$ embedded membranes. In the case of 4% titania loadings, nanoparticles induce an apparent aggregate phenomenon inside the pores and on the membrane surface. On Figure 3.6. it can be easily noticed, that nanoparticle aggregation results pore blockage and thus, membrane flux and membrane efficiency decrease. Yang et al. explains this phenomenon with quick increase of suspension viscosity at high filler concentrations (4% by weight in this study), therefore nanoparticles move with difficultly in polymer solution and generate a resistance to shrinkage of the polymer (Yang et al., 2006).

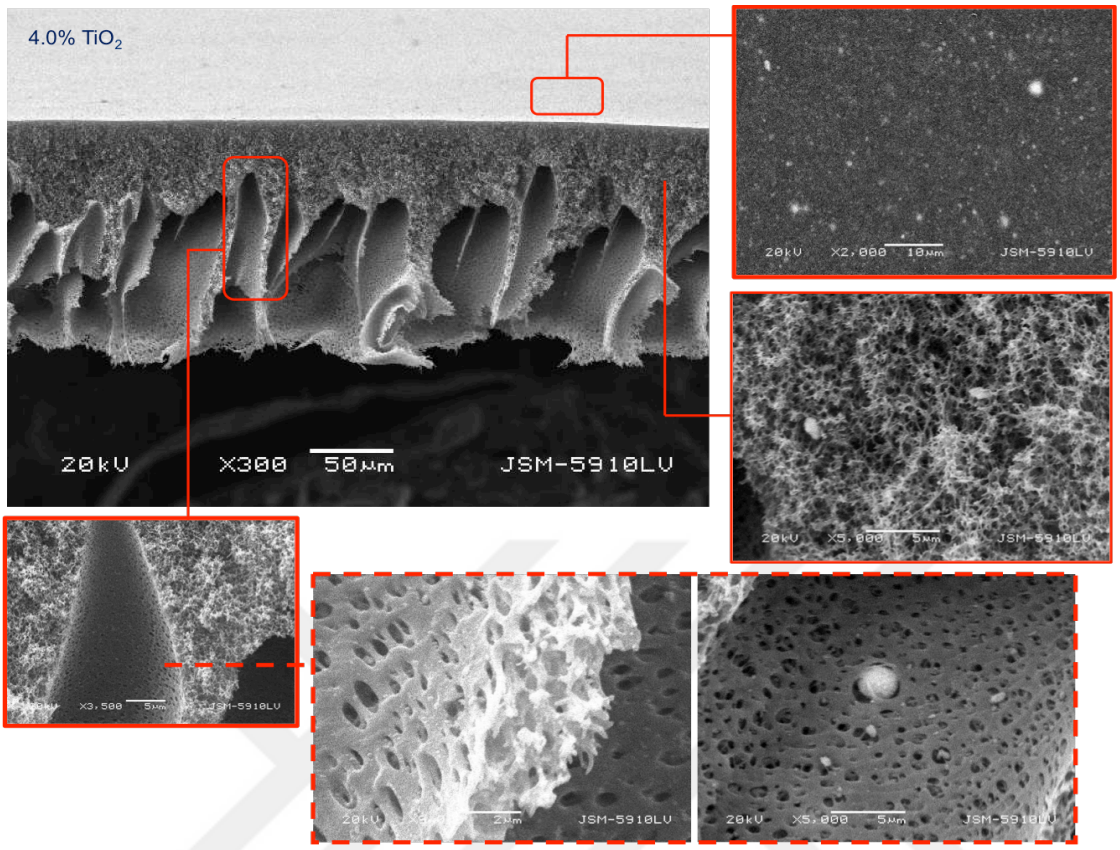


**Figure 3.6.** SEM picture of 4% $TiO_2$ embedded membrane

To testify the identity of aggregate nanoparticles on Figure 3.6., elemental analysis was carried out by energy dispersive spectrometer (EDS) , which can be seen on Figure 3.7.. The spectrum indicates that there was no impurity other than we expected. Gold (Au) and palladium (Pd) elements were used to cover membranes before SEM and EDS investigation.

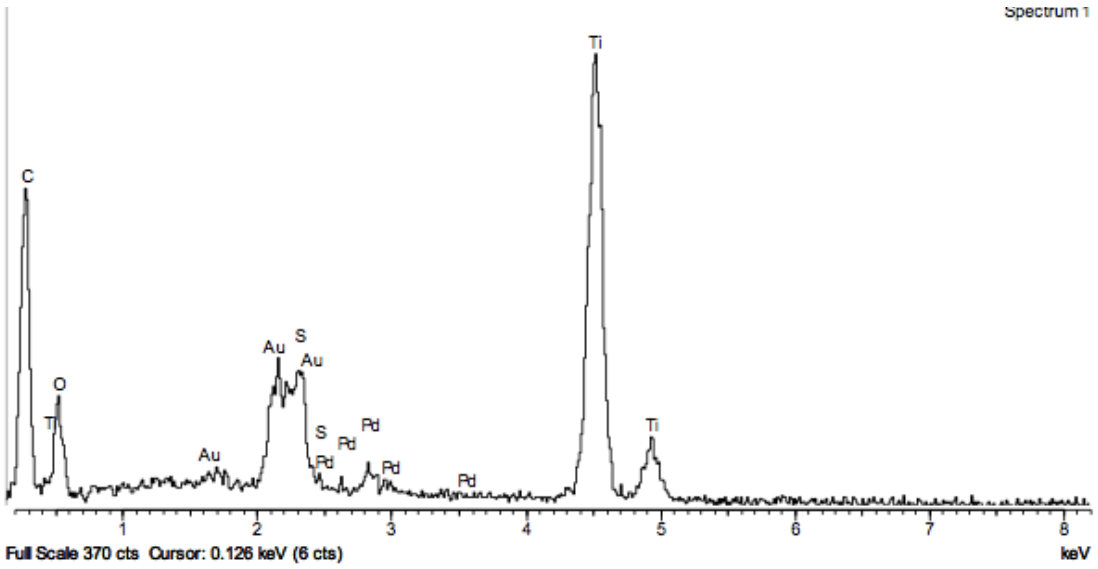


| Spectrum | O | Ti | Total |
|---|---|---|---|
| At.Ag rt | 49.47 | 50.53 | 100.00 |
| At.Syrt | 74.57 | 25.43 | 100.00 |

**Figure 3.7.** Energy dispersive spectrometry of TiO2-NP

### 3.1.3. Rejection

MWCO is a characteristic feature of membrane pores and is related to rejection for a certain molecular weight of a solute (Kanagaraj et al., 2014). In this study membrane rejection is evaluated by filtration of 100 ppm PEG having 35,000 molecular weight. If the molecular weights of the molecule larger than the molecular weight cut-off of a membrane, molecule will retain on the membrane. For the determination of permeates concentration TOC measurements and calculations were done according to equation below.

$$\text{Rejection } (\%) = \left(1 - \frac{\text{Cp}}{\text{Cf}}\right) * 100$$

Commercial membrane with 20 kDa MWCO showed a rejection of 61.50 % for the filtration of 100 ppm PEG. On the other hand, in laboratory fabricated membrane, which is 4% titania loaded, showed 32.18% rejection to 100 ppm PEG filtration. When this ratios were evaluated,

it can be seen, that fabricated membranes are rejecting approximately two times less than commercial membrane with 20 kDa MWCO. Thus, this approach would be proper, that molecular weight cut-off of fabricated membrane is close to 40 kDa.

### 3.1.4. Flux Decline

Membrane flux decline and membrane fouling were investigated by surface water and alginic acid sodium salt (alginate) solution filtration. The whole filtration process was characterized by reversible flux, irreversible flux and total flux decline before backwash for both solutions. Figure 3.8. is a representation of filtration and cleaning periods. Alginate is a model compound that is representing extracellular polymeric substances (EPS) since it is a polysaccharide molecule.

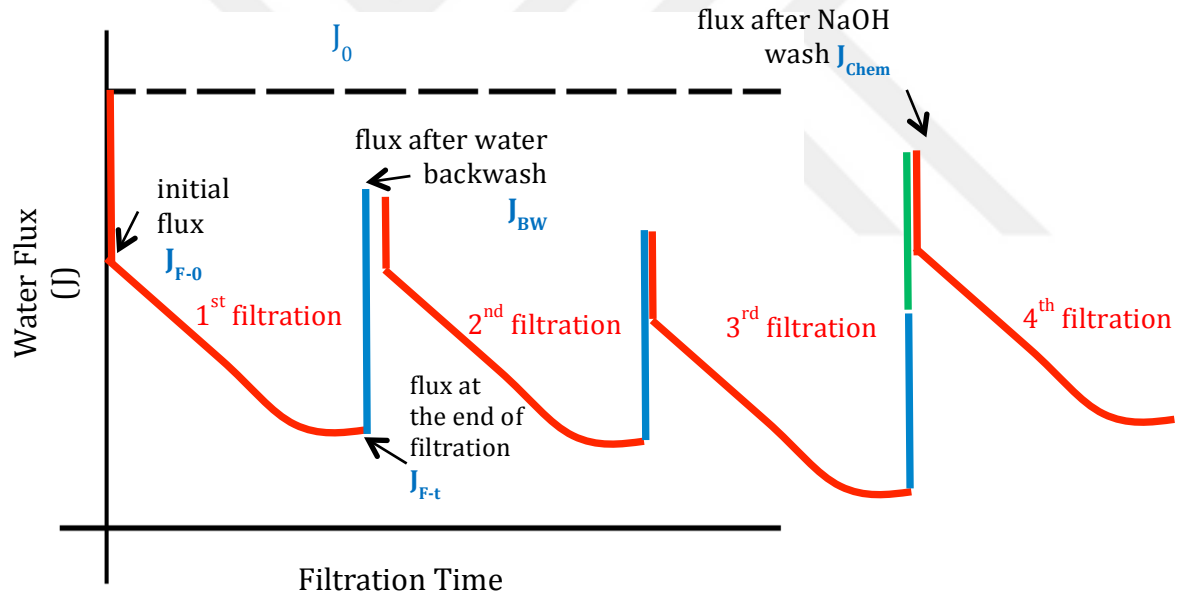


**Figure 3.8.** A representative figure as a model for filtration and cleaning periods

Water fluxes were recorded and evaluated according to the protocol given on figure 2.17 in chapter two.

J: Permeate flux at 100 kPa, L/m$^2$/h

$J_0$: Clean membrane pure water flux at 100 kPa, L/m$^2$/h

Individual units of trendline in the figure represent each 60-minute filter runs. Water backwash (or hydraulic cleaning) after each run recovers some portion of the lost flux as

solids and weakly bound organics are flushed from the membrane surface. However, all of the flux is not recovered and a long-term decline in terms of performance is observed (as the 2nd and 3rd backwashes in Figure 3.8.). Chemical cleaning is necessary for the foulants that are not able to be removed during hydraulic cleaning. The loss of flux that can be recovered with chemicals is called chemically reversible cleaning (the cleaning cycle before the 4th filtration run in Figure 3.8).

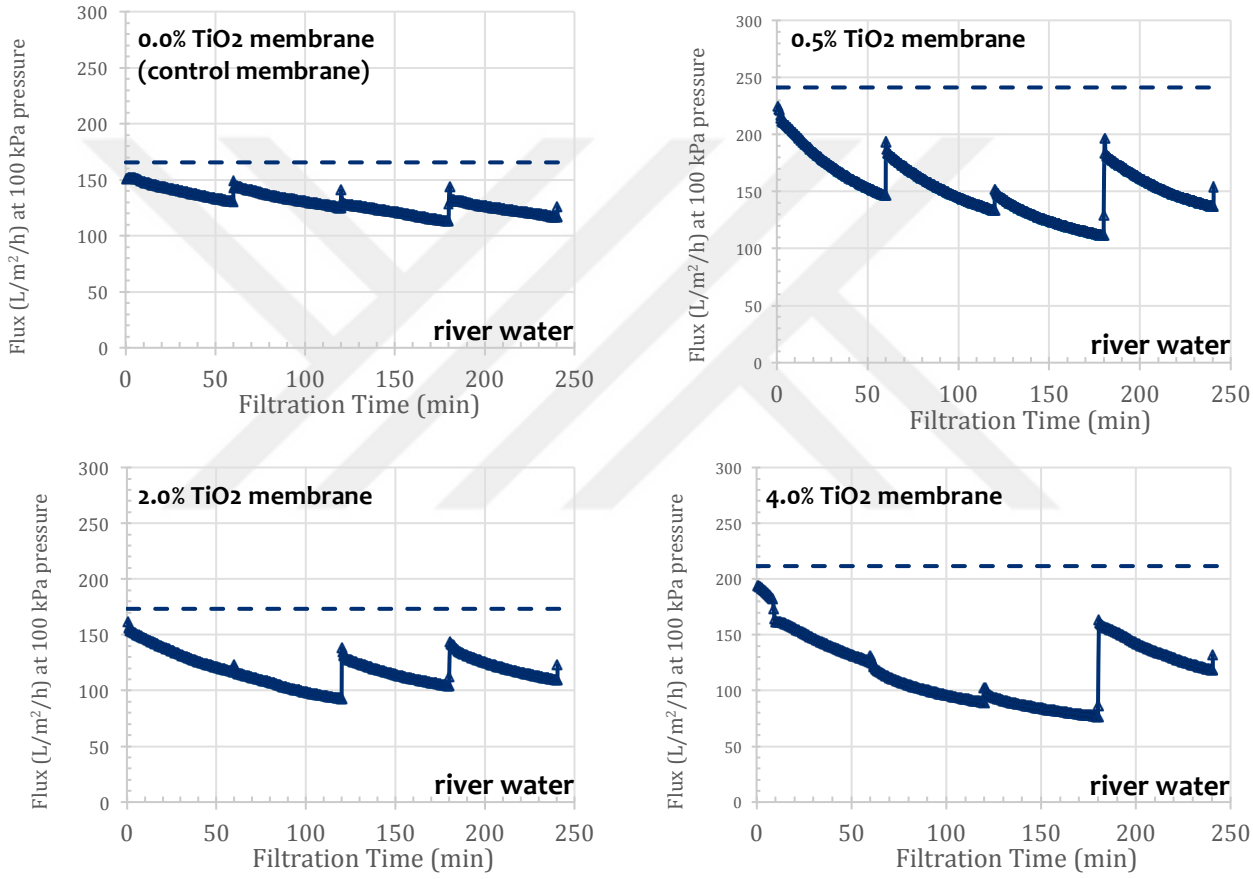


**Figure 3.9.** Permeate flux during river water filtration at different titania loadings.

Figure 3.9. shows flux behavior during river water filtration at all titania loadings, which are 0.0%, 0.5%, 2.0%, 4.0% $TiO_2$- NP by weight. Dashed and linear lines of each graph represent pure membrane flux in clean state of membranes. Figure 3.9. shows us that 0.5% $TiO_2$-NPs loaded membranes have the highest pure membrane flux among all other titania loadings, while those membranes have a bigger propensity to fouling during river water

filtration than neat membranes (0.0% $TiO_2$ –NPs embedded membranes). But, 0.5% titania loaded membranes' flux can be easily recovered after chemical backwash, even if those membranes tend to be fouled quickly in comparison to neat membranes. In the case of 4.0% titania loaded membranes it is observed that there is a more severe fouling during river water filtration than the case of 2.0% titania loaded membranes.

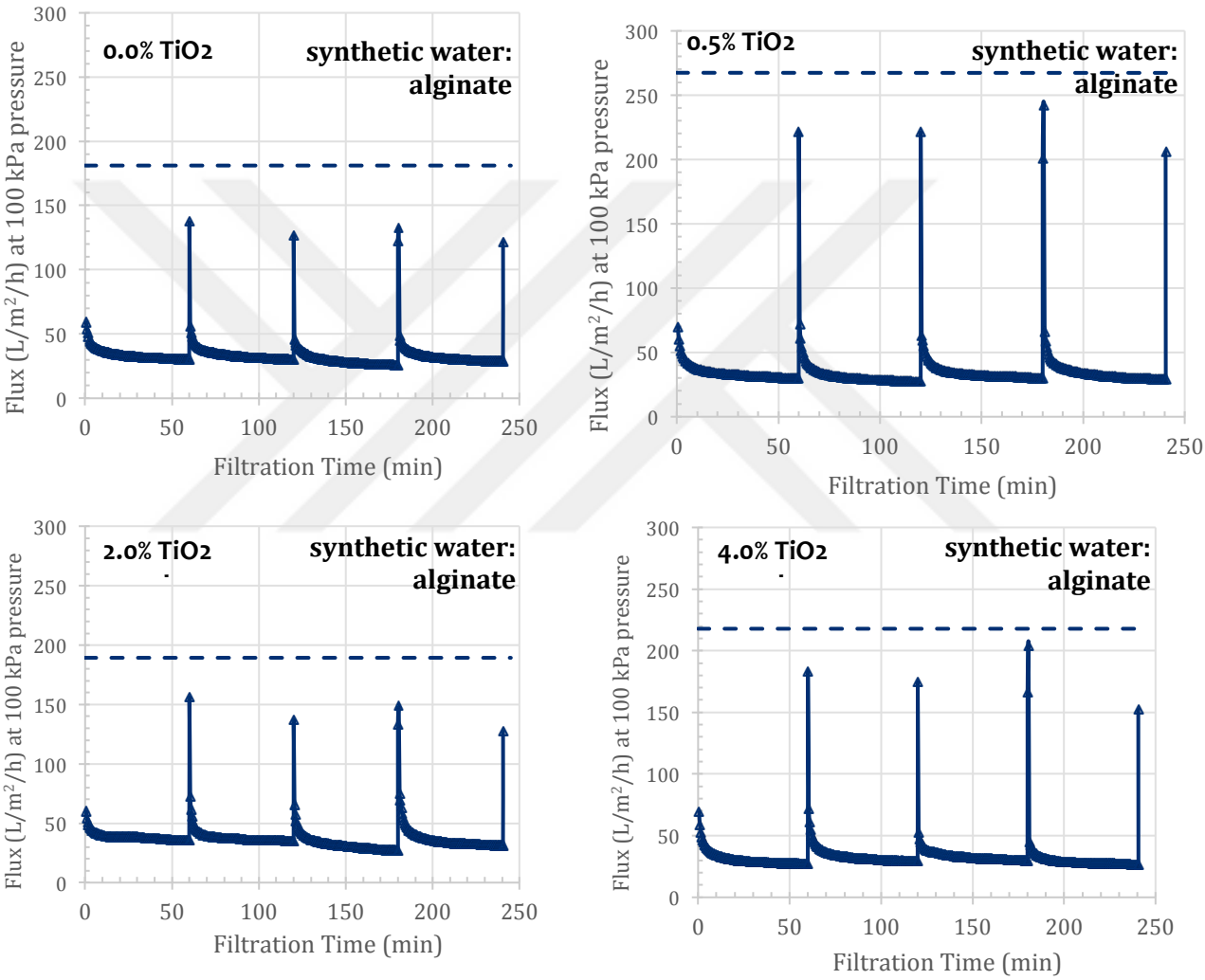


**Figure 3.10.** Permeate flux during synthetic water (alginate) filtration at different titania loadings

Figure 3.10. shows flux behavior during synthetic water (alginic acid sodium salt) filtration at all titania loadings, which are 0.0%, 0.5%, 2.0%, 4.0% $TiO_2$- NP by weight. It can be

reported about alginate filtration that membranes at all titania loadings tend to foul very rapidly while they are exposed to alginic acid filtration.

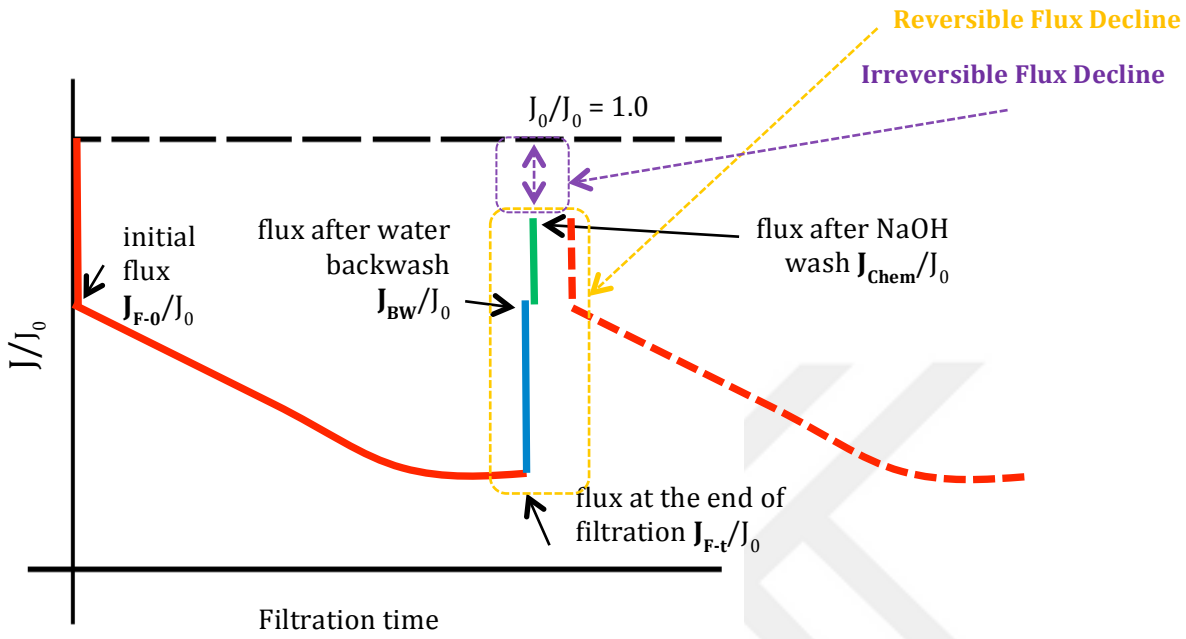


**Figure 3.11.** A representative figure of reversible and irreversible flux decline calculations

In order to calculate normalized water flux permeate fluxes at 100 kPa were divided by clean membrane pure water flux at 100 kPa ($J/J_0$). To make normalized initial water flux of a membrane, clean membrane water flux, which is initial water flux, was divided by itself ($J_0/J_0$). This is the reason that highest value on the graph is 1.0.

Irreversible flux and reversible flux values were calculated as it is below:

Irreversible Flux Decline = $1-J_{BW}$

Irreversible Flux Decline = $1-J_{chem}$

Reversible Flux Decline (with BW) = $J_{BW}- J_{F-t}$

Reversible Flux Decline (with NaOH) = $J_{chem}- J_{BW}$

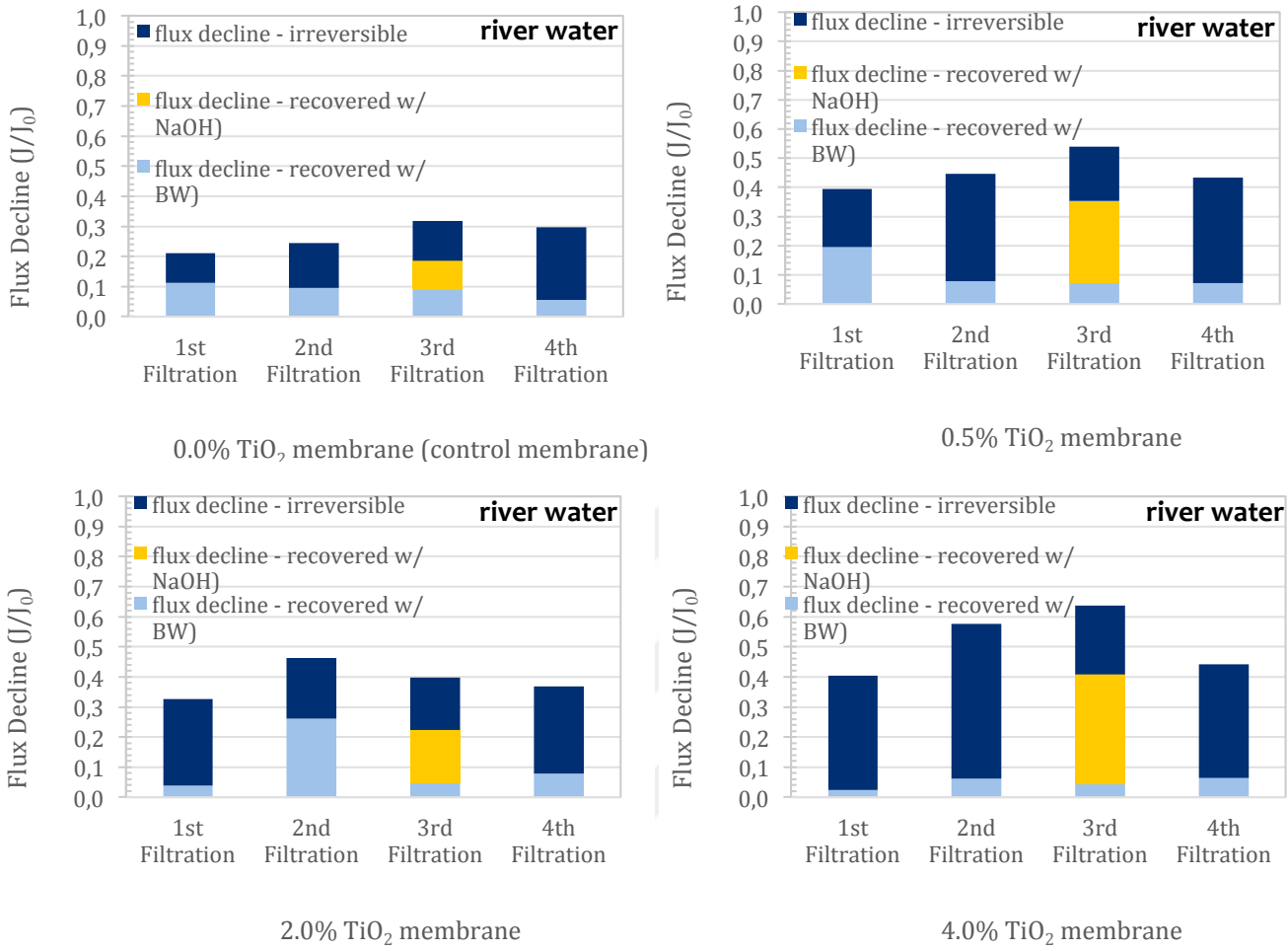


**Figure 3.12.** Flux decline during river water filtration for 0.0% - 0.5% - 2.0% - 4.0% $TiO_2$-NP loadings, respectively

Figure 3.12. shows flux decline behavior during river water filtration at all titania loadings, which are 0.0%, 0.5%, 2.0%, 4.0% $TiO_2$- NP by weight. Dark blue parts of the bars are representing irreversible flux decline, light blue parts of the bars are representing flux decline which is recovered by water during backwash and yellow parts of the bars are standing for the flux decline, which is recovered by NaOH during chemical backwash. As it can be seen on figure 3.12, with the addition of nanoparticles irreversible flux decline values are not decreasing. On the other hand, the more nanaoparticle embedded, the easier to regain water flux after chemical wash, which can be read from the yellow parts of the bars on figure 3.12.

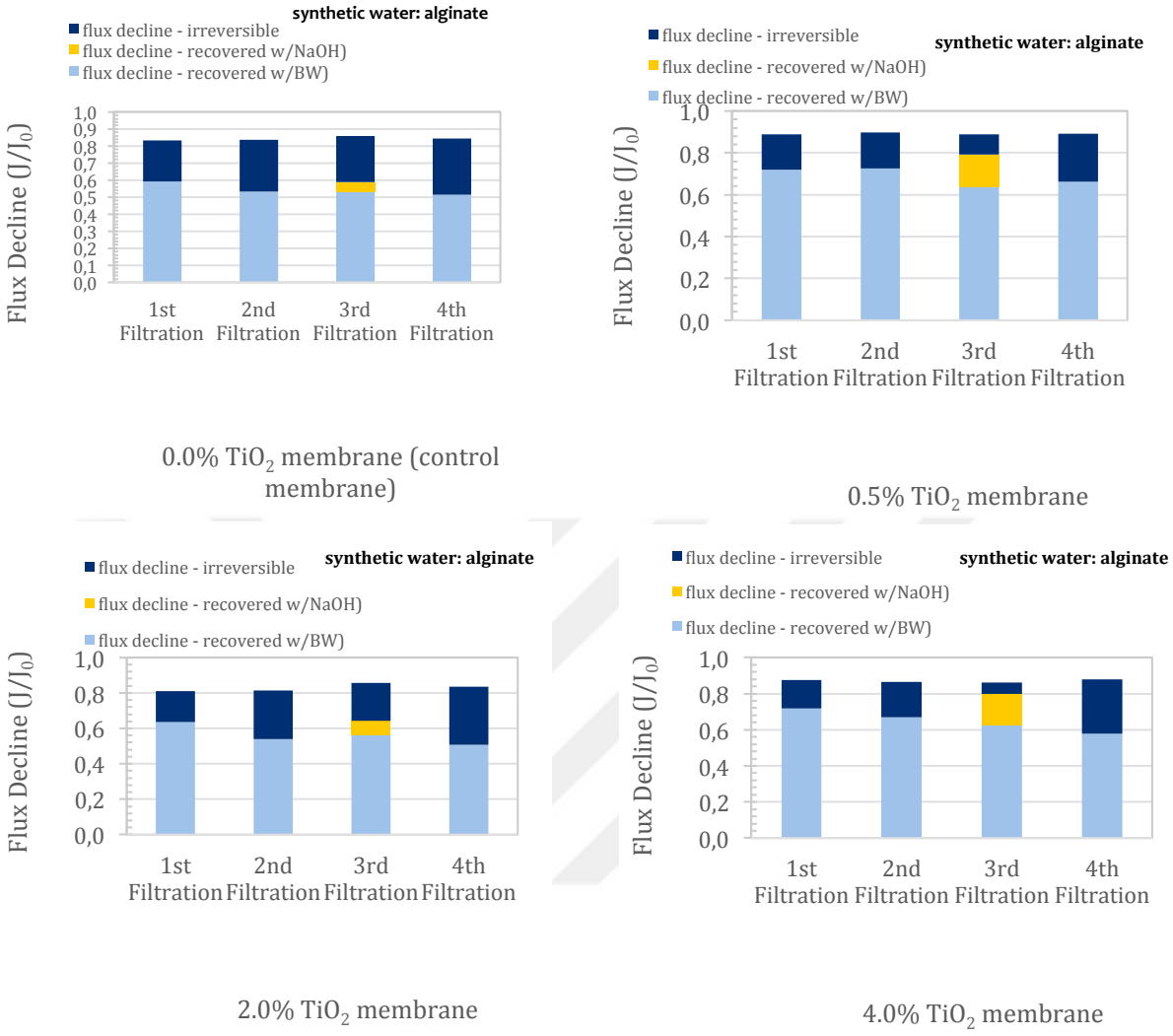


**Figure 3.13.** Flux decline during alginate filtration for 0.0% - 0.5% - 2.0% - 4.0% $TiO_2$- NP loadings, respectively

Figure 3.13 shows flux decline behavior during synthetically prepared water (alginate) filtration at all titania loadings, which are 0.0%, 0.5%, 2.0%, 4.0% $TiO_2$- NP by weight. Dark blue parts of the bars are representing irreversible flux decline, light blue parts of the bars are representing flux decline which is recovered by water during backwash and yellow parts of the bars are standing for the flux decline, which is recovered by NaOH during chemical backwash. In the case of alginate filtration, flux recovery with water backwashes and chemical cleaning is relatively high comparing to river water filtration. It can be reported that 0.5% titania embedded membranes have the biggest propensity to be recovered after each filtration run.

### 3.1.5. Total Water Production Potential

Fouling derives from specific interactions between the membrane and the components in the raw water. It leads a quick and usually irreversible loss of permeability through membrane. In order to avoid the effects of fouling, generally a periodic hydraulic backwash is applied. During hydraulic backwash, water performs a partial removal of deposited matter. Owing to the backwash process membrane regains its permeability to a certain extent. But, membrane fouling cannot be totally reversed by backwash. Some part of the deposited matter on and inside the membrane cannot be removed and that causes the irreversible fouling (Katsoufidou et al., 2007).

In order to examine the affectivity of membranes, which are entrapped with $TiO_2$-NPs, to fouling, flux recovery ratios were calculated according to the data obtained from river water filtration. Figure 3.14 represents total water production potential, product water and lost due to fouling through an illustration.

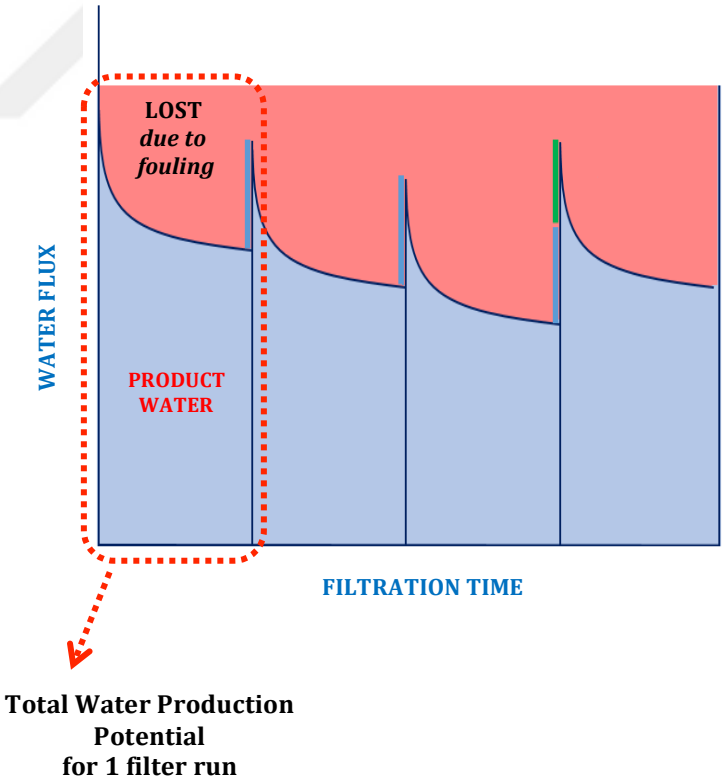


**Figure 3.14.** Illustration of total water production potential

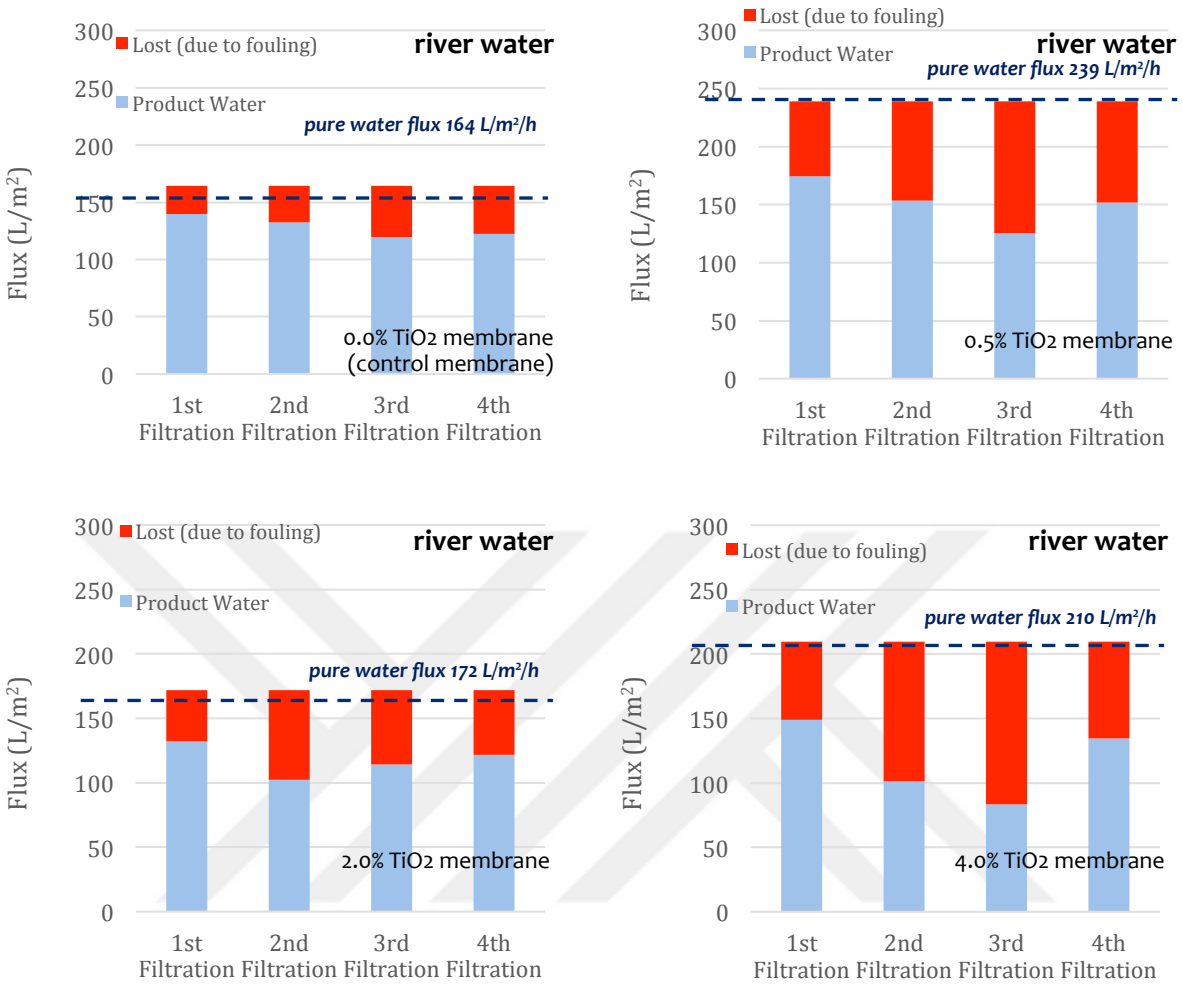


**Figure 3.15.** General view of total water production potential of 0.0% - 0.5% - 2.0% - 4.0% $TiO_2$- NP loaded membranes, respectively.

Figure 3.15 represents product water and lost (due to fouling) during river water filtration for 0.0% - 0.5% - 2.0% - 4.0% $TiO_2$- NP loaded membranes. Red parts of the bars stand for lost and blue parts of the bars show product water. As it can be seen on the figure 0.5% titania entrapped membranes have the highest product water amount and 4% $TiO_2$-NP loaded membranes have the lowest product water amount.

To overview total water production potential for each $TiO_2$-NP loadings, all values were calculated in itself to get a result by percent. Figure 3.16 shows us total water production potential by percent of 0.0% - 0.5% - 2.0% - 4.0% $TiO_2$- NP loaded membranes. It must be noted that all values were reached according to the results of each titania loadings separately.

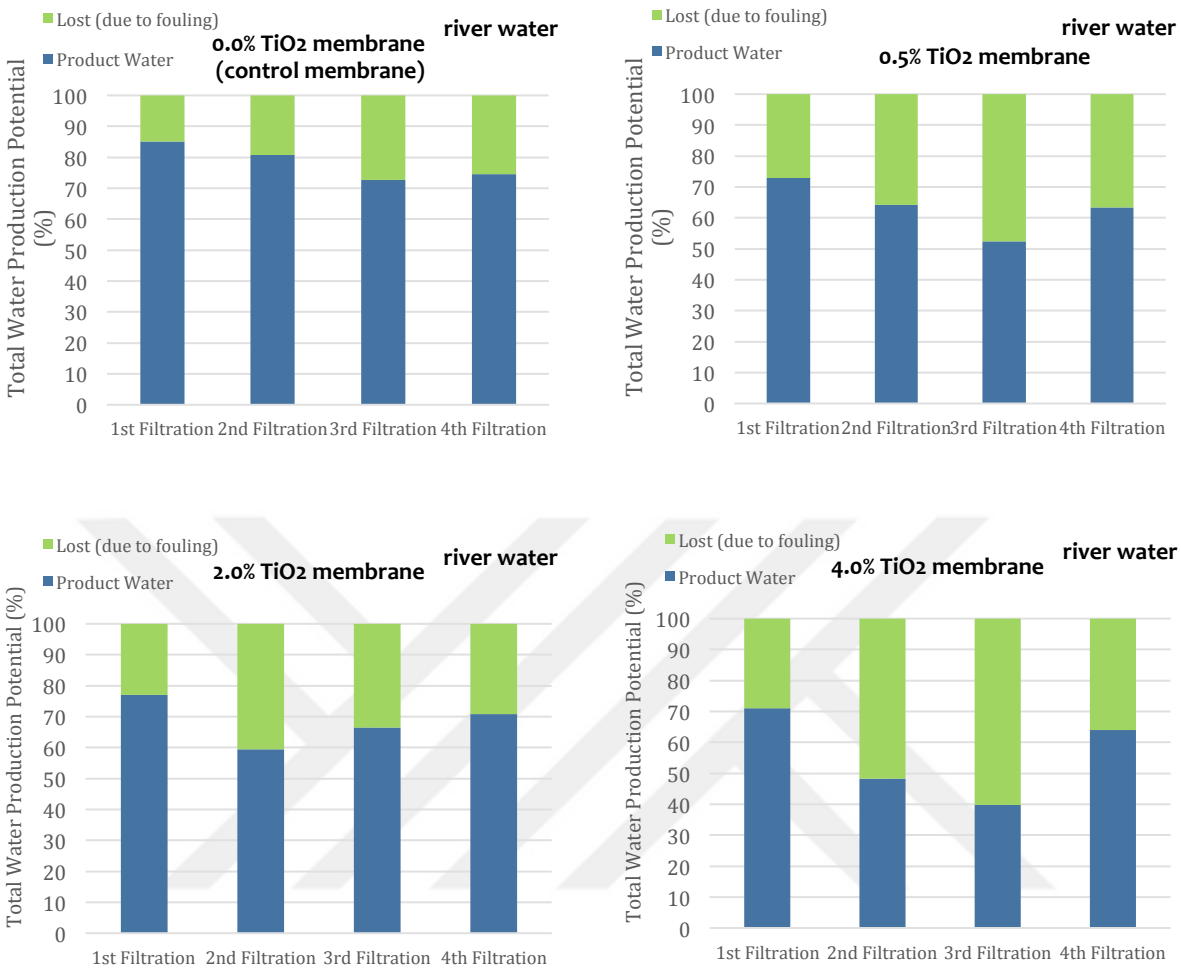


**Figure 3.16.** Total water production potential by percent of 0.0% - 0.5% - 2.0% - 4.0% $TiO_2$- NP loaded membranes

On figure 3.16 each bars of the graphs were representing filtration steps. Blue parts of the bars stand for product water and green parts of the bars show lost (due to fouling). According to figure 3.16 4% $TiO_2$- NP embedded membranes have the lowest product water value with the amount of less than 71% and also the highest lost (due to fouling) value.

### 3.1.6. Effect of Membrane Cleaning Agents

To examine the change of membrane performances with chemical cleaning agents fabricated membranes were exposed to 1N HCl, 1N NaOH and 500 ppm NaOCl for specific periods of time and then pure water fluxes evaluated. In order to achieve a comparative analysis all flux values were calculated as normalized water flux values.

Figure 3.17, figure 3.18, figure 3.19, figure 3.20 are showing flux change of membranes, which are 0.0 wt.%, 0.5wt. %, 2.0wt.% and 4.0wt. % titania loaded, after certain periods of time exposure to 1N HCl, 1N NaOH and 500 ppm NaOCl. If pure water fluxes of membranes are changing dramatically, it means that that specific cleaning agent leads to a progressive deterioration of membrane performance.

When membranes are not loaded with titania nanoparticles, all chemical cleaning agents cause decline on membrane pure water fluxes, which can fall till 21.57% for the case of NaOCl.

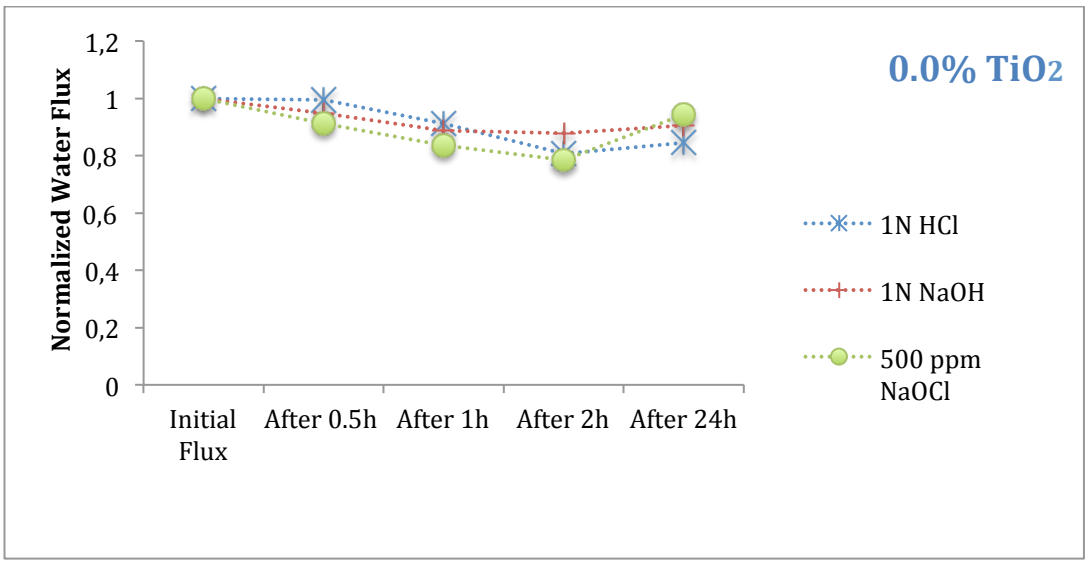


**Figure 3.17.** Normalized pure water flux changes at 100 kPa for 0.0% TiO2-NP embedded membrane after cleaning agents' exposure

During the experiments carried out with 0.5% $TiO_2$ loaded membrane under NaOCl exposure, membrane got damaged at first 30-minutes period. Therefore data belonging to 0.5h, 1h and 2h exposure cannot be found on 3.23. For the case of 0.5% $TiO_2$ loaded membranes it can be mentioned that NaOH causes a slight decline after 2h exposure at the ratio of 7.88%.

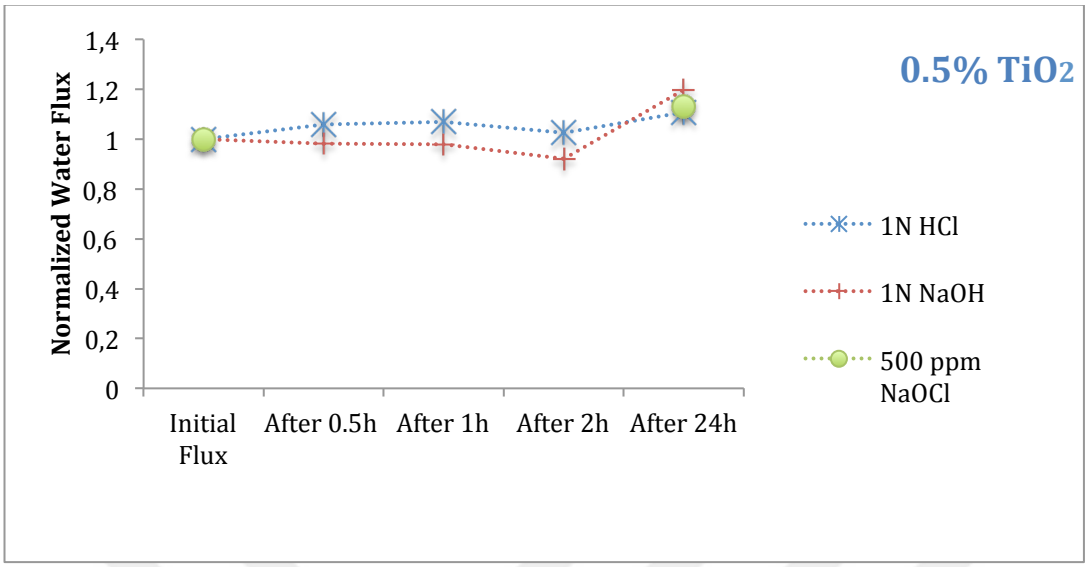


**Figure 3.18.** Normalized pure water flux changes at 100 kPa for 0.5% TiO2-NP embedded membrane after cleaning agents' exposure

As it can be seen on figure 3.18 and figure 3.19 sodium hypochlorite (NaOCl) is the most aggressive cleaning agent. After 24h exposure of NaOCl it led 14.31% and 31.9% increase at 2.0 % and 4.0% titania loadings, respectively. For the case of 2% titania loaded membranes, 1N NaOH has the most convenient characteristics since it did not cause intense change on membrane permeabilities.

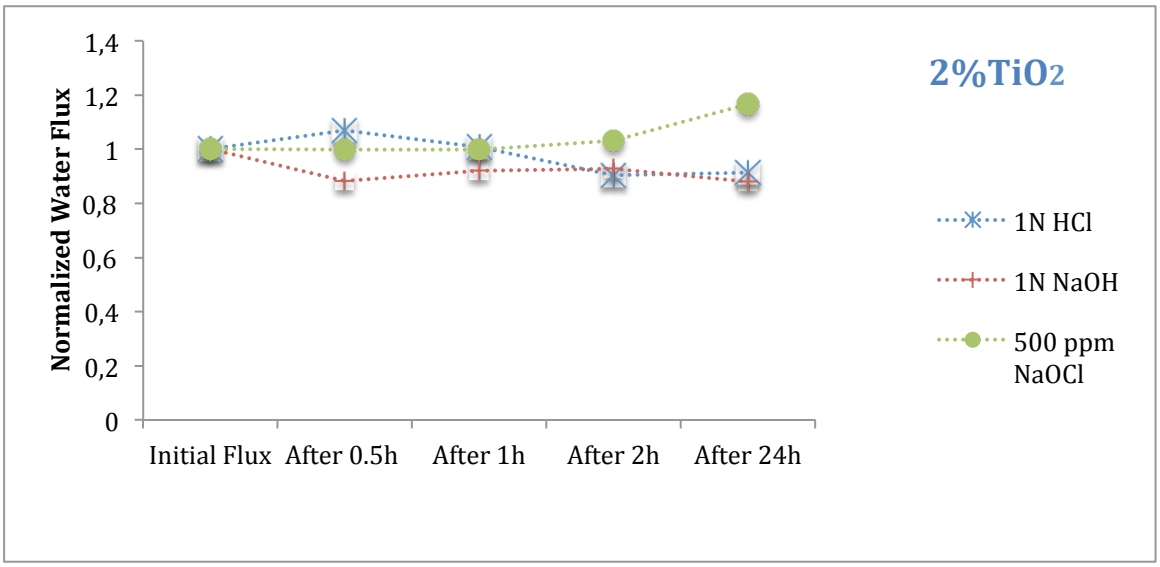


**Figure 3.19.** Normalized pure water flux changes at 100 kPa for 2% TiO2-NP embedded membrane after cleaning agents' exposure

In order to chemically clean 4wt.% $TiO_2$ loaded membrane 1N NaOH or 1N HCl can be chosen. Because both cleaning agents are not affecting membrane permeability dramatically and they show similar trendline (Figure 3.20).

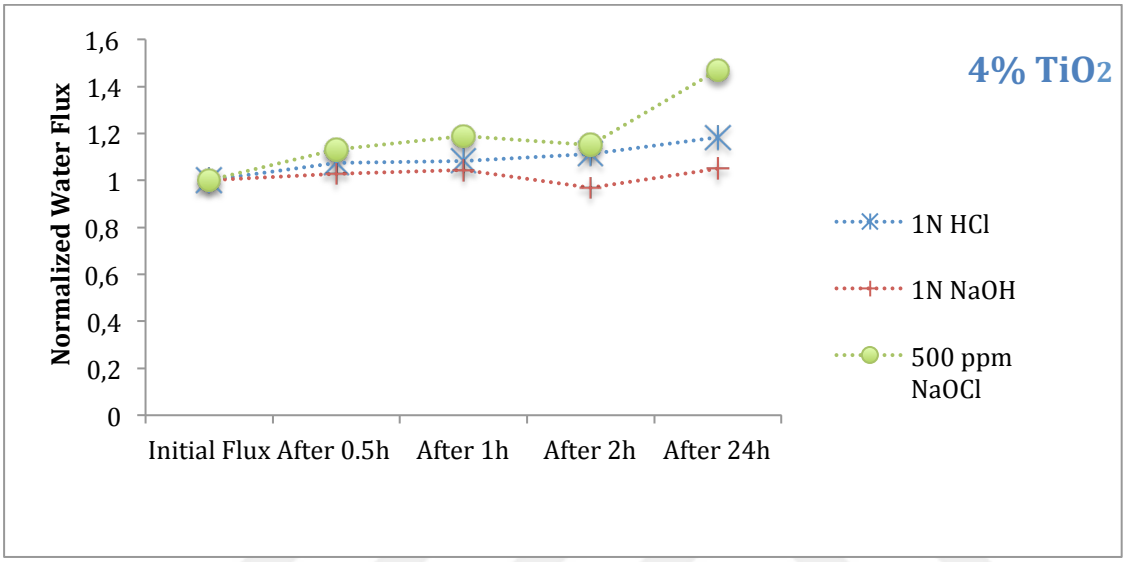


**Figure 3.20.** Normalized pure water flux changes at 100 kPa for 4% TiO2-NP embedded membrane after cleaning agents' exposure

Pure water flux at 100 kPa is increasing by the time of exposure of 500 ppm NaOCl when the concentration of titania loadings are 2% and 4%. This aforesaid incline confirms the aggregation phenomenon, which previously helped to explain pure water flux of clean membranes and membrane morphology. This idea and behavior will also be confirmed by titania release study. Because, $TiO_2$-NPs greatly tend to be released under hypochlorite exposure especially for 4% titania concentration. The more nanoparticles are embedded into membrane, the more they have propensity to aggregate and thus, pure water flux of membranes increases, when nanoparticles leave membrane under aggressive chemicals exposure.

### 3.1.7. Mechanical Tests

To examine the relationship between tensile strength and loaded nanoparticle concentration stress-strain tests were done under certain circumstances, which were

already given in material and methods chapter. Reported values are the average value of at least five samples (Figure 3.21).

With the loading amount of $TiO_2$ nanoparticles increasing from 0% to 4% by weight, tensile strength decreased from 18.01 kg/cm$^2$ to 7.4 kg/cm$^2$. It means that the more nanoparticle embedded into membrane the less intense it becomes. Li et al. also investigated mechanical strength of PES membranes with the loading of titania nanoparticles in terms of breaking strength and elongation ratio, but they reported that membrane intensity increases with addition of $TiO_2$ nanoparticles (Li et al., 2009). Yang et al. also confirms these results for the case of PSf membranes in 2006.

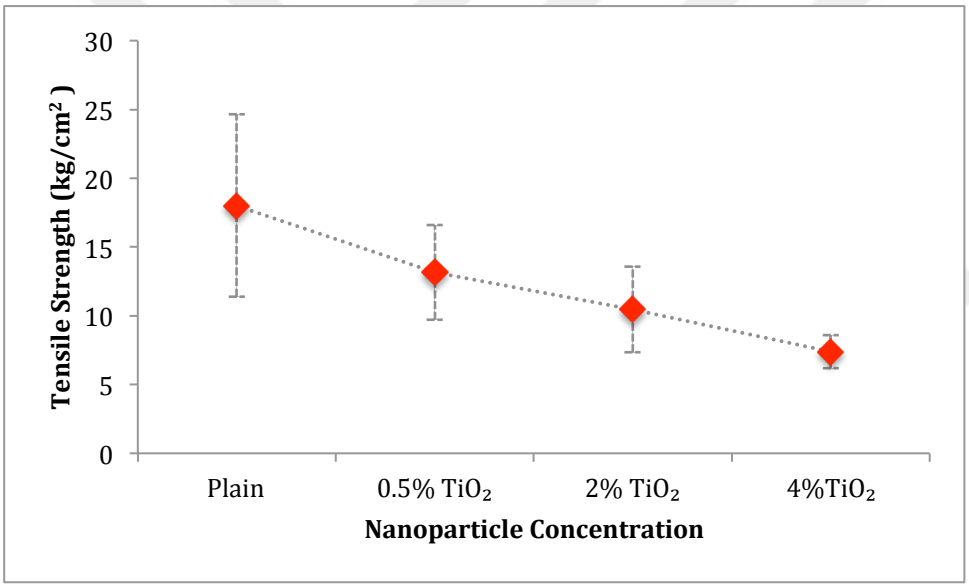


**Figure 3.21.** Tensile Strength vs. Titania-NP Concentration

### 3.1.8. Nanoparticle Size

In order to determine the size of nanoparticles after ultrasonication with solvent (NMP) and after ultrasonication and blended with polyvinypyrrolidone (PVP), nanoparticle size measurements were carried out. Results of analyses are listed in Table 3.1.

According to Goh et al. (2015) evaluation of particle size and dimension is an important part of the study to determine the efficiency of titania, when it is incorporated to polymer matrix.

As it can be seen on table 3.1., when the concentration is 0.5% by weight, particle size is very close to initial powder size (40 nm). As the concentration rises up to 2wt.% and 4wt.%, particles become 4.46 and 5.7 times bigger than 0.5wt. % $TiO_2$ case, respectively. With PVP blended particles are 3.6, 1.6 and 2.4 times bigger than neat particles of 0.5% $TiO_2$, 2.0% $TiO_2$ and 4.0% $TiO_2$, respectively.

According to the results given in table 3.1., blending titania nanoparticles with PVP after ultrasonication process induces an apparent increase in particle size. The reason could be coating of PVP with nanoparticles, which makes the size bigger than it should be in neat state. Besides, with the addition of titania, agglomeration of particles in solution becomes faster and more intense.

**Table 3.1.** Particle size of embedded nanoparticles in isolated and with PVP incorporated positions

| **Quantity of Nanoparticles (by weight)** | **Particle Size (nm)** |
|---|---|
| 0.5% $TiO_2$ | 56.56 |
| 2.0% $TiO_2$ | 252.1 |
| 4.0% $TiO_2$ | 324.2 |
| PVP + 0.5% $TiO_2$ | 205.7 |
| PVP + 2.0% $TiO_2$ | 394.2 |
| PVP + 4.0% $TiO_2$ | 787.7 |

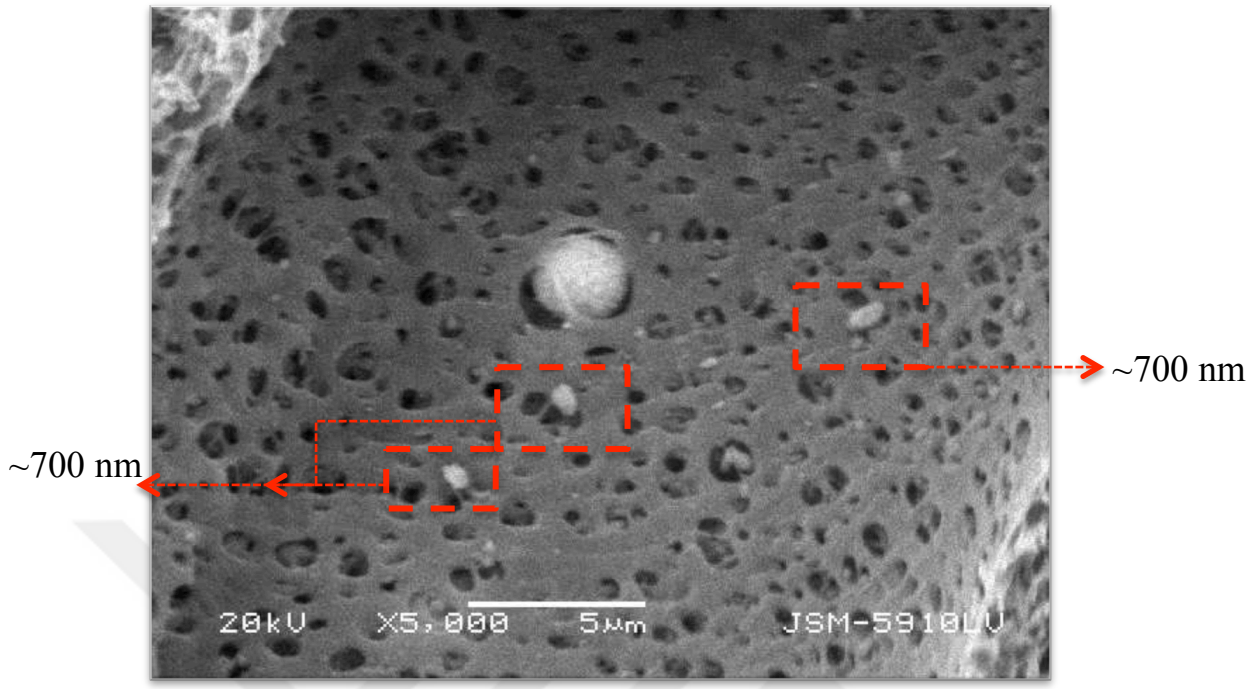


**Figure 3.22.** Cross-section morphology of 4% titania embedded membrane

SEM pictures of 4wt. % titania entrapped membrane in 5μ magnitude confirm particle size evaluation (Figure 3.22). Because, nanoparticles exist in PVP blended state when they are in membrane solution. As it can be seen on figure 3.21, several agglomerated $TiO_2$ nanoparticles are located in membrane cross-section and these agglomerations are approximately 700 nm, which is expected according to particle size experiments.

### 3.2. Titania Release

Unique part and the motivation of this study is to investigate release behavior of enhanced membranes, which provided by titania nanoparticles before. Following figures represent titanium release characteristics of certain amount of $TiO_2$ embedded membranes under chemical cleaning agents (1N HCl, 1N NaOH and 500 ppm NaOCl) over time. First bar on the graphs below stands for 30 minutes exposure, second bar represents continuing 30 minutes, third bar represents continuing 1 hour, fourth bar stands for another 2 hours, fifth bar represents continuing 20 hours and the last bar speaks for total release at the en of 24 hours.

After each periods of time chemicals were collected and stored, but membrane coupons were not changed. With a new solution of cleaning agents was poured on membranes and another contact time with chemicals was started.

As it has already been mentioned in chapter two, released titanium amounts were analyzed by ICP-MS and after analysis calculations and comparisons below were done.

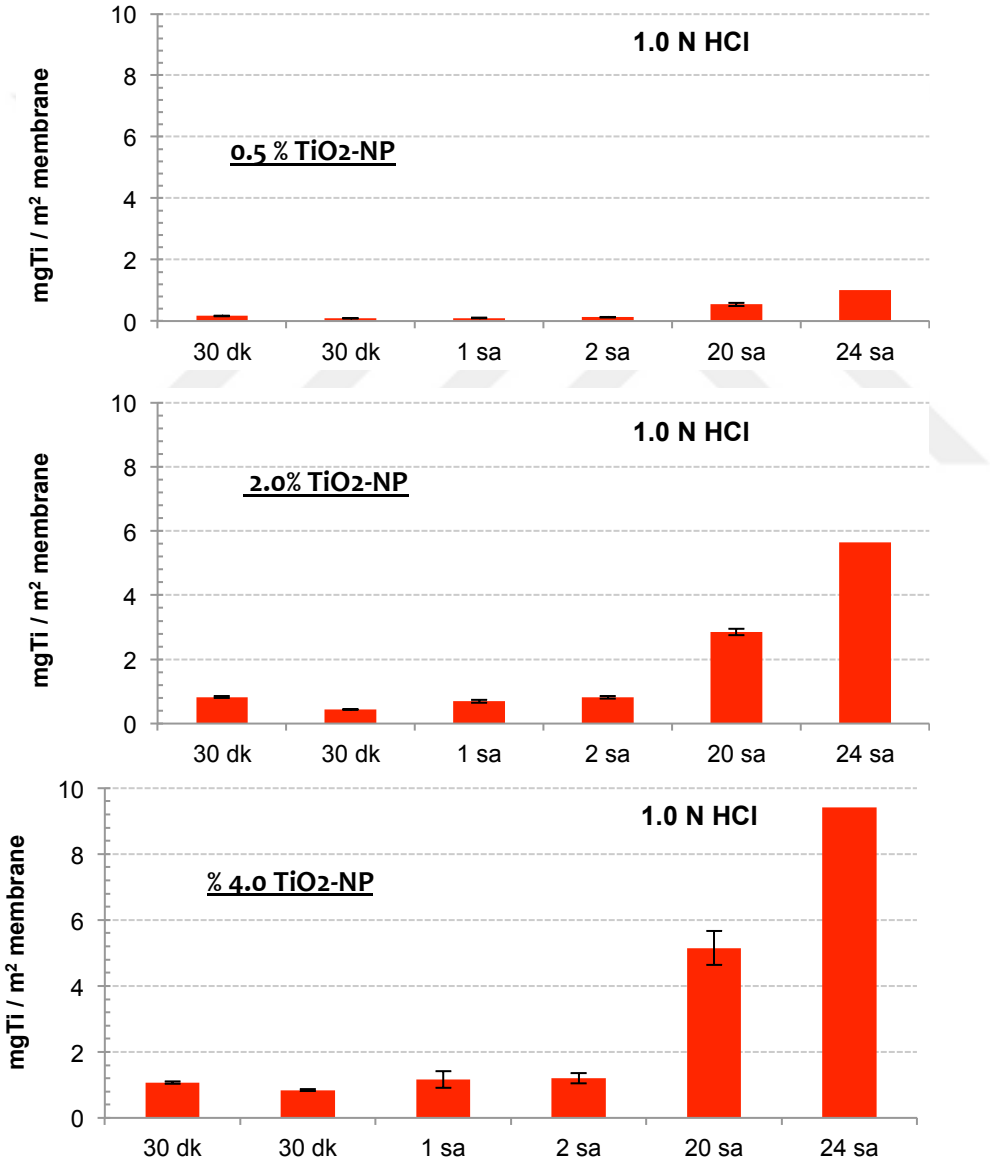


**Figure 3.23.** Titania release under 1N HCl exposure for 0.5%-2%-4% by weight titania loaded membranes

In case of 1.0 N HCl exposure to all concentrations of nano-composite membranes released titanium amounts are increasing with the increase of exposure time. This observation indicates that entrapped $TiO_2$ comes to an end after periods of times of cleaning that we have chosen. In addition to first observation is that released titanium is increasing with the rising concentration of loaded titania, which is naturally expected due to aggregate phenomenon of high amounts of nanoparticles.

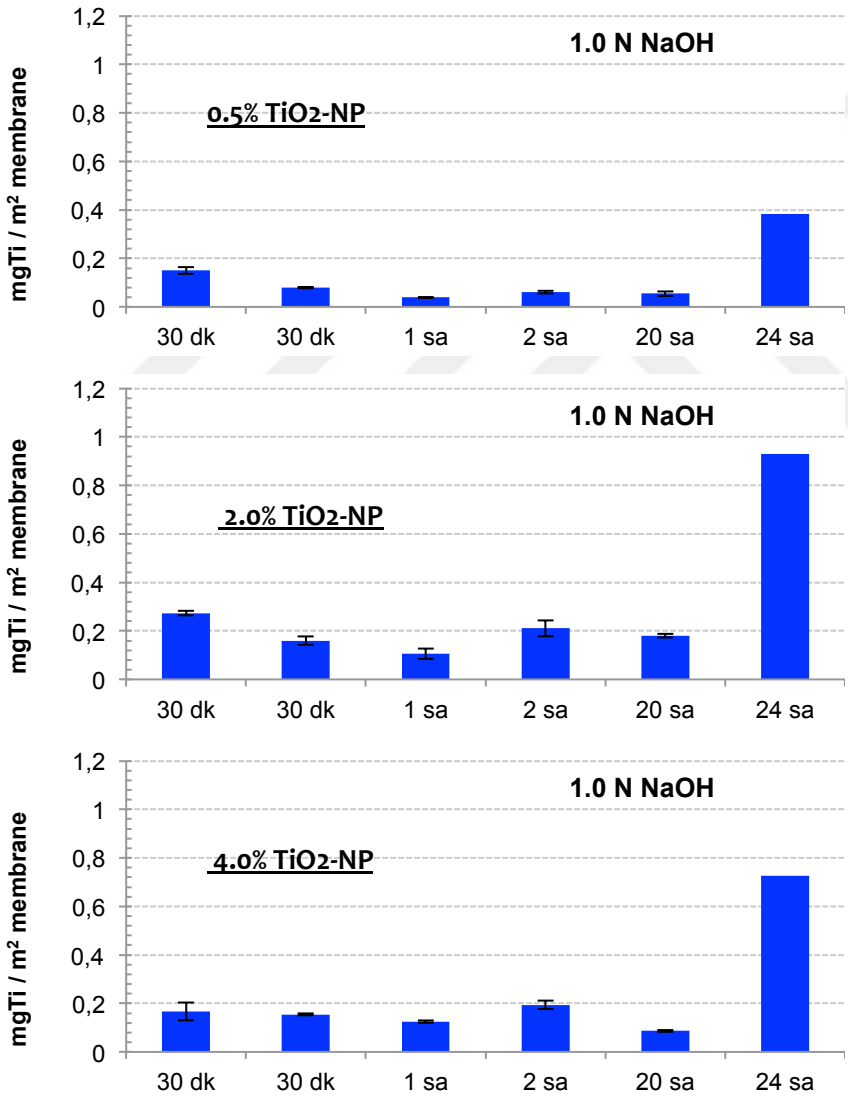


**Figure 3.24.** Titania release under 1N NaOH exposure for 0.5%-2%-4% by weight titania loaded membranes

Titanium, which is embedded inside membranes, has a less susceptible behavior, when it is exposed to 1N NaOH, as it can be seen on figure 3.24. Released Ti amount is too low, so that causes nonlinear incline in terms of exposure duration and loaded titania concentration. For example, the amount of released Ti for 4wt. % $TiO_2$ after 2 hours of exposure is higher then released Ti amount after 20 hours of exposure. Furthermore, total released Ti of 2 wt.% $TiO_2$ is slightly higher than 4 wt. % $TiO_2$ embedded membranes. But, when the concentration is 0.5wt. % $TiO_2$, total amount of Ti at the end of 24 hours is still the lowest compared to other concentrations.

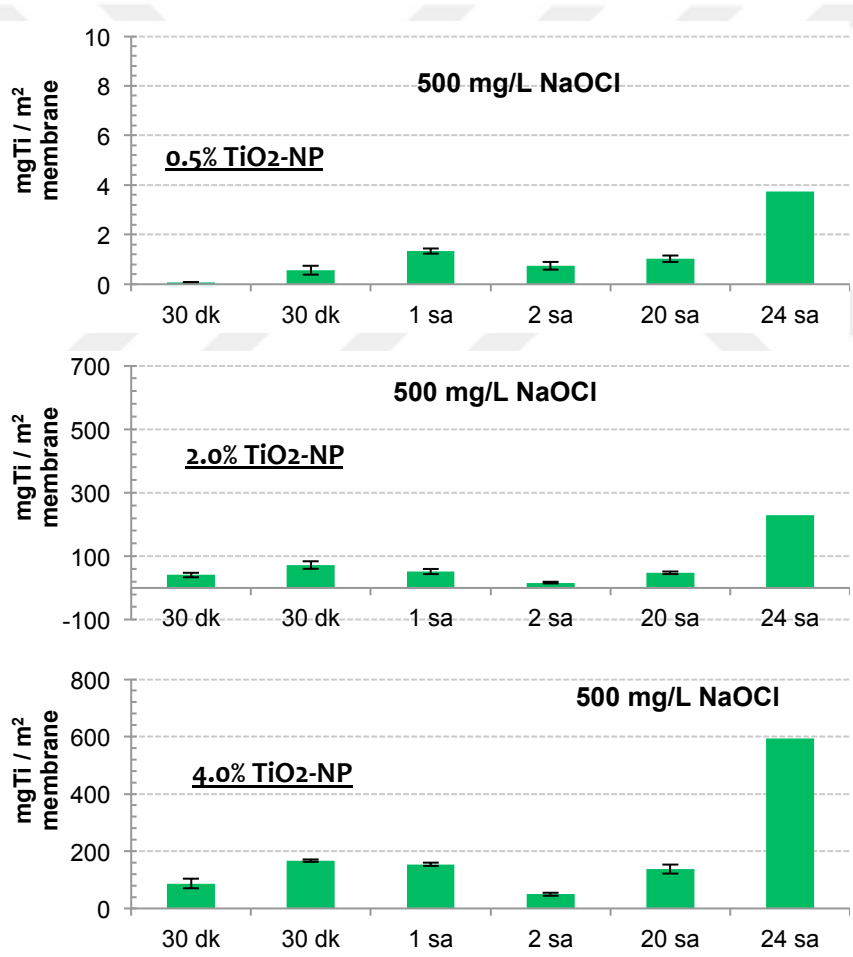


**Figure 3.25.** Titanium release under 500 ppm NaOCl exposure for 0.5%-2%-4% by weight titania loaded membranes

In the case of 500 ppm NaOCl, it can be easily said that all membranes of each concentration level are remarkably susceptible to this environment (Figure 3.26). Released Ti amounts per $m^2$ are substantially high comparing to other two cleaning agents' environment. Ti is so vulnerable to sodium hypochlorite that 4wt. % $TiO_2$ embedded membranes release more during second 30 minutes than during 20 hours exposure. On the other hand, 0.5 wt. % $TiO_2$ loaded membranes show a very stable behavior in comparison to other concentrations, but still most released titanium amount is the highest under NaOCl exposure for 0.5 wt. % $TiO_2$ as well. Again, released titanium is increasing with the rising concentration of loaded titania and that confirms once again the aggregate phenomenon.

On following graphs total released titanium amounts per square meter were shown (Figure 3.26). First bars on each three graphs are representing HCl environment, second bars are standing for NaOH environment and the third ones are representing NaOCl environment.

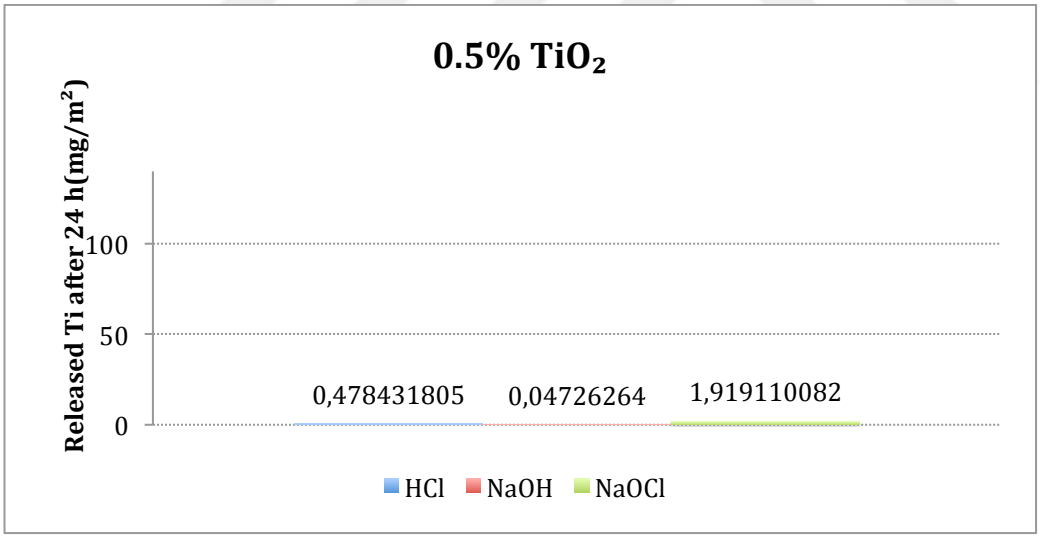

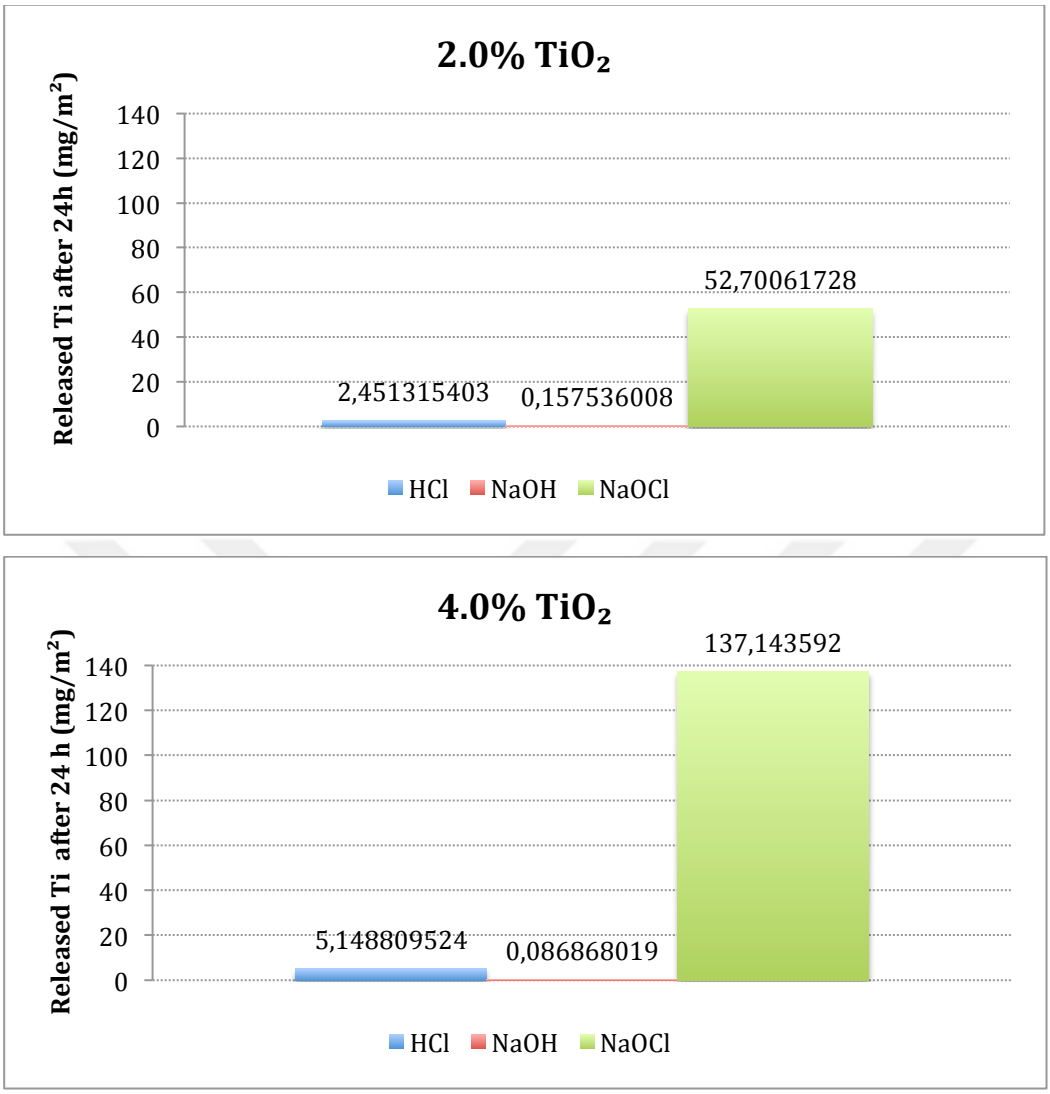


**Figure 3.26.** Titanium release under 1N HCl, 1N NaOH and 500 ppm NaOCl 24h long exposure for 0.5%-2%-4% by weight titania loaded membranes

On figure 3.26 it can be easily observed that release behavior in hypochlorite environment is remarkably high at 2% and 4% titania concentrations. On the other hand, in case of 0.5% titania concentration release behaviors are quite slightly changing. As it has already been mentioned that membranes at all concentrations level are very stable to NaOH exposure, which can be seen very clearly on figure asdfg. Furthermore, titanium is released 75.1%, 95.3% and 96.2% less at 0.5% $TiO_2$, 2.0% $TiO_2$, 4.0% $TiO_2$ concentration levels in HCl environment compared to NaOCl environment, respectively.

As it can be seen on figure below (figure 3.27), released titanium amounts are approximately %2.5 from total Ti amount, which is 4% by weight as titania embedded inside the membranes, even if membranes were cleaned with the most aggressive chemical agent, NaOCl. Besides that, when membranes were exposed to HCl agent on the purpose of cleaning, released titanium amount is less than one percent.

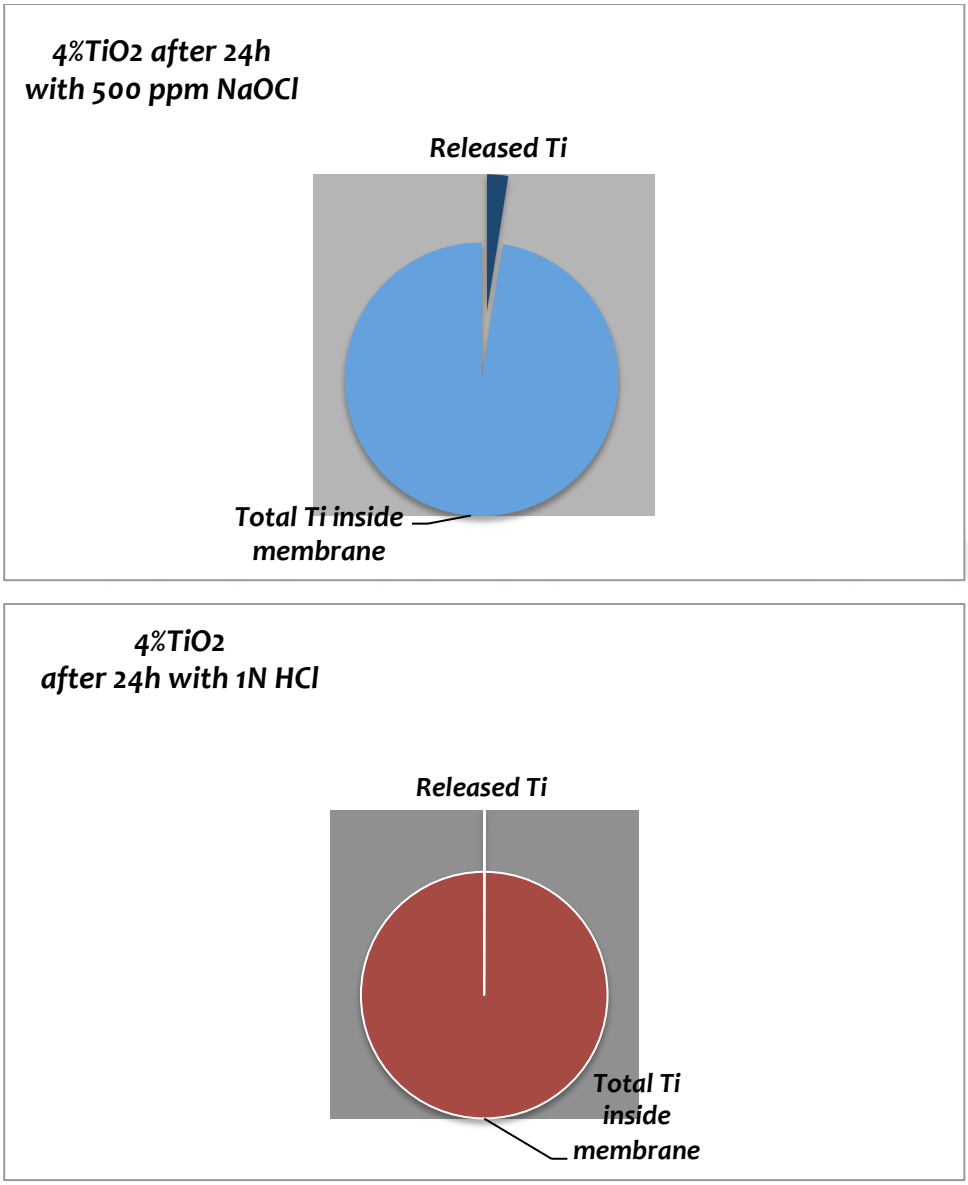


**Figure 3.27.** Representative figure of released titanium from total titanium inside membrane under *i)* 500 ppm NaOCl, *ii)* 1N HCl exposure of 4% $TiO_2$ embedded membranes

### 3.3. Effect of UV Irradiation

$TiO_2$ is the most widely used catalyst in heterogeneous photocatalysis, because of its photostability, nontoxicity, low cost, and stability in water. Large amount of reactive oxygen species such as hydroxyl radicals (·OH) and superoxide radical anion ($\cdot O_2$) are produced on the surface of $TiO_2$ under UV-light irradiation, and these reactive radicals are responsible species for the degradation of organic matter (Zhang et al., 2014). This photocatalytic activity of titania constitutes a basis for solar oxidation experiments done in this study. Titanium dioxide solutions were prepared based on the highest released titanium characteristics, which was shown by 4% $TiO_2$ embedded membranes under NaOCl exposure.

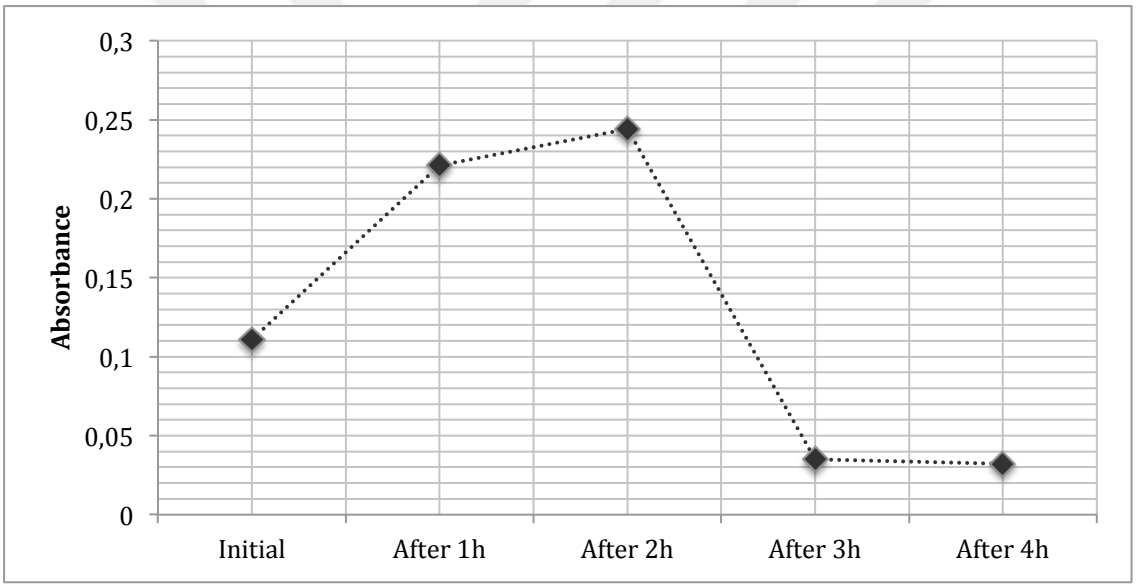


**Figure 3.28.** Absorbance of $TiO_2$ + HA solution after UV-light treatment vs. time

254 nm is considered as the characteristic peak of benzene ring. As can be seen on figure 3.28 above, absorbance at 254 nm increases in the first 2 hours of irradiation. This can be explained by the formation of some benzene intermediate compounds (Damodar et al., 2009).

Figure 3.28 also shows the altering absorbance of HA and titania mixture after UV-light exposure for certain amount of time. As it can be easily observed that after 3 hours of UV-light irradiation there is a remarkable decline of absorbance under 254 nm, which is 68.47% less than initial absorbance. It is necessary to mention here that

initial absorbance of HA alone was 0.108 and that is not so different from the initial absorbance of HA-$TiO_2$ mixture. Degradation of humic acid into smaller molecules leads that decrease of UV absorbance. During last period of UV-light irradiation absorbance and degradation stay stable.

# 4. CONCLUSIONS

In this study membranes were prepared by phase inversion method using polysulfone (PSf), polyvinylpyrrolidone (PVP) in solvent N-methyl-2 pyrrolidone (NMP) with three different loadings of titania nanoparticles ($TiO_2$-NPs), 0.0%, 0.5%, 2.0% and 4.0% by weight.

Because of its unique characteristics, such as obtaining high water flux, semi-conductivity, potential in photocatalytic membrane reactions, titania has been gaining more attention for producing nanoparticles embedded membranes. Therefore, this study is focused on the production and characterization of titania ($TiO_2$) nanoparticles entrapped membrane sheets.

The morphology of the fabricated membranes was analyzed by using scanning electron microscope (SEM). The membranes were subjected to ultrafiltration tests, such as measurement of pure water flux, fouling behavior including flux decline and flux recoveries. Besides, this study includes particle size evaluation of nanoparticles, mechanical tests, water uptake and contact angle measurements of fabricated membranes,. Titania release under interaction with different chemical agents (HCl, NaOH and NaOCl) and photocatalytic activity of released titania were also investigated.

18% PSf and 15% PVP polymer composition was chosen after evaluating several polymer ratios since this composition enables the production of membranes with similar and reliably consistent pure water fluxes, which are in the scale of ultrafiltration permeabilites.

0.5% $TiO_2$ embedded memranes showed highest pure water flux among all the membranes fabricated (0.0%, 0.5%, 2.0% and 4% $TiO_2$ loaded membranes). It was possible to distribute the nanoparticles homogeneously, when the composition of titania nanoparticles is 0.5% by weight. The further increase in nanoparticle concentration can cause reduction in membrane permeability and an increase in filtration resistance. Observed decrease in pure water fluxes at 100 kPa for the membranes with 2.0% and 4.0% $TiO_2$-NPs loadings is 19.5% and 6.9%, respectively. For the case of higher concentration than 2% by weight of titania, nanoparticles perform aggregation phenomenon, which prevents dispersion of nanoparticles inside polymer matrix.

The water uptake tests and the results of equilibrium water content showed that while the $TiO_2$ – NP content increases in membranes the water uptake percentage decreases. The water uptake of 0.5% $TiO_2$ loaded membrane slightly differentiates from plain membrane, but is the highest. On the other hand, 4.0% $TiO_2$ embedded membrane shows the lowest water uptake

propensity with the difference of ~4% and ~5% from 2.0% and 0.5% $TiO_2$ entrapped ones, respectively.

According to contact angle measurements 4% titania loaded membranes are the most hydrophilic membranes among 0.5%, 2% and 4% $TiO_2$-NP loadings. As the measurement results show that contact angle decreases, while the concentration of titania nanoparticles inside the membrane increases.

Cross-section images of the membranes showed similar morphologies. The membranes have the asymmetric morphologies and the loading of titania nanoparticles did not change the membrane structure. The skin layer of membranes thickens with the increase of filler concentration. In the case of 4 wt.% titania loaded membranes have much thicker skin layer, which causes low pure water permeation. SEM images also showed that addition of $TiO_2$-NPs at high amounts resulted in the agglomeration of nanoparticles inside the membrane structure.

Experiments during which the membranes were exposed to NaOCl showed that the membranes were damaged with the mechanism through which the permeability has increased. When membranes are loaded with 2% titania by weight NaOH did not cause intense change on membrane permeabilities. Considering these results, in order to chemically clean 4wt.% $TiO_2$ loaded membrane NaOH or HCl can be chosen. Because both cleaning agents do not affect membrane permeability dramatically and they show similar nanoparticle release.

The more nanoparticles are embedded into membrane, the more they have propensity to aggregate. This non-homogeneous distribution causes the membrane to lose more nanoparticles during the exposure to chemical agents (HCl, NaOH, NaOCl). As a result of nanoparticle release membrane permeability increases.

Of all the three chemical agents, NaOH caused the smallest damage to the membrane, which can be summarized as: NaOCl> HCl> NaOH.

It is found that cleaning the PSf/PVP-$TiO_2$-NPs composite membranes with NaOH would mostly preserve the homology and morphology of the membrane-nanoparticle composites.

In this study with the loading amount of $TiO_2$ nanoparticles increasing from 0% to 4% by weight, tensile strength decreased from 18.01 $kg/cm^2$ to 7.4 $kg/cm^2$. It means that the more nanoparticle embedded into membrane the less intense it becomes.

According to the nanoparticle size evaluation blending titania nanoparticles with PVP after ultrasonication process induces an apparent increase in particle size. The reason could be coating of PVP with nanoparticles, which makes the size bigger than it should be in neat state. Besides, with the addition of titania, agglomeration of particles in solution becomes faster and more intense.

When the concentration of titania nanoparticles increases, reversible flux recovery becomes easier during river water filtration. 0.5% $TiO_2$-NPs loaded membranes have the highest pure membrane flux among all other titania loadings, while those membranes have a bigger propensity to fouling during river water filtration than neat membranes (0.0% $TiO_2$ –NPs embedded membranes). But, 0.5% titania loaded membranes' flux can be easily recovered after chemical backwash, even if those membranes tend to be fouled quickly in comparison to control membranes. 4% titania loaded membranes are tend to be fouled severely during river water filtration than 2.0% titania loaded membranes. On the other hand, all titania loadings tend to foul very rapidly while they are exposed to alginic acid filtration. According to river water filtration the more nanaoparticle embedded, the easier to regain water flux after chemical wash. In the case of alginate filtration 0.5% titania embedded membranes have the biggest propensity to be recovered after each filtration run.

At 0.5% $TiO_2$-NPs loading, total water production potential and amount of product water were increased. Besides, 4% $TiO_2$- NP embedded membranes have the lowest product water value with the amount of less than 71% and also the highest lost (due to fouling) value.

Released titanium amounts are approximately %2.5 from total Ti amount, which is 4% by weight as titania embedded inside the membranes, even if membranes were cleaned with the most aggressive chemical agent, NaOCl. Besides that, when membranes were exposed to HCl agent on the purpose of cleaning, released titanium amount is less than one percent.

Titanium dioxide solutions were prepared based on the highest released titanium characteristics, which was shown by 4% $TiO_2$ embedded membranes under NaOCl exposure. The possible benefits of titania release can be oxidation of organics in the fouling layer if the membranes are exposed to UV light during chemical cleaning. After 3 hours of UV-light irradiation there is a remarkable decline of absorbance under 254 nm, which is 68.47% less than initial absorbance.

# REFERENCES


American Water Works Association, American Society of Civil Engineers, (2005). *Water Treatment Plant Design*. The McGraw-Hill Companies Inc., USA.

Crittenden, J.C.; Trussell, R.R.; Hand, D.W.; Howe, K.J. and Tchobanoglous, G., (2012). *MWH's Water Treatment Principles and Design 3rd Edition*. John Wiley & Sons, Ltd.

Yang, Y.; Zhang, H.; Wang, P.; Zheng, Q.; Li, J., (2007). *The influence of nano-sized $TiO_2$ fillers on the morphologies and properties of PSF UF membrane.* Journal of Membrane Science 288 (2007) 231–238.

Li, J.; Zhu, J.; Zheng, M., (2006). *Morphologies and Properties of Poly(phthalazinone ether sulfone ketone) Matrix Ultrafiltration Membranes with Entrapped $TiO_2$ Nanoparticles*. Journal of Applied Polymer Science, 103, 3623–3629.

Richards, H.L.; Baker, P.G.L.; Iwuoha, E., (2012). *Metal Nanoparticle Modified Polysulfone Membranes for Use in Wastewater Treatment: A Critical Review.* Journal of Surface Engineered Materials and Advanced Technology, 2, 183-193.

Goh, P.S.; Ng, B.C.; Lau, W.J.; Ismail, A.F., (2015). *Inorganic Nanomaterials in Polymeric Ultrafiltration Membranes for Water Treatment*. Separation & Purification Reviews, 44, 216–249.

Zhang, X.; Du, A.; Lee, P.; Sun, D.; Leckie, J., (2008). *$TiO_2$ nanowire membrane for concurrent filtration and photocatalytic oxidation of humic acid in water.* Journal of Membrane Science, 313 (2008), 44–51.

Sotto, A.; Boromand, A.; Balta, S.; Darvishmanash, S.; Kim, J.; Van der Bruggen, B., (2011). *Nanofiltration membranes enhanced with $TiO_2$ nanoparticles: a comprehensive study.* Desalination and Water Treatment, 34(2011), 179-183.

Teli, S.B.; Molina, S.; Sotto, A.; Calvo, E.; Abajo, J., (2013). *Fouling Resistant Polysulfone−PANI/$TiO_2$ Ultrafiltration Nanocomposite Membranes*. Ind. Eng. Chem. Res.

2013, 52, 9470−9479

You, S.; Guo, M., (2013). *Combination of $TiO_2$-Film Photocatalysis and Ultrafiltration to Treat Wastewater.* International Journal of Photoenergy.

Vatanpour, V.; Madaeni, S.S.; Khataee, A.R.; Salehi, E.; Zinadini, S.; Monfared, H.A., (2012). *$TiO_2$ embedded mixed matrix PES nanocomposite membranes: Influence of different sizes and types of nanoparticles on antifouling and performance*. Desalination, 292, 19-29.

Barron, A.R.; Rose, J.; Wiesner M.R., (2007). Ch. 9 Membrane Processes. In Wiesner M.R.; Bottero, J (Eds.), *Environmental Nanotechnology Applications and Impacts of Nanomaterials.* The McGraw-Hill Companies Inc., USA

Ding, X.; Fan, Y.; Xu, N., (2006). *A new route for the fabrication of $TiO_2$ ultrafiltration membranes with suspension derived from a wet chemical synthesis***.** Journal of Membrane Science 270, 179-186

Mackenzie L.D., (2010). *Water and Wastewater Engineering Design Principles and Practice.* The McGraw-Hill Companies Inc., USA.

Baker, R.W., (2004). *Membrane Technology and Applications Second Edition.* John Wiley & Sons, Ltd.

Lalia, B.S.; Kochkodan, V.; Hashaikeh, R.; Hilal, N., (2013). *A review on membrane fabrication: Structure, properties and performance relationship*. Desalination, 326, 77–95.

Natarajan, C.; Fukunaga, N.; Nogami, G., (1998). *Titanium dioxide thin film deposited by spray pyrolysis of aqueous solution.* Thin Solid Films, 322, 6-8.

Macleod, H.A., (1999). Thin-Film Optical Filters Third Edition. Institute of Physics Publishing, Bristol.

Frank, S. N.; Bard A.J., (1977). *Heterogeneous Photocatalytic Oxidation of Cyanide Ion in Aqueous Solution at $TiO_2$ Powder.* Journal of the American Chemical Society, 99, 303-304.

Zhao, C.; Xue, J.; Ran, F.; Sun, S., (2013). *Modification of polyethersulfone membranes – A*

*review of methods.* Progress in Material Science, 58, 76-150.

Monteiro-Riviere N.A.; Orsiere T., (2007). Ch.11 Toxicological Impacts of Nanomaterials. In Wiesner M.R.; Bottero, J (Eds.), *Environmental Nanotechnology Applications and Impacts of Nanomaterials.* The McGraw-Hill Companies Inc., USA.

Poluncheck, L.; Elbel, J.; Eckert, J. Blum, E. Wintermantel, H. M. Eppenberger, "*Titanium dioxide ceramics control the differentiated phenotype of cardiac muscle cells in culture"*, Biomaterials, 21, 539-550

Zhang, T.; Wang, X.; Zhang, X., (2014). *Recent Progress in TiO2-Mediated Solar Photocatalysis for Industrial Wastewater Treatment.* International Journal of Photoenergy, 607954.

Shi, H.; Magaye, R.; Castranova, V.; Zhao, J., (2013). *Titanium dioxide nanoparticles: a review of current toxicological data*. Particle and Fibre Toxicology, 10:15.

Rincon, A.; Pulgarin, C., 2004. *Effect of pH, inorganic ions, organic matter and $H_2O_2$ on E. coli K12 photocatalytic inactivation by $TiO_2$. Implications in solar water disinfection.* Applied Catalysis B: Environmental, 51, 283–302.

Maness, P.; Smolinski, S.; Blake D.M.; Huang, Z.; Wolfrum, E.J.; Jacoby, W.A., 1999. *Bactericidal Activity of Photocatalytic TiO2 Reaction: toward an Understanding of Its Killing Mechanism*. Applied and Environmental Microbiology, 4094-4098.

Chakrabarty, B.; Ghoshal, A.K.; Purkait, M.K., (2008). *Preparation, characterization and performance studies of polysulfone membranes using PVP as an additive.* Journal of Membrane Science, 315, 36-47.

Arthanareeswaran, G.; Mohan, D.; Raajenthiren, M., (2009). *Preparation, characterization and performance studies of ultrafiltration membranes with polymeric additive.* Journal of Membrane Science, 350, 130-138.

Kanagaraj, P.; Neelakandan, S.; Nagendran, A., (2014). *Preparation, characterization and*

*performance of cellulose acetate ultrafiltration membranes modified by charged surface modifying macromolecule.* The Korean Institute of Chemical Engineers, 31(6), 1057-1064.

Tweddle, T.A.; Kutowy, O.; Thayer, W.L.; Sourirajan, S., (1983). *Polysulfone Ultrafiltration Membranes*. Industrial & Engineering Chemistry Product Research and Development, 22, 320-326.

Oh, S.J.; Kim, N.; Lee, Y.T., (2009). *Preparation and characterization of PVDF/$TiO_2$ organic–inorganic composite membranes for fouling resistance improvement*. Journal of Membrane Science, 345, 13-20.

Yang, Y.; Wang, P.; Zheng, Q., (2006). *Preparation and Properties of Polysulfone/$TiO_2$ Composite Ultrafiltration Membranes*. Journal of Polymer Science, 44, 879-887.

Katsoufidou, K.; Yiantsios, S.G.; Karabelas, A.J., (2007). *Experimental study of ultrafiltration membrane fouling by sodium alginate and flux recovery by backwashing*. Journal of Membrane Science, 300, 137-146.

Li, J.; Xu, Z.; Yang, H.; Yu, L.; Liu, M., (2009). *Effect of TiO2 nanoparticles on the surface morphology and performance of microporous PES membrane*. Applied Surface Science, 255, 4725-4732.

Damodar, R.A.; You, S.; Chou, H., (2009). *Study the self cleaning, antibacterial and photocatalytic properties of TiO2 entrapped PVDF membranes*. Journal of Hazardous Materials, 172, 1321-1328.